



# BRNO UNIVERSITY OF TECHNOLOGY

VYSOKÉ UČENÍ TECHNICKÉ V BRNĚ

## FACULTY OF MECHANICAL ENGINEERING

FAKULTA STROJNÍHO INŽENÝRSTVÍ

## INSTITUTE OF PHYSICAL ENGINEERING

ÚSTAV FYZIKÁLNÍHO INŽENÝRSTVÍ

# DESIGN OF MOBILE VACUUM CHAMBER FOR LOADING SAMPLES INTO HIGH-FREQUENCY ELECTRON PARAMAGNETIC RESONANCE SPECTROMETER

NÁVRH PŘENOSNÉ VAKUOVÉ KOMORY PRO ZAKLÁDÁNÍ VZORKŮ DO VYSOKOFREKVENČNÍHO  
PARAMAGNETICKÉHO REZONANČNÍHO SPEKTROMETRU

## MASTER'S THESIS

DIPLOMOVÁ PRÁCE

### AUTHOR

AUTOR PRÁCE

Bc. Tomáš Láznička

### SUPERVISOR

VEDOUCÍ PRÁCE

Ing. Petr Neugebauer, Ph.D.

BRNO 2020



# Specification Master's Thesis

Department: Institute of Physical Engineering  
Student: **Bc. Tomáš Lázníčka**  
Study programme: Applied Sciences in Engineering  
Study branch: Physical Engineering and Nanotechnology  
Supervisor: **Ing. Petr Neugebauer, Ph.D.**  
Academic year: 2019/20

Pursuant to Act no. 111/1998 concerning universities and the BUT study and examination rules, you have been assigned the following topic by the institute director Master's Thesis:

## **Design of mobile vacuum chamber for loading samples into high-frequency electron paramagnetic resonance spectrometer**

### **Concise characteristic of the task:**

The goal of the project is to design a vacuum transfer system for loading samples into high frequency electron paramagnetic resonance (HF-EPR) spectrometer. The design will provide solution allowing transfer of samples from vacuum preparation chamber (or glow box) without contamination. Thanks to this solution, measurements of sensitive samples to oxidation or air contamination will be possible. The design should be fully compatible with existing HF-EPR spectrometer working in frequency range 80–1100 GHz, temperature 1.8–300 K and use strong magnetic field of 16 T.

### **Goals Master's Thesis:**

1. Literature review of EPR spectroscopy with focus on samples sensitive to atmospheric contamination and its use.
2. Design of a system for the transfer of atmosphere-sensitive samples from a vacuum apparatus or a glow box to the EPR spectrometer at CEITEC.
3. Testing the setup and performing first measurements of atmosphere-sensitive samples.

### **Recommended bibliography:**

MOBIUS, K. a A. SAVITSKY. High-field EPR spectroscopy on proteins and their model systems: characterization of transient paramagnetic states. 2nd edition. Cambridge UK: Royal Society of Chemistry, 2009. ISBN 978-0-85404-368-2.

NEUGEBAUER, P., D. BLOOS, R. MARX, et al. Ultra-broadband EPR spectroscopy in field and frequency domains. Physical Chemistry Chemical Physics. 2018, 20(22), 15528-15534. DOI: 10.1039/C7CP07443C. ISSN 1463-9076.

GRINBERG, O. a L. J. BERLINER. Very High Frequency (VHF) ESR/EPR. 1st edition. New York: Springer Science Business Media, 2004. ISBN 978-144-1934-420.

WEIL, J. A. a J. R. BOLTON. Electron paramagnetic resonance: elementary theory and practical applications. 2nd edition. Hoboken: Wiley-Interscience, 2007. ISBN 978-0-471-75496-1.

Deadline for submission Master's Thesis is given by the Schedule of the Academic year 2019/20

In Brno,

L. S.

---

prof. RNDr. Tomáš Šikola, CSc.  
Director of the Institute

---

doc. Ing. Jaroslav Katolický, Ph.D.  
FME dean

## Abstract

In order to be able to characterize atmosphere sensitive samples in high-frequency electron paramagnetic resonance spectrometer (HF-EPR), a system of vacuum transportation is needed. The scope of this thesis is to design and develop a vacuum transport system which will allow this transportation. The vacuum system, which consists of a mobile vacuum suitcase, palette holder and airlock, was designed, assembled and tested. The pressure of  $4.3 \cdot 10^{-10}$  mbar was achieved, which will ensure inert condition for sample transportation. The transport of the sample from an ultra-high vacuum (UHV) cluster to the HF-EPR spectrometer was performed. The contamination of the test samples was characterized using x-ray photoelectron spectroscopy. It was found that there is no detectable contamination if the sample is in the vacuum system for less than 16 hours. The extension for transportation of the samples from a glove box and sample palette for graphene were proposed, but their production has not been performed yet. The developed vacuum system is fully functional and provides the alternative to commercially available products, thus it will be further used in the investigation of an atmosphere sensitive samples in CEITEC Nano laboratories.

## Abstrakt

Aby bylo možné charakterizovat atmosfericky citlivé vzorky ve vysokofrekvenčním elektronovém paramagnetickém rezonančním spektrometru (z angl. *high-frequency electron paramagnetic resonance spectrometer*, HF-EPR), je potřebné mít vakuový transportní systém. Cílem této práce je navrhnout a vyvinout tento vakuový přepravní systém, který umožní tuto přepravu. Vakuový systém, který se skládá z mobilního vakuového kufru, držáku palety a přechodové komory, byly navrženy, sestaveny a testovány. Bylo dosaženo tlaku  $4,3 \cdot 10^{-10}$  mbar, což zajistí inertní podmínky pro transport vzorků. Byl proveden transport vzorku ze systému ultravysokého vakua (UHV) do HF-EPR spektrometru. Kontaminace testovacích vzorků byla charakterizována pomocí rentgenové fotoelektronové spektroskopie. Bylo zjištěno, že nedochází téměř k žádné detekovatelné kontaminaci, pokud je vzorek přepravován pomocí vakuovém systému méně než 16 hodin. Bylo navrženo rozšíření pro přepravu vzorků z rukavicového boxu a paletky pro grafen, ale jejich výroba dosud nebyla provedena. Vyvinutý vakuový systém je plně funkční a poskytuje alternativu ke komerčně dostupným produktům, a proto bude dále používán při zkoumání vzorků citlivých na atmosféru v laboratořích CEITEC Nano.

## Keywords

UHV suitcase, palette holder, airlock, HF-EPR,

## Klíčová slova

UHV kufřík, držák paletky, přechodová komory, HF-EPR,

LÁZNIČKA, Tomáš. *Design of mobile vacuum chamber for loading samples into high-frequency electron paramagnetic resonance spectrometer*. Brno, 2020. 71 p. Master's thesis. Brno University of Technology. Faculty of Mechanical Engineering. Supervised by Petr NEUGEBAUER.

I hereby declare that I have written my master's thesis on the theme of *Design of mobile vacuum chamber for loading samples into high-frequency electron paramagnetic resonance spectrometer* independently, under the guidance of the master's thesis supervisor, Ing. Petr Neugebauer, Ph.D., and using the technical literature and other sources of information which are all properly quoted in the thesis and detailed in the list of literature at the end of the thesis.

.....  
Place and date

.....  
Bc. Tomáš Lázníčka

## ACKNOWLEDGMENT

I would like to thank my supervisor Ing. Petr Neugebauer, Ph.D. for mentoring and consulting during the writing of my master's thesis. I am also grateful to all of my colleagues, especially to Ing. Antonín Sojka, and Ing. Jakub Hrubý, because their advice has always been very helpful. I would also like to thank doc. Ing. Jan Čechal, Ph.D. for his hints and never-ending fruitful discussions about samples and holders. I would also like to thank Ing. Tomáš Krajňák and Ing. Veronika Stará for their help with measuring, testing UHV suitcase in clean rooms and for correcting my thesis. I am thankful also to prof. Joris van Slageren for the opportunity to work on such interesting projects during my Erasmus at the University of Stuttgart, to his group, namely MSc. Dennis Schäfter, MSc. Mario Winkler, MSc. David Hunger and Ing. Michal Kern for unforgettable moments spent there. Furthermore, I would like to thank my classmates, with whom I spent an amazing piece of my life at BUT, which I will never forget. Special thanks go to Kubina, Tesi, Káťa, Ondra, Ivoš, and Endží for the great moments spent at CEITEC while we were writing the master's thesis. Thanks also go to everyone who took turns playing table football during this time. And last but not least, I thank to my family, my brother and both of my parents, without whom none of this would be possible.

Bc. Tomáš Láznička

CzechNanoLab project LM2018110 funded by MEYS CR is gratefully acknowledged for the financial support of the measurements/sample fabrication at CEITEC Nano Research Infrastructure.

# Contents

<b>1. Introduction</b>	<b>1</b>
<b>2. Introduction to electron paramagnetic resonance</b>	<b>3</b>
2.1. Historical perspective	3
2.2. EPR as a tool	5
2.3. Principles of EPR	6
2.3.1. Zeeman effect	8
2.4. Applications of EPR	9
2.5. HF-EPR spectrometer	11
Microwave source	12
Quasi-optics and waveguides	12
Superconducting magnet with Cryostat	13
Detection	13
<b>3. Molecular nanomagnets</b>	<b>15</b>
3.1. Properties	15
3.2. Applications and challenges	18
3.3. MNMs on the surface	19
<b>4. Requirements and materials</b>	<b>21</b>
4.1. UHV conditions	22
4.1.1. Leaks and Mechanical joints	22
4.1.2. Low desorption of gases from the materials and mechanical stability at elevated temperatures	24
4.2. Materials in low temperatures	25
4.3. Materials in magnetic field	27
4.4. Compatibility with UHV, low temperature, and magnetic field	28
<b>5. Design of the sample transfer system</b>	<b>30</b>
5.1. UHV suitcase	30
5.2. Various sample palettes	35
5.2.1. Samples	35
5.2.2. Sample palettes	36
5.3. Palette holder for EPR measurements	38
5.4. Airlock	40
5.5. Simple suitcase	41
<b>6. Performance of the sample transfer system</b>	<b>43</b>
6.1. Palette holder testing	43
6.2. UHV suitcase testing	45

6.2.1. Transport and compatibility with UHV cluster . . . . .	47
6.2.2. Compatibility with HF-EPR spectrometer . . . . .	52
6.3. Sample test in HF-EPR . . . . .	56
<b>7. Conclusion</b>	<b>58</b>
<b>References</b>	<b>60</b>
<b>List of abbreviation and symbols</b>	<b>67</b>
<b>List of attachments</b>	<b>68</b>
<b>A. Appendix</b>	<b>i</b>
A.1. Helmholtz magnetic coils . . . . .	i
A.2. Support system . . . . .	ii
A.3. UHV suitcase . . . . .	ii

# 1. Introduction

In times when there were no vacuum systems, it was difficult or even impossible to fabricate thin layers or microscopic structures of high quality. With the advent of vacuum systems, the production of high-quality thin films and very clean surfaces has begun. Before, this was not possible, as the mentioned objects suffered from sensitivity to oxidation and decomposition in natural ambient conditions. However, devices for the characterization and investigation of such sensitive structures must be directly connected with the systems, in which the structures are prepared – otherwise, quality of such structures might be deteriorated.

To maintain the clean character of the spoken structures, ultra-high vacuum (UHV) conditions are crucial, as they minimize the detrimental effects and prevent samples from decomposition. Such conditions can be already provided in multi-purpose vacuum clusters. However, the proposed UHV suitcase enables to transfer a sample between two otherwise unconnected vacuum devices. Specifically, the proposed suitcase was designed primarily to connect the UHV cluster apparatus and high-frequency electron paramagnetic spectrometer (HF-EPR) at Central European Institute of Technology (CEITEC) Nano. Further, a part of this thesis has been dedicated to designing a palette holder that will serve for inserting a new type of sample palette for graphene samples into HF-EPR under the vacuum conditions at CEITEC Nano. The design and manufacture of the airlock, which is the last segment of the vacuum transport of the sample, as it is mounted on the magnet of the HF-EPR spectrometer and enables the connection of the UHV suitcase to it, are presented, too. A simple case that would expand the possibilities of sample transport from the glove box to other devices with an inert atmosphere is proposed. With the exception of this case and the sample palette suitable for graphene samples, all of the proposed components have been assembled and used within the functional setup for sample transport. Additionally, the quality of all of these components has been probed intensively.

The presented thesis is structured into seven chapters. After a brief introduction, the second chapter provides a review of literature on electron paramagnetic resonance (EPR) spectroscopy and its applications in many scientific fields. Further, the HF-EPR spectrometer at CEITEC Nano is described. The third chapter contains a brief preview of molecular nanomagnets, their use, future utilization, and concisely describes molecular nanomagnets on the surface. In the fourth chapter, the emphasis was put on the requirements for the design of the UHV suitcase, palette holder, and the palette itself, which eventually serves for the support of the studied samples. The requirements for the materials given by the physical purpose of the designed apparatus are addressed, too. The fifth chapter deals with the design of the constructional requirements of the sample transfer system. This includes the proposal of the UHV suitcase, the palette holder, the palette, and the airlock. Additionally, a simple case for the connection of a glove box is proposed. The sixth chapter describes the performance of the sample transfer system and addresses

the quality testing processes of individually manufactured components before and after they were assembled to their final form. Further, the first transfer of the samples from the UHV cluster to the HF-EPR spectrometer is described. Finally, the last chapter concludes the results obtained from tests and measurements. An outline of the possibilities for further improvements is provided along with the future treatment of this topic.

## 2. Introduction to electron paramagnetic resonance

This chapter introduces the reader to the technique of EPR. It will start with a brief description of the history of EPR, through a functional description of this technique and depiction of EPR as a powerful tool used in many areas of science and technology. The last part of this chapter will describe the newly developed HF-EPR spectrometer located in CEITEC Magneto-Optical and THz Spectroscopy (MOTeS) laboratories in Brno. This theoretical part of the author's thesis is drawn mainly from two books: Electron Paramagnetic Resonance: Elementary Theory and Practical Applications [1] and Electron Spin Resonance [2] written by J.A. Weil and J.R. Bolton in 2007, B.C. Gilbert, M.J.Davies and K.A. Mclauchlan in 2000 respectively.

### 2.1. Historical perspective

The technique of EPR spectroscopy is an extension of the well-known Stern-Gerlach experiment [3]. In the 1920s, Stern and Gerlach showed that an electron magnetic moment in an atom can only take discrete orientations in a magnetic field. In the meantime, Uhlenbeck and Goudsmit connected the concept of electron spin angular momentum with



**Figure 2.1:** Experimental setup of the first EPR measurement made by Zavoisky in 1944. Photographed and provided author's friend Dennis Schäfer at the Zavoisky Museum Lab, Kazan Federal University, Russia.

electron magnetic moment [4]. The first observation of an electron paramagnetic resonance was made in Kazan (USSR, nowadays Russia) by Zavoisky in 1944 (Figure 2.1) when he detected a radiofrequency absorption line of  $\text{CuCl}_2 \cdot \text{H}_2\text{O}$  sample. Zavoisky found resonance at a magnetic field of 4.73 mT for a frequency of 133 MHz. In this case, the Zeeman factor  $g$  was approximately 2. Later, Frenkel interpreted Zavoisky's results as showing paramagnetic resonance absorption. Experiments using higher (microwave) frequencies in the magnetic field of 100-300 mT demonstrated the advantage of the use of higher fields and frequencies.

The rapid development and boom of paramagnetic resonance started after World War II due to the widespread availability of complete microwave systems used in the military. For instance, microwave devices in the 9 GHz frequency region (X-band) were used in the military for radar devices, and thus, the components could be easily obtained at a reasonable price. Until the 1970s, the problem of higher frequencies was not to be solved, and since this time, significant progress has been made to higher frequencies. The group of Lebedev implemented the first 148 GHz EPR spectrometer [5], Möbius reported EPR spectrometer operating at 94 GHz [6] and Freed, and his group pushed the limits frequencies of EPR to 250 GHz [7]. During the 1980s, the emphasis was given on the research of electron spin, the interconnection of physical properties, and material science, which increased the demand of EPR [8]. The first HF-EPR spectrometer built by a group of Schmidt in 1989 operated at 95 GHz [9]. Simultaneously with the first pulsed EPR, a new multi-frequency as well as pulsed 600 GHz HF-EPR spectrometer operating at the field as high as 19 T was developed in Grenoble [10][11]. The group of P.C. Reidi in 1998 reported about quasi-optics used for HF-EPR in the form, which is now used in HF-EPR laboratories around the world, and it is a crucial element, which is for today's scientific field very beneficial [12].

Further progress in this field came from the University of Stuttgart, specifically from F. El Hallak, J. van Slageren and M. Dressel in 2010. They developed and used a macro-cantilever, where the sample was on the cantilever, and it was irradiated by microwaves. They were able to record a broadband EPR signal by capacitive detection of the cantilever, and the name of this method is Torque Detected Electron Spin Resonance [13].

Nowadays, EPR methods are progressing very fast. Technological progress has been made by quasi-optics with modern cryostats, which achieved high-quality signals with lower noise and higher and more stable magnetic fields [14–16]. To a large extent, pulsed X-band (8 to 12 GHz), Q-band (33 to 50 GHz), and W-band (75 to 110 GHz) spectrometers were included into the commercial applications applicable to industrial applications, and pulsed EPR experiments have become an indispensable part of some production processes. To a greater extent, the HF-EPR technique has recently begun to be combined with the Nuclear Magnetic Resonance technique into the Dynamic Nuclear Polarization of experiments where the polarization of nuclei via electronic cross-relaxation is carried out [17]. In the last few years, the HF-EPR technology has begun to expand with the so-called rapid-scan regime [18]. This technique uses fast frequency sweeps and provides access to the extremely short relaxation times of the molecules. Thanks to this regime, an investigation of spin dynamics at terahertz frequencies can be possible. This is fundamentally important for the problems of quantum computation. Very few people around the world use this technique, and it is a potential extension of pulsed EPR spectrometers and, in some aspects (e.g., lower relaxation times), surpasses these spectrometers [19].

## 2.2. EPR as a tool

Electron paramagnetic resonance, also known as Electron Spin Resonance (ESR), is a sensitive spectroscopic method suitable for studying various systems and substances with unpaired electrons. Thanks to this method, various properties of different substances can be observed, such as hyperfine interaction,  $g$ -factor, fission in zero external magnetic fields. It is also possible to gain a clearer insight into many of the fundamental concepts of quantum mechanics [20].

EPR is based on the interaction between electromagnetic radiation and magnetic moments. The structure of matter is revealed by analyzing the absorption spectra of diverse samples and materials. They are obtained by measuring the attenuation versus frequency (or wavelength) of electromagnetic radiation passing through a sample. Lines or bands in a spectrum represent transitions between energy levels of the absorbing sample. Electromagnetic radiation is the synchronized oscillation of an electric  $\mathbf{E}$  and magnetic  $\mathbf{B}$  field perpendicular to the direction of propagation  $\mathbf{k}$  and it is shown in Figure 2.2. Both of these fields oscillate at the frequency  $\nu$ , which is in the field of EPR commonly between 1 and 1 000 GHz, which corresponds with the magnetic field from 35.7 mT to 35.7 T

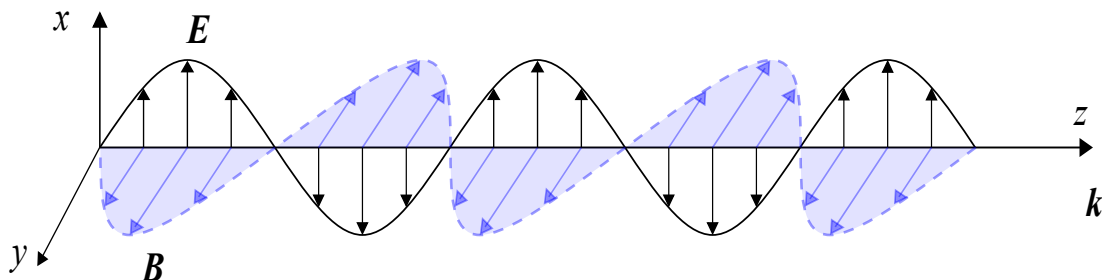


**Figure 2.2:** Illustration of propagating plane-polarised and monochromatic electromagnetic wave with propagation vector  $\mathbf{k}$  along  $z$ -axis.

Electromagnetic radiation can be imagined as a stream of particles called photons. Energy of these photons is given by  $h\nu$ , where  $h$  is Planck constant<sup>1</sup>. When a photon is emitted or absorbed by an electron, atom or molecule, the system's energy and angular momentum must be conserved. In many spectroscopic studies, it is the electric field component of the radiation, which interacts with the molecules [21]. There are two conditions, that must be fulfilled for absorption to occur:

1. The energy  $E = h\nu$  of the radiation quantum must correspond to the energy separation between certain energy levels in the molecule,
2. The oscillating electric field component of the radiation must be able to interact with an oscillating electric dipole (or higher-order) moment.

Likewise, a molecule with a magnetic dipole is expected to interact with the oscillating magnetic component of the radiation. This is a fundamental concept for magnetic resonance spectroscopy. Commonly, in the case of EPR, there is also an external magnetic field  $\mathbf{B}_s$  applied.

In any atom or molecule exist many electronic states. In the scope of EPR, the energy of photons is small (e.g., 9.5 GHz  $\approx$  0.039 3 meV) and thus, most of the electron states can

<sup>1</sup>Planck constant in SI units:  $h \doteq 6,626 \times 10^{-34} \text{ J} \cdot \text{s}$

be neglected except for the ground state, or several surrounding excited states. All atoms and molecules in a paramagnetic state or can be put into it, for example by irradiation, can be studied with EPR. A paramagnetic state is a condition, which has a non-zero-sum of all angular momenta of the electrons (usually spin angular momenta). The following systems meet these conditions:

1. Free Radicals in the solid, liquid or gaseous phases. A free radical can be atom, molecule or ion containing one unpaired electron.
2. Transition metal ions including actinide ions (shown in Figure 2.3). These can contain up to seven unpaired electrons.
3. Point defects (localized imperfections, trapped electrons, electron vacancies).
4. Systems with more than one unpaired electron in general. These include
  - (a) Triplet – state system – strong interaction between two unpaired electrons,
  - (b) Biradicals – a system with weak interaction between two unpaired electrons,
  - (c) Multiradicals – a system with more than two unpaired electrons interaction.
5. Systems with conducting electrons (semiconductors and metals).

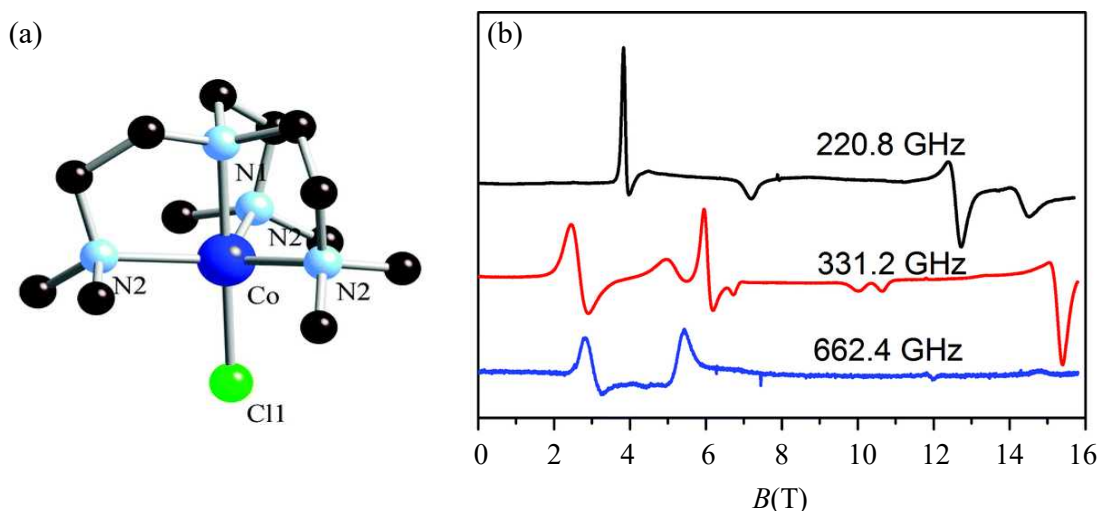


**Figure 2.3:** Example of molecular complex with a central transition metal ion - cobalt, (a) illustration of the molecular structure of the  $[\text{Co}(\text{Me}_6\text{tren})\text{Cl}]^+$  (b) EPR spectrum in 220.8 GHz, 331.2 GHz and 662.4 GHz. Taken and adapted from [22].

## 2.3. Principles of EPR

Particle such as electron, free or bonded to the nucleus of the atom, has an intrinsic angular momentum called electron spin  $\mathbf{S}$  and electron magnetic dipole momentum  $\boldsymbol{\mu}_s$  proportional to the  $\mathbf{S}$ . Spin is usually showed as a particle spinning around its own axis. The resulting electron magnetic dipole momentum is given by

$$\boldsymbol{\mu}_s = -\frac{g_e}{2m_e}\mathbf{S}, \quad (2.1)$$

where  $m_e$  is the electron mass<sup>2</sup> and  $g_e$  is the electronic  $g$ -factor. Electrons also move in the space around the nucleus of the atom and generate a magnetic field. Electrons have a magnetic momentum (called orbital magnetic angular moment  $\boldsymbol{\mu}_L$ ) related with orbital angular momentum  $\mathbf{L}$ . The orbital magnetic angular moment is expressed

$$\boldsymbol{\mu}_L = -\frac{e}{2m}\mathbf{L} = -\mu_B\frac{\mathbf{L}}{\hbar}, \quad (2.2)$$

where  $\hbar = \frac{h}{2\pi}$  is a reduced Planck constant,  $e$  is electron charge<sup>3</sup> and  $\mu_B$  is the Bohr magneton, given by

$$g_B = \frac{e\hbar}{2m_e} \doteq 9.274 \times 10^{-24} \text{ J} \cdot \text{T}^{-1}. \quad (2.3)$$

The total angular momentum is then given by

$$\mathbf{J} = \mathbf{S} + \mathbf{L}. \quad (2.4)$$

It is important to note, that all moments in equation (2.4) are quantized

$$\mathbf{S} = \sqrt{s(s+1)}\hbar, \quad s = 0, \frac{1}{2}, 1, \dots; \quad (2.5)$$

$$\mathbf{L} = \sqrt{l(l+1)}\hbar, \quad l = 0, 1, 2, \dots, \quad (2.6)$$

$$\mathbf{J} = \sqrt{j(j+1)}\hbar, \quad j = 0, \frac{1}{2}, 1, \dots; \quad (2.7)$$

where  $s$  is the spin quantum number, for electron  $s = 1/2$ ,  $l$  is orbital quantum number and  $j$  is the angular-momentum quantum number. Projection of the spin quantum number to  $z$ -axis can have just two values

$$\mathbf{S}_z = m_s\hbar, \quad m_s = \pm\frac{1}{2}, \quad (2.8)$$

where  $m_s$  is spin magnetic quantum number (generally  $m_s = -s, -s+1, \dots, s$ ). In the presence of an external magnetic field oriented along the  $z$ -axis is the projection of the magnetic moment to the  $z$ -axis  $\mu_z$  for free electron given by

$$\mu_z = -g_e\mu_B m_s. \quad (2.9)$$

The energy of a magnetic dipole in a static magnetic field  $B_0 = (0,0,B_0)$  oriented along the  $z$ -axis is

$$E = -\boldsymbol{\mu}_z \cdot \mathbf{B}_0, \quad (2.10)$$

After substituting equation (2.9) into equation (2.10) we obtain the energy of a specific electronic spin state as

$$E_s = g_e\mu_B m_s B_0. \quad (2.11)$$

Nucleus have the same number of protons and neutrons and has its total spin zero. The same principle applies to it as to spin of electron. Generally, orbital magnetic quantum number have the values  $m_l = -l, -l+1, \dots, l$ .

<sup>2</sup>Electron mass in SI units:  $m_e \doteq 9,109 \times 10^{-31}$  kg

<sup>3</sup>Electron charge in SI units:  $e \doteq 1,602 \times 10^{-19}$  C

The interaction of the atom or molecule in a paramagnetic state with a constant magnetic field is given by the hamiltonian  $\mathcal{H}$

$$\mathcal{H} = \mathcal{H}_{\text{elect}} + \mathcal{H}_{\text{ef}} + \mathcal{H}_{\text{LS}} + \mathcal{H}_{\text{SS}} + \mathcal{H}_{\text{Ze}} + \mathcal{H}_{\text{HFS}} + \mathcal{H}_{\text{Q}} + \mathcal{H}_{\text{N}}, \quad (2.12)$$

where the various terms have the following typical forms and magnitudes [23]:

$\mathcal{H}_{\text{elect}}$	electronic energy (optics)	$10^4 - 10^5$	$\text{cm}^{-1}$
$\mathcal{H}_{\text{ef}}$	crystal field energy	$10^4 - 10^5$	$\text{cm}^{-1}$
$\mathcal{H}_{\text{LS}}$	spin-orbit interaction	$10^2$	$\text{cm}^{-1}$
$\mathcal{H}_{\text{SS}}$	spin-spin interaction	$0 - 10^1$	$\text{cm}^{-1}$
$\mathcal{H}_{\text{Ze}}$	Zeeman energy	$0 - 10^1$	$\text{cm}^{-1}$
$\mathcal{H}_{\text{HFS}}$	hyperfine structure	$0 - 10^2$	$\text{cm}^{-1}$
$\mathcal{H}_{\text{Q}}$	quadrupole energy	$0 - 10^{-2}$	$\text{cm}^{-1}$
$\mathcal{H}_{\text{N}}$	nuclear spin energy	$0 - 10^{-3}$	$\text{cm}^{-1}$

The greatest influence on a given signal obtained from EPR measurements is given by term of the Zeeman energy, which will be described in the following section.

### 2.3.1. Zeeman effect

The energy levels of one unpaired electron have the same energy without the presence of a magnetic field. Under the influence of an external magnetic field, one energy level has then different energy. For this reason, the energy levels are split into two lines, and the phenomenon is called the Zeeman effect is shown in Figure 2.4. This phenomenon can be observed in the transition of electrons from the individual energy levels in the atoms. When electrons are excited to higher energy levels, these electrons can spontaneously relax to the lower levels, emitting electromagnetic radiation (in the form of photons) with a characteristic wavelength. In a simple example of free electron, the spin is equal to  $1/2$ . It means that if no external magnetic field is applied, both energy states of electron magnetic spin  $m_s = \pm 1/2$  are degenerate. After applying a magnetic field, the energy of these two-electron states can be by described by writing the equation (2.11) into the form

$$E_s = \pm \frac{1}{2} g_e \mu_B B_0. \quad (2.13)$$

The energy difference between the two spin states is

$$\Delta E_s = E_+ - E_- = g_e \mu_B B_0. \quad (2.14)$$

When the system is irradiated by electromagnetic radiation at a suitable frequency, it is absorbed when the energy difference value of the electron energy is exactly the same as the energy absorbed by the photons. This gives us the fundamental equation of paramagnetic resonance, the resonance condition:

$$\Delta E_s = g_e \mu_B B_0 = h\nu, \quad (2.15)$$

where  $\nu$  is the frequency of the photon. To achieve this resonance condition, there are 2 options. First, the frequency of the electromagnetic radiation is constant and the magnetic field is continuously changed, or the frequency of the electromagnetic radiation is gradually changed in the static magnetic field. In most cases, the first option is used. In simple

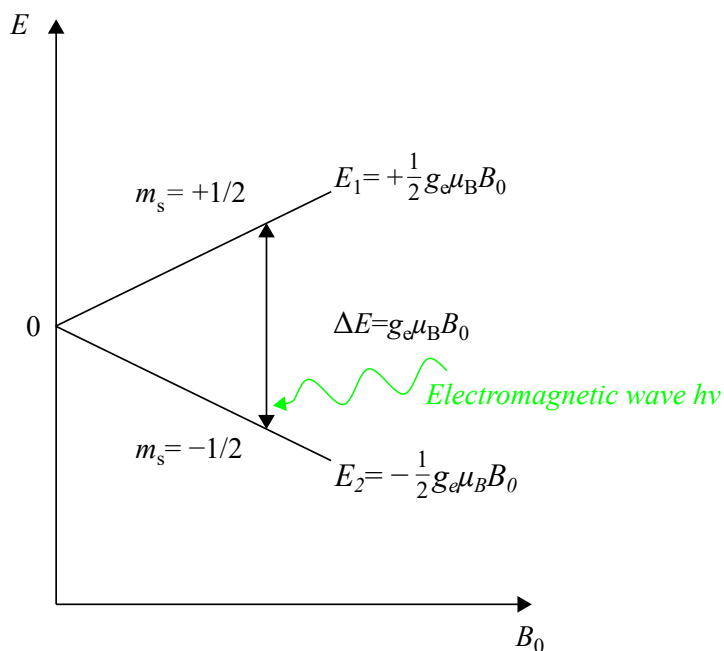


**Figure 2.4:** Scheme of energy-level diagram for free electron with a spin  $s = \pm 1/2$  as a function of applied magnetic field  $B_0$ .  $E_1$  and  $E_2$  are energies corresponding to  $m_s = \pm 1/2$  states.

systems with just one unpaired electron, the resonance occurs at value of magnetic field  $B = 0.34$  T and frequency  $\nu = 9.5$  GHz.

Resonance condition in equation (2.15) also gives an interesting factor that contains information about the substance. The elements appearing in the equation are either constants or can be changed by the influence of external effects, except one—the electronic  $g$ -factor. The  $g$ -factor was derived for free electron or hydrogen atom with one electron, but substances do not always have only one electron. Generally the  $g$ -factor is given

$$g = \frac{h\nu}{\mu_B B} \quad (2.16)$$

and depends on the orientation of the substance in the external magnetic field. Its value is not only a number, but a tensor of the second order represented by nine values arranged in a 3x3 matrix. By selecting a suitable coordinate system (eg. Cartesian), the matrix can in most cases be converted to a diagonal form, reducing the number of members from nine to three, specifically  $g_{xx} = g_x$ ,  $g_{yy} = g_y$ ,  $g_{zz} = g_z$ .

## 2.4. Applications of EPR

Electron paramagnetic resonance includes a wide range of applications in various scientific fields, but also in industry. Several exciting applications of EPR spectroscopy as a diversification of the theoretical part are indicated in this section.

EPR is mostly used in chemistry, where it can help to understand many areas of research. For instance, photocatalytic oxidation of organic pollutants is frequently carried out using semiconducting polycrystalline powders, such as  $\text{TiO}_2$ . A hydroxyl radical is easily formed by light irradiation of  $\text{TiO}_2$  and detected by EPR using spin traps. In electrochemistry to identify and investigate free radicals thrived from both organic and

inorganic compounds. Inorganic dyes can be used to improve the efficiency of solar cells. To optimize the ligands, one must understand the electronic structure of the dye [24]. EPR has proven itself as a useful tool in homogeneous catalysis research for the characterization of paramagnetic complexes and reactive intermediates. EPR spectroscopy is a particularly useful tool to investigate their electronic structures, which is fundamental to understand their reactivity [25].

Medical biological and life science applications also exist in EPR. Although radicals are very reactive and do not typically occur in high concentrations in biology, special reagents have been developed to spin-label molecules of interest. These reagents are particularly useful in biological systems. Specially-designed nonreactive radical molecules can attach to specific sites in a biological cell, and EPR spectra can then give information on the environment of these so-called spin labels or spin probes. Spin-labeled fatty acids have been extensively used to study a dynamic organization of lipids in biological membranes, lipid-protein interactions [26, 27]. EPR provides information about the local environment of the spin-label that has unpaired electrons and can measure inter-spin label distances when two spin labels are introduced inside the protein. It is also used in conjunction with spin trapping to detect and identify high-molecular-weight species generated as a result of reactive oxygen species induced damage to biological macromolecules, such as DNAs and RNAs. The destruction or alteration of these materials is known to play a critical role in a large number of cellular injuries and diseases. In this field also enzyme reactions can be studied, as many enzyme reactions involve one-electron oxidation steps with a formation of paramagnetic transition states of the enzyme. The paramagnetic center, where the unpaired electron is located, is usually centered at a transition metal (metalloproteins) or is an amino acid derived radical. Detection and identification of the paramagnetic centers are essential to understand the function of the enzymes. For example, in the native superoxide dismutase [Cu-Zn] enzyme, the active site contains one Cu(II) ion that gives a characteristic EPR spectrum [28].

Radiation sterilized food have been examined with EPR spectroscopy, reaching the benefits of irradiation to consumer and the food industry. Radiation doses can affect fruit ripening or reduce or eliminate microorganisms. The packaging of food and its subsequent exposure to radiation is also taken into account. Various polymers (polyvinyl chloride, polyethylene, polypropylene, polystyrene, polyamides, and flexible laminates) used in food packaging and their effect on food after irradiation are also studied [29].

In material science, EPR spectroscopy is used, for example, for studying polymer degradation due to light exposure, it leads to decoloration of the polymer and a decrease in the mechanical properties. This spectroscopy is also used for studying polymer structures like polyelectrolyte multilayer films. Multilayers of polyelectrolytes (polymers having dissociated ionic groups) are formed by the alternating adsorption of oppositely charged polyelectrolytes, so-called layer-by-layer technique. EPR studies polyelectrolyte multilayer films composed of a strong polycation and weak polyanion that is usually spin-labeled with free nitroxide (4-amino-2,2,6,6-tetramethylpiperidino-1-oxyl). The growth of the polyelectrolyte multilayer films is monitored, and quantitative EPR analysis provides information about each double layer. Another exciting field is the properties of paint. It can be studied, for example, a signal in paint indicating deterioration after UV exposure [30].

EPR in physics is used for studying transition metals, inner-transition ions, which are members of the 3d, 4d, 5d, 4f, and 5f groups. One aspect that makes transition elements exciting subjects for study by EPR is their variable valence. In the field of quantum

computing, pulsed EPR is used to control the state of electron spin qubits in materials such as diamond, silicon, and gallium arsenide, which will also be mentioned in the next chapter [31].

EPR is also widely used in the industry. It plays an important role in the characterization of solar cells and silicon in them. Specific characterization of paramagnetic defects can be done by EPR to gain insight into how paramagnetic centers induced by degradation influence the efficiency of solar cell active layers. It's also used for another example, especially for quantifying nitrogen centers and hence provide a tool for color grading. It can also be used to distinguish between synthetic and natural diamonds. Czech citizens much appreciate the use of EPR to improve beer brewing procedures. Hops used in the brewing process contain a mixture of active components that include humulones, cohumulones, adhumulones, beta acids, and essential oils. Some forms of these components are photo-active. Light exposure of beer leads to the formation of free radicals that combines with sulfur compounds and gives unpleasant flavor and odor to the beer [32].

EPR also has been used by archaeologists for the dating of teeth. Radiation damage over a long time creates free radicals in tooth enamel, which can then be examined by EPR and, after proper calibration, dated. Alternatively, a material extracted from the teeth of people during dental procedures can be used to quantify their cumulative exposure to ionizing radiation. People exposed to radiation from the Chernobyl disaster have been examined by this method [33, 34].

EPR can also be used to measure microviscosity and micropolarity within drug delivery systems, detection of microacidity, and characterization of colloidal drug carriers. It is also possible to perform pH measurements. It is possible to study unique information on drug release mechanisms and kinetics[8][35].

## 2.5. HF-EPR spectrometer

In 2018, MOTeS group led by Petr Neugebauer was established at CEITEC Nano with a focus on the development of a newly-built heterodyne HF-EPR spectrometer with applications, especially in material and biological science. It is a possibility to perform experiments on a variety of samples ranging from biomolecules over coordinated metal centers to magnetic and solid-state materials, in a very broad spectral range from 80 to 1 100 GHz, at cryogenic temperatures (1.8 K – 300 K) and very high magnetic fields (16 T).

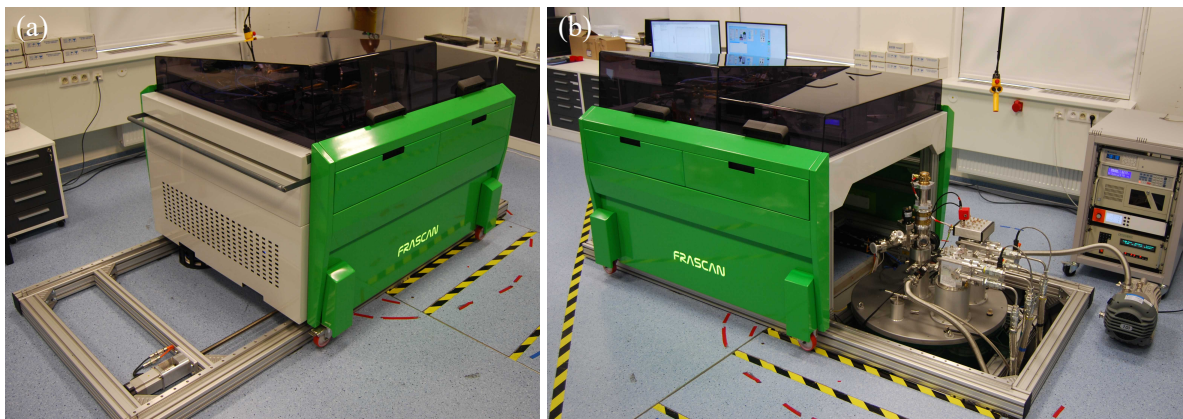


**Figure 2.5:** A newly-built HF-EPR spectrometer in CEITEC Nano MOTeS laboratory. (a) In the measurement position. (b) In the waveguide loading position.

The heterodyne specification of the spectrometer (briefly described in Figure 2.6) is an arrangement of two types of signals, one passing through the sample and the second one, the reference, which has frequency usually about 0.1 GHz higher than the first signal. It goes through the quasi-optics and has the same optical path as the first one. It is used for subsequent mixing, filtering out unwanted signals, and achieving better resolution.

A new HF-EPR spectrometer is shown in Figure 2.5. The key components of the HF-EPR system are briefly described below.

### Microwave source

Most of the millimeter and submillimeter microwave sources for EPR can be divided into two groups: vacuum-tube oscillators and solid-state oscillators. Vacuum-tube oscillators are used as a coherent mm-wave source, but nowadays, they are being replaced by solid-state oscillators, which are smaller, easier to operate, and reach excellent performance. Noise performance, output power, tuning bandwidth, durability, and of course, the price are part of the selection criteria for suitable microwave solid-state source. Moreover, the solid-state sources do not require high control voltage, additional cooling and are generally less sensitive to stray fields from the cryomagnet. They deliver, however, only low output power compared to vacuum-tube devices. EPR solid-state sources generally employ negative-resistance devices based on Gunn diodes (GaAs, InP). Gunn diodes are sources used in the frequency range up to 150 GHz. For frequencies above 50 GHz, it is necessary to employ one or more stages of frequency multiplication. These multipliers can be doubled, even tripled of the frequency, but the efficiency drops rapidly. Typically, the power of 200 mW at 90 GHz is available prior to multiplication. Output power of 20 mW can be obtained after doubling to 180 GHz and 5 mW at 280 mW after tripling. [36] Nowadays, the solid-state sources are slowly replaced by microwave synthesizer with subsequent amplification and multiplication. It is also the case of a new HF-EPR spectrometer in CEITEC Nano, where signal generator extension from Virginia Diodes Inc. is used. This source provides high-performance frequency extension of microwave signal generators into THz range. The desired microwave frequency can be obtained by multiplication of the base frequency from 8 GHz to 12 GHz generated by the microwave synthesizer. The highest available frequency of the spectrometer is 1 100 GHz.

### Quasi-optics and waveguides

To propagate the microwave, in the HF-EPR, a low loss free-space quasi-optical table from company Thomas Keating Ltd. The microwave in the form of the Gaussian beam is propagated from feedhorns. It is then focused by elliptical mirrors placed within certain distances. The microwave also goes through several filters and polarizers that can filter undesirable polarisation components of the beam. For small losses and excellent conduction of the microwave beam, the solution is to use quasi-optical elements - mostly off-axis mirrors. Metallic mirrors are also used to reflect and extend a propagation length. The microwave is subsequently reflected in the waveguide through a teflon window to separate the waveguide and space outside the magnet. The waveguide is a hollow metal tube. Sometimes waveguides have grooves inside to propagate radiation and reduce losses, which is also the case of this waveguide. At the end of the waveguide, there are various types of sample holders with samples. The reflective mirror is, in most cases, placed under the sample to reflect incoming radiation.

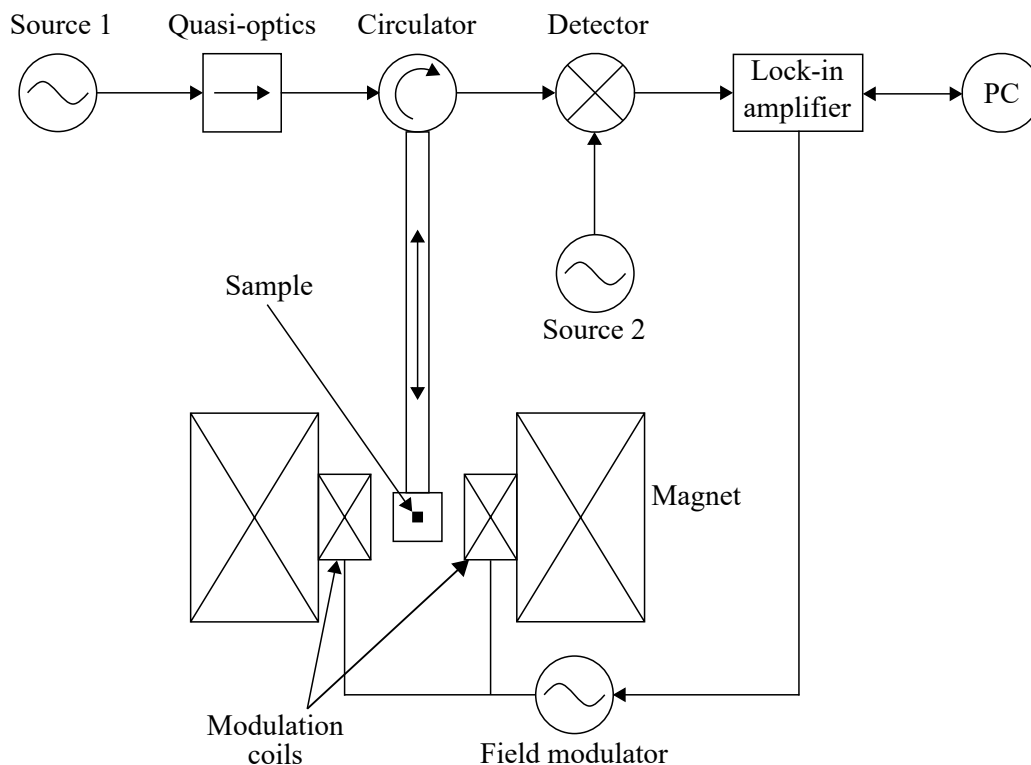


**Figure 2.6:** A schematic of a typical HF-EPR spectrometer with a heterodyne detection system.

### Superconducting magnet with Cryostat

By moving to high magnetic fields, better spectral resolution and new phenomena can be studied. The spectral resolution is described in Figure 2.7, where two systems of different  $g$ -factor are shown. In low fields, the two signals are indistinguishable, but with an increasing magnetic field, the signals become more distinguishable. Thanks to these necessities, normal electromagnet (which is usually used in EPR with typical strength of 1 T) cannot be used. For HF-EPR, the magnetic field of several tesla is needed. Therefore Superconducting magnet, usually up to 16 T, is used.

Furthermore, low temperatures must be used for better resolution. As the system temperature decreases, the probability of occurrence of particles in the atom or molecule in the ground state increases. The lower temperature of the entire system (sample), the higher is the absorption of the sample. Also, to achieve a better spectral resolution, one of the possibilities is to increase the microwave frequencies. In the case of the HF-EPR spectrometer at CEITEC Nano, the cryogen-free measurement system from a company Cryogenic Ltd is used. The base system is made up of a cryogen-free superconducting magnet with the Variable Temperature Insert (VTI), where the waveguide with samples is inserted. This magnet is based on a helium closed circuit. The principle is similar to the freezer. The VTI enables to control the inner temperature in the range from 1.8 K to 300 K.

### Detection

Microwave detectors are usually divided into the two types: bolometers and diode detectors. Bolometers are usually used for broad frequency range detection. Their advantage is exceptionally low noise, but they need to be cooled down to cryogenic temperatures,

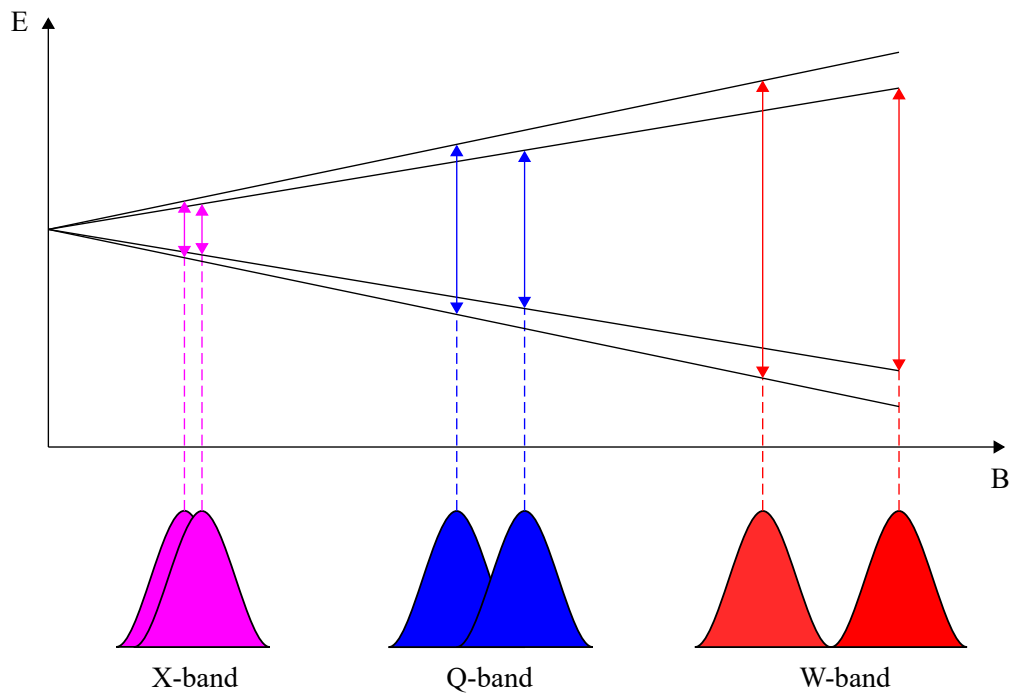


**Figure 2.7:** A simplified energy level diagram 2 species of different  $g$ -values. In the X-band frequency range, they are close to each other and are almost indistinguishable. After applying a higher magnetic field, the situation in the Q-band region is better, and the individual spectra can be distinguished. In the W-band frequency range are spectra fully distinguishable.

and their detection is relatively slow. For this reason, they are used mostly for single frequency detection. The second type of detectors are diode detectors, especially Schottky barrier type. Diode detectors have a narrow band of the frequency range. It means that the detection of frequencies is limited by the choice of the diode. Each diode should be specially designed for a given frequency range. They have a fast response to the received signal. In the case of the HF-EPR spectrometer in CEITEC MOTeS laboratory, diodes are used as mixers, which mix incoming signals with the reference signal at which is the frequency usually a little bit higher. After applying a low pass filter, other frequencies are filtered, only low frequencies remain, and these can be processed as a final signal. The modulation of the signal is used via modulation coils to increase the signal to noise ratio.

## 3. Molecular nanomagnets

This chapter provides information about molecular nanomagnets (MNMs) and their possible use in the future. It should be mentioned that the author's primary goal of this thesis is to design a mobile vacuum transfer system for loading samples into high-frequency electron paramagnetic resonance spectrometer, at which the given experiments will be performed later, and other successors and users will examine the samples. Interest in measurement and characterization of samples is just an added value for this work. Therefore this chapter will not be analyzed in full detail and will provide a brief overview of molecular magnets and several applications. The content of this chapter was partially taken from the book: Molecular nanomagnets [37].

### 3.1. Properties

MNMs are coordination compounds that exhibit properties similar to classical magnets. They can be defined as molecules containing central metal atoms connected by organic ligands. Their biggest advantages are a low density, mechanical elasticity and strength, the possibility of modification by chemical means, compatibility with polymers, and bio-

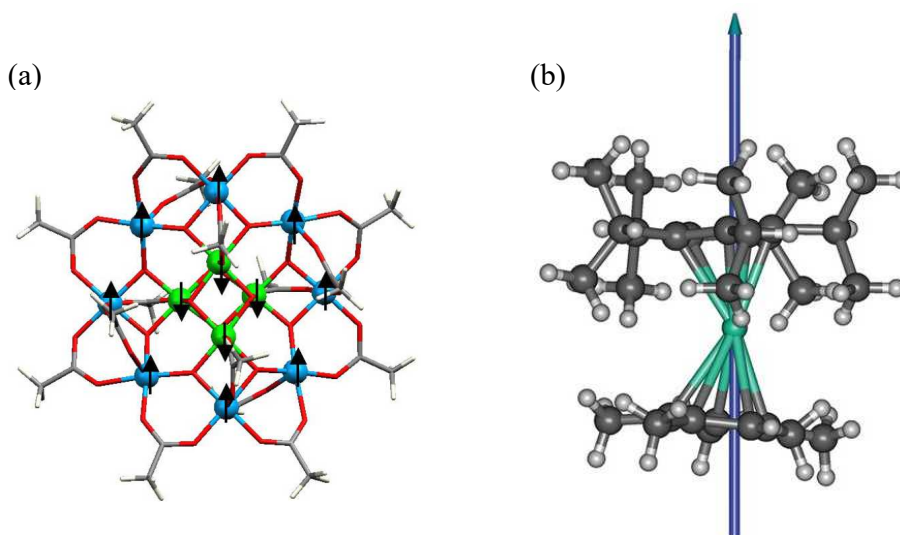


**Figure 3.1:** (a) View of the first studied molecular material  $\text{Mn}_{12}\text{O}_{12}(\text{CH}_3\text{COO})_{16}(\text{H}_2\text{O})_4$ . The four inner  $\text{Mn}^{3+}$  ions (green color) and their magnetization is pointing down. Eight outer  $\text{Mn}^{4+}$  ions (blue color) each have spins of  $S=2$  and are pointing up. The spins coupled together give the resulting spin  $s=10$  pointing up in the direction of  $\text{Mn}^{4+}$  [38]. (b) A breakthrough of the first high-temperature (77 K) SMM with  $\text{Dy}^{3+}$  as a central atom published in 2018 [39].

compatibility. According to the dimensions of the structure of MNMs, they are divided into single-molecule magnets (SMMs), single-ion magnets (SIMs), single-chain magnets (SCMs), planes and planar layers or networks of nanomagnets. SMMs were at the beginning of the formation of molecular magnets and were gradually expanding to larger scales. Nanometer materials exhibit slow relaxation of magnetization (return into equilibrium) at lower temperatures and interesting quantum effects, which can be used in applications involving high-density data recording. In this area, new molecular magnets are being rapidly developed and prepared (the first molecular magnet  $\text{Mn}_{12}\text{O}_{12}(\text{CH}_3\text{COO})_{16}(\text{H}_2\text{O})_4$  (abbreviated:  $\text{Mn}_{12}\text{Ac}$ ), shown in Figure 3.1 (a), with slow relaxation of the magnetization was first studied in 1993 [40, 41]). The need for smaller components in devices and the application of quantum mechanics is becoming more relevant. Investigation of these systems was enabled by techniques such as Atomic Force Microscopy (AFM), Scanning Tunneling Microscopy (STM), and Scanning Electron Microscopy (SEM). The application of MNMs is related to the number of spins on the surface and the ability to influence them. Figure 3.2 shows a comparison of microscopic and macroscopic scales with different numbers of spins.

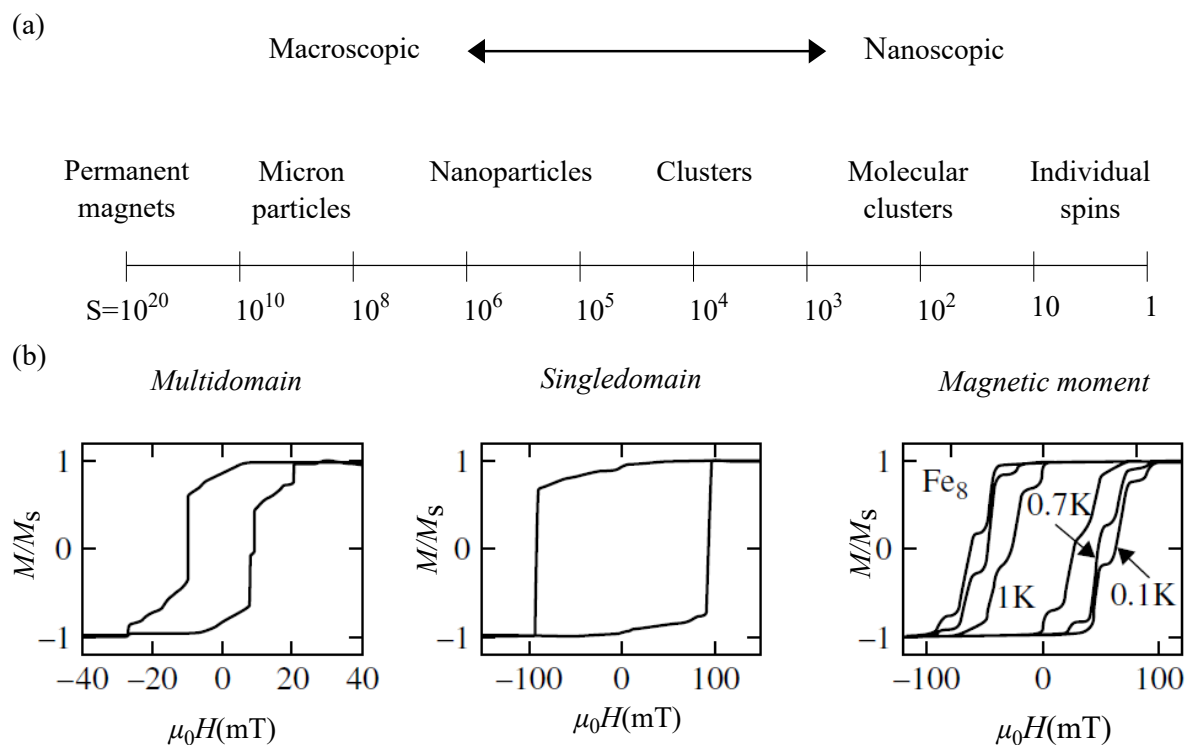


**Figure 3.2:** (a) overview ranging from macroscopic to microscopic scale of magnets, (b) various hysteresis dependencies of magnetization  $M$  and intensity of the magnetic field  $H$  are shown, from the multidomain through the single domain to the individual magnetic moments. Adapted from [37].

On a macroscopic scale, particles are concentrated in a large volume with a large number of spins that are interconnected and react collectively to external influences. By forming spins into magnetic domains, energy is minimized. The orientation of the magnetic moments in the magnetic domains is random if there is no external magnetic field, and the resulting magnetization is zero. When a magnetic field is applied, and the sample is magnetized, all magnetic moments will be parallel to each other, and the magnetization will reach saturation value. If the field effect decreases, the formation of magnetic domains

will not be reversible in such a way that the magnetization at zero magnetic field will not be zero, like in the non-magnetized case. The finite value of the magnetization at zero field is called the remanent magnetization. For sample demagnetization, it is necessary to go to a negative magnetic field, the value when the magnetization at zero is called the coercive field. This value is used to classify the bulk magnets. The small value is typical for soft magnets, while for hard magnets, the coercive field is large. The M/H plot in Figure 3.2(b) shows hysteresis loops, which tell us how the value of the magnetization of the sample depends on its history. It is the basis of the use of magnets for storing information.

The SMM also exhibits a superparamagnetic behavior below a certain blocking temperature. The smallest in size MNMs can act as a nanomagnet. The preparation route is utilizing synthetic chemistry. In most cases, the structure of SMM is a metallic center like transition metal, lanthanide, or actinide, which are surrounded by various organic ligands.

Magnetic interactions in molecular systems are, in principle, the same as can be observed in continuous lattices. These magnetic interactions can be described by the spin Hamiltonian. It usually consists of two main parts: The Zeeman term and ZF terms, which describe the internal magnetic behavior of the system in the absence of an applied magnetic field.

The Zeeman Hamiltonian can be written as

$$\mathcal{H}_Z = -\mathbf{H} \cdot \mathbf{m} = \mu_B \mathbf{H} \cdot \mathbf{g} \cdot \mathbf{S}, \quad (3.1)$$

where  $\mathbf{H}$  is applied magnetic field,  $\mathbf{g}$  is a tensor linking the magnetic field and the spin vectors, and  $\mathbf{S}$  is a spin operator. The magnetic moment  $\mathbf{m}$  is given by

$$\mathbf{m} = -\mu_B \mathbf{g} \cdot \mathbf{S}. \quad (3.2)$$

The zero-field splitting Hamiltonian can be generally described by the Stevens operators [42] as

$$\mathcal{H}_{ZFS} = \sum_{k=2,4,6..} \sum_{q=-k}^k B_k^q O_k^q, \quad (3.3)$$

where the coefficients  $B_k^q$  are real and operators  $O_k^q$  are Hermitian. In systems with total spin  $\leq 2$ , terms up to second order are usually sufficient to describe system; namely, the uniaxial anisotropy term  $DS_z^2$  and the transverse anisotropy term  $E(S_x^2 - S_y^2)$ . Then the full spin Hamiltonian can thus be written as

$$\mathcal{H} = \mathcal{H}_Z + \mathcal{H}_{ZFS} = \mu_B \mathbf{H} \cdot \mathbf{g} \cdot \mathbf{S} + DS_z^2 + E(S_x^2 - S_y^2) + \text{higher order anisotropy terms}. \quad (3.4)$$

The first part on the right side of the equation (3.4) represents the Zeeman energy contribution from the interaction of the spin of the molecule with an external magnetic field. The second term represents the uniaxial anisotropy resulting from the spin-orbit interaction defines an "easy axis" from the magnetic moment of the molecule, and establishes an energy barrier  $DS_z^2$  separating opposite spin projections. The remaining terms correspond to transverse anisotropies ( $S_x^2, S_y^2$ ) and inter- or intra-molecular interactions such as dipolar, exchange, or hyperfine interactions [43].

## 3.2. Applications and challenges

There are many potential uses of SMMs, or generally MNMs. Thanks to the typically large anisotropy, SMMs are promising for using as the smallest unit for magnetic memory. It means that one molecule can be seen as one bit that the combination of a large spin of the molecules with an easy-axis magnetic anisotropy results in an energy barrier that hampers the reversal of the magnetization. However, the barrier can be cross-cut by a tunneling mechanism for some particular magnetic field values. These data storages composed of individual molecules use spin flips for a binary system and provides a considerable data density up to 300 times larger than nowadays commercial hard disk drive (HDD) [44] and 100 times larger than nowadays still expanding and newer solid-state drive (SSD) [45]. HDD consists of atoms, which communicate with their neighbors and create magnetic domains.

On the other hand, SMMs do not require these interactions to retain their magnetic memory because their memory effect arises from quantum mechanics. Atoms and molecules are much smaller than the magnetic domains. They can be used individually rather than in groups. It causes their size to be small compared to magnetic domains, and therefore they can be much closer to each other, and thus, the data density increases enormously [46].

The advantage of quantum computers arises from the way they encode a bit, fundamental unit of information. The state of a bit in a classical digital computer is specified by one number, 0 or 1. An  $n$ -bit binary word in a typical computer is accordingly described by a string of  $n$  zeros and ones. A quantum bit, called a qubit, might be represented by an atom in one of two states, which can also be denoted as 0 or 1. Two qubits, similar to two classical bits, can have attained for different well-defined states (0 and 0, 0 and 1, 1 and 0, 1 and 1). Nevertheless, unlike classical bits, qubits can exist simultaneously as 0 and 1, with the probability for each state given by a numerical coefficient. In general,  $n$  qubits demand  $2^n$  numbers, which rapidly becomes a sizable set for larger values of  $n$ . A quantum computer promises to be immensely powerful because it can be in multiple states at once a phenomenon called superposition and because it can act on all its possible states simultaneously. Instead of focusing on spin transport, attention is paid to the handling of electron spins and their implementation as qubits, which are fundamental units for the quantum computer mentioned above. However, the function of qubits is still not fully understood. There is a need for an even better understanding and especially control of the magnetic properties of SMMs.

Molecular spintronics is another field of study that aims to use electron spins for electronics applications with potential advantages of non-volatility, increased data processing speed, decreased electric power consumption, and high integration density compared to conventional semiconductor devices [47]. On the other hand, the disadvantage of some SMMs is their instability in the atmosphere. Usually, synthesis of some types of SMMs is time consuming, and they must be prepared and kept under the inert conditions (argon, nitrogen, or UHV conditions). Such molecules are decomposed in contact with oxygen or air moisture. It can lead to decomposition or oxidation number change and, thereby, change the molecule properties. Unstable SMMs can be generally divided into two groups, SMMs with the sensitive ligands (e.g., cyclopentadienyl [39]) and SMMs with the central atom in unstable (such as Co(II)) or non-typical oxidation numbers [such as Fe(I)] [48]. SMMs with non-typical oxidation numbers, especially with Fe(I), are SMMs, which also exists without an external magnetic field, and they have a rare oxidation state. SMMs

with the central atom in unstable oxidation numbers as a mentioned molecule in Figure 3.1(b). Research of SMMs with promising high blocking temperature, like SMM with central atom  $\text{Dy}^{3+}$ , is crucial to discover these molecules with the best performing properties for use in a promising application. However, they are expensive to manufacture, very time consuming, and from that it means, they have to be prepared, transported, and measured in inert conditions. Therefore, the sample transfer system, including the UHV suitcase, is developed to carry these molecules between systems with inert conditions, and it will be useful for measuring properties of SMMs.

### 3.3. MNMs on the surface

The behavior of MNMs at the nanoscale and their transport to the solid surface is of particular interest. The production of nanostructured SMMs thin films and their transport to the solid-state surfaces can be done in various ways, such as via wet-chemistry protocol from a solution or by physical deposition and sublimation of SMMs from the solid phase by using effusion evaporator [49]. For transporting and attaching SMMs to the surfaces are also used methods such as Langmuir-Blodgett film method, the self-assembled monolayer (SAM) method [50] and electrospray deposition [51]. Molecule-based nanomagnets can be directly attached and assembled on the surface by magnetically coupling several arranged metal centers using organic ligands. The adsorption on the surface can modify the chemical and electronic state of both components. Notably, the magnetic moments of the metal centers can be reduced or even quenched due to screening by surface electrons. Chemisorbed organic ligands may also undergo appreciable electron transfer and associated bond ordering [52]. However, there are already articles in which the properties of MNMs did not change after deposition to the surface [53]. The most commonly used substrates for the studies of MNMs are electrically conductive crystals. The use of conductive substrates allows the inclusion of STM to investigate the structure at an atomic scale. Besides, the local electronic properties are similar to the magnetic properties of molecules within the supramolecular structure examined by STM methods [54].

Due to the correct arrangement of molecules on the surface, it is necessary to have it atomically clean. For this reason, the preparations are very limited by certain conditions. The preparation of clean surfaces in the solution is available, but preparation under the UHV conditions is much more common. Then the properties of the molecules on the surface of the substrate can be influenced mainly by the rate of deposition and the temperature of the substrate. The arrangement of the molecules is determined by molecule-molecule interactions and molecule-substrate interactions.

Graphene is a monolayer of carbon in the hexagonal crystal lattice. Since graphene is a zero bandgap semiconductor, its scope can be extended by implementing a bandgap through disturbances. Furthermore, graphene can be affected by doping, i.e., changing the density of the charge carriers and changing the bandgap. The quality of graphene depends crucially on the method of preparation and selected substrate. There are various interactions between graphene and the substrate. They affect its transport properties, and therefore the mobility of charge in graphene is a suitable measure of its quality. The aim is to prepare graphene on the substrate, which is very similar to the structure of graphene, and thus there is a small interaction between graphene and the substrate.

A well-known example is a low-interaction system of graphene on iridium monocrystal Ir(111). The interaction defines the orientation of the graphene to the substrate. It does not significantly modify the unique electronic structure of graphene on iridium, and

it is very similar to the structure of free-standing graphene or graphene on insulating substrates [54].

Thanks to the ability to control the electrical properties of graphene, it becomes a suitable substrate for the MNMs and their applications. Due to the low reactivity of graphene, it is possible to form structures with a dominant molecule-molecule interaction. Possibility to change the charge carriers in graphene by changing the external electric field makes graphene the suitable substrate for the growth and deposition of molecular layers [55]. For external tuning of the electrical properties of graphene, it has to be placed on the insulating substrate. Therefore, most studies focus on the growth of graphene on metallic substrates or insulating substrates such as SiC crystals.

## 4. Requirements and materials

The goal of this thesis is the design of the vacuum transfer system for loading samples into HF-EPR (Figure 2.5). In the following chapter, the material requirements for individually designed components will be discussed. This chapter is focused on a description of these requirements and outline their solutions. For UHV suitcase is the compatibility with many UHV systems crucial, mainly the UHV cluster at CEITEC Nano. Compatibility with HF-EPR must also be a condition. Furthermore, a simple connection of the UHV suitcase, transportability, and handling with the samples itself is also essential. The requirements for the palette holder are a little bit different. A specification for vacuum compatibility is required, but more attention is focused on the compatibility with the helium atmosphere. In HF-EPR, the palette holder will be inside the helium in the cryostat. It must withstand very low temperatures up to 1.8 K and be made of non-magnetic materials because it will be inside the magnetic field that reaches up to 16 T. Similar demands are placed on the sample palette with a sample. The additional requirements are compatibility with UHV conditions, where studied samples will be prepared and analyzed and reach higher temperatures because some types of samples will be annealed to remove surface contaminants and impurities to achieve a clean surface. This chapter will also describe requirements for multiple environments and materials, which can be used in these ambiances.

### UHV cluster

The Ultra High Vacuum Preparation and Analytical System, abbreviated UHV cluster, is a complex UHV system combining preparation and in-situ analysis with specific devices focused on studying especially thin films and surfaces. The scheme of the UHV cluster in CEITEC Nano is shown in Figure 4.1. To maintain high purity during the preparation and subsequent analysis of the samples is the whole complex maintained under very high vacuum conditions (listed under  $2 \cdot 10^{-10}$  mbar) [56]. The system includes eight separate devices for sample preparation and characterization, which are interconnected by a linear transfer system (transfer line), allowing sample transfer under UHV conditions and storing samples. Part of this system is also a loading chamber for inserting samples into the UHV cluster from the atmosphere, which is also connected to the transfer line. This load lock chamber will be used to connect a UHV suitcase and transfer various types of samples from the UHV cluster described above.

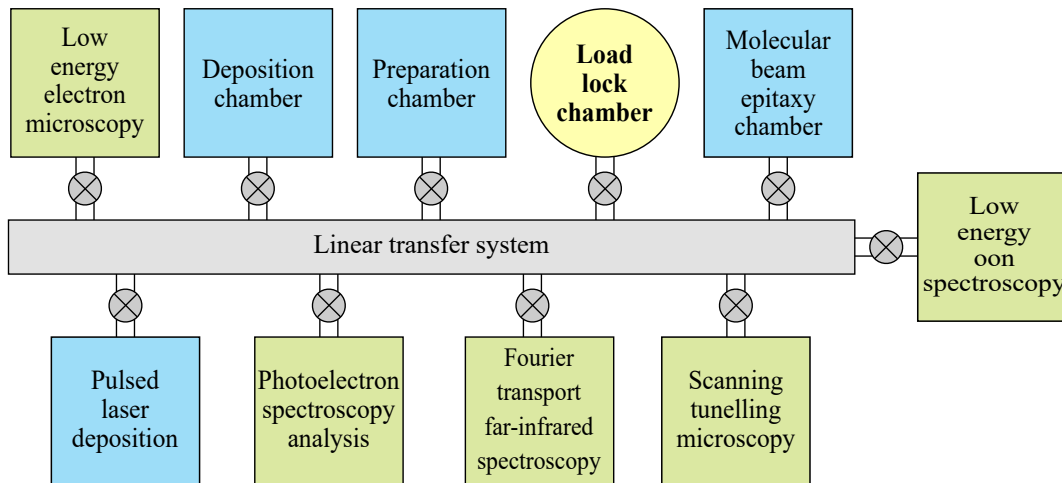


**Figure 4.1:** Schematic representation of the UHV cluster in the clean rooms in the institution CEITEC Nano.

## 4.1. UHV conditions

UHV environment brings some limitations, especially in terms of material used. A certain group of materials meet the appropriate conditions, and this group is further reduced with an increasing vacuum. It is from the low vacuum pressure (LV,  $10^0 - 10^{-5}$  mbar), through the high vacuum (HV,  $10^{-5} - 10^{-9}$  mbar) up to UHV ( $10^{-9} - 10^{-12}$  mbar). In addition, some materials require special machining procedures [57][58]. UHV conditions are essential to maintain an extremely high purity of the sample surface. Many surface applications and analysis require this level of vacuum. Atomically clean surfaces are essential for the preparation of surfaces and thin films and their study. Method for analysis such as XPS, low energy ion spectroscopy (LEIS), or low energy electron microscopy (LEEM) also requires UHV conditions for the transmission of electron or ion beams to avoid collision these particles with molecules and impurities flying in the chamber.

For materials used in vacuum systems, there are two main requirements [59]:

### 4.1.1. Leaks and Mechanical joints

One of the biggest problem to achieve the desired vacuum are leaks in the system. If the leaks are too large, the required pressure may not stabilize in the chamber. Furthermore, the system may be affected by small leaks. During measurement, transport, and storage, the sample may become contaminated and impaired. Leaks can be divided into external and internal, more often referred to as virtual leaks. External leaks are caused by the connection of individual parts of the chamber. It may be due to bad welds during welding of the individual chamber components or damaged flange blades and their subsequent leaks. In exceptional cases, a poorly designed connection of components may occur, which causes leakage through the seal. Virtual leaks are usually caused by an incorrect design of parts or their connection, mechanical machining, or wrongly selected material. These include virtual leaks that cause gas desorption from the cracks in the material, cavities of the pores material, or construction of the closed cavities, which could not be pumped very well and deterioration of the level of vacuum. The example of virtual leak and solutions to eliminate this problem is shown in Figure 4.2. It is also worth mentioning that the formation of unwanted microcracks during production should be avoided.

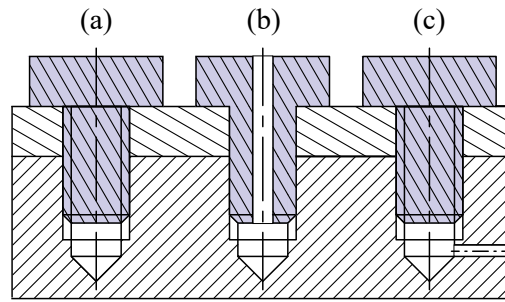
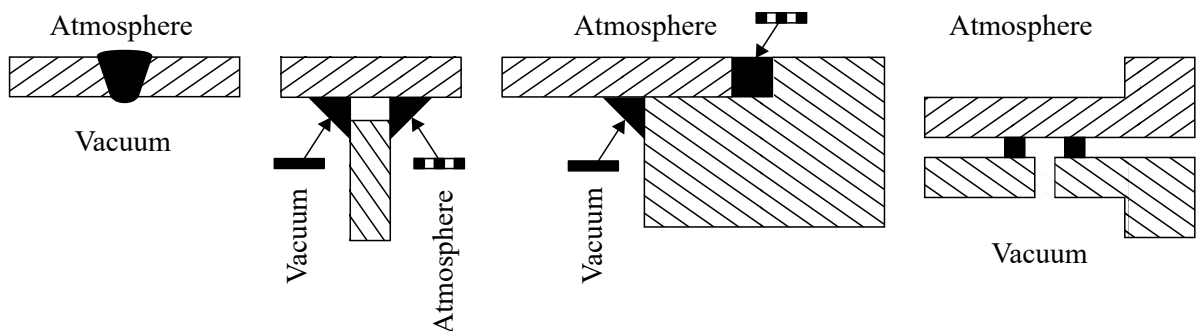


**Figure 4.2:** Schema of virtual leaks including: (a) the cavity under the screw, (b) the possibility to avoid the cavity by the screw with a hole, (c) by drilling the hole to the cavity from the side. Adapted from [60].

Virtual leaks can also be created due to unsuitable types of welding as well as soldering due to bad technological processes. Therefore, all of the parts used in the vacuum chamber has to meet strict criteria for reducing the gas desorption. It is necessary to follow the procedures of creating the right mechanical connections and avoid creating virtual leaks. Several types of correct and incorrect welds are shown in Figure 4.3.

In the design of vacuum chambers, it is necessary to pay attention to efficiently pump gas from the systems. All pipes leading to the vacuum pumps have to be as short as possible, as wide as possible, and without sharp edges and bends to reduce the pumping time of the entire system.

Acceptable welds:



Unacceptable welds:

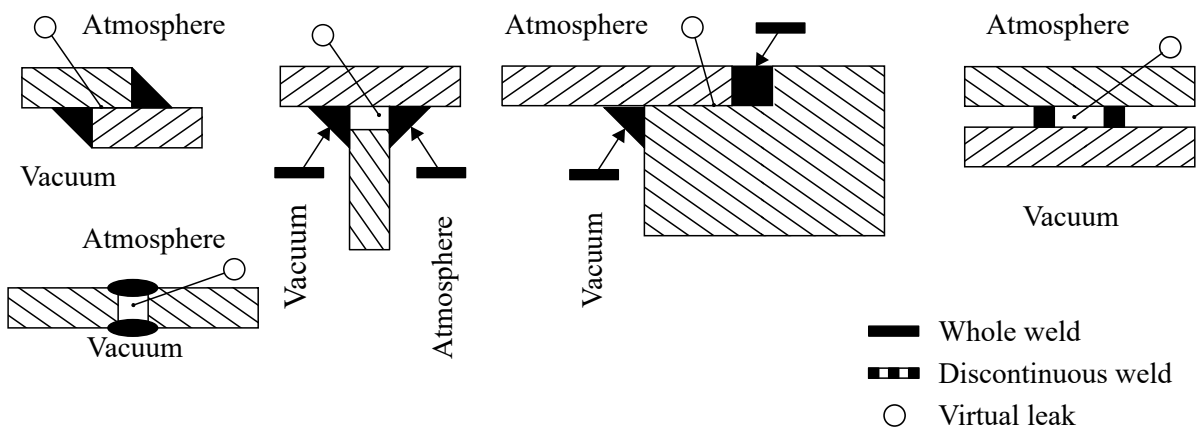


**Figure 4.3:** The cases of vacuum acceptable and unacceptable welds. Adapted from [60].

Permanent joints are usually made with electron welding and arc welding in a protective atmosphere [59]. For soldering is, in most cases, used hard solders as silver, gold, or copper alloys for a low gas throughput and excellent stability. Subsequent mechanical processing should take place after these thermal connection processes.

In the case of devices and systems used in different temperatures, it is necessary to be aware of different extensibility of materials. Fastening or shaped joins can be released by the influence of temperature changes and their different thermal expansion.

Mechanical connections of materials with various additives may also contaminate the vacuum system. For that reason, parts used in the UHV conditions must be adequately cleaned. These are mainly residues of oils and lubricants during machining because of their low saturated vapor pressure. Other impurities are paint, corrosion, or possible fingerprints. All machined parts are cleaned, preferably individually. The most common cleaning process is deionized water, followed by chemical cleaning and degassing in a vacuum furnace. Subsequently, all parts are assembled. Also, for all vacuum components, the surface quality is essential due to the adsorption and desorption of gases. Surfaces should be smooth and free of pores and cracks. To process and achieve the required quality, it uses sandblasting and mechanical or electrochemical polishing [61].

#### 4.1.2. Low desorption of gases from the materials and mechanical stability at elevated temperatures

The pressure in the chamber, assuming a perfect seal, can be expressed by the equation

$$p = \frac{QA}{S} \quad (4.1)$$

where  $S$  is pumping speed of vacuum system,  $A$  is total surface area in the chamber, and  $Q$  is a desorption coefficient in the chamber. The pressure depends on the spontaneous release of the particles inside the vacuum system. It may be the release from the chamber surface, eventually from the whole volume of things inside the vacuum chamber, such as sample holders. For this reason, material selection is crucial in the design of the vacuum-compatible devices. The main requirement is the low value of desorption. The materials should also be as clean as possible and with a minimum of gases bound within the material. Both requirements greatly affect the pumping of the vacuum chamber also mentioned above.

Vacuum chambers and devices in them can be heated over 200°C, even 300°C during baking. Baking is a procedure of removing water and other undesirable substances settled on the chamber's inner walls, which have adsorbed on the walls over time. Usually, parts of the chamber are wrapped with heated tapes, which are further wrapped in aluminium foil to keep the heat inside. There is also a cover with built-in heating inside, which is designed specifically for the device, where it is enclosed and heated. It also exists chambers, where smaller devices are enclosed and are heated. Materials used in vacuum chambers have to be resistant to this temperature to maintain their mechanical properties at the desired level. Desorption of used material or other parts must not overstep the required limit even at these high temperatures. The choice of vacuum materials should also be subject to any requirements for their electric and magnetic properties. For the components used in UHV, a variety of materials are used. These are mainly metals, glass, ceramic materials, or types of polymers. Materials should be easy to machine and strength stable at different temperatures. Furthermore, it must be considered for the given application, whether it

is necessary to use materials with low thermal conductivity (thermal insulators) or with high thermal conductivity (for cooling and heating systems).

The most widely used vacuum construction material is stainless steel with various alloying elements and classes. The advantages of stainless steel are their mechanical properties and stability. Some types of stainless steels are not suitable for UHV conditions due to additive elements such as selenium or sulfur. Stainless steel is used both for the production of vacuum systems themselves and as components inside chambers. The second most used material is aluminium and especially its alloys (dural). They are light, cheap, easy to machine, and they have low gas desorption. The disadvantages are worse durability to high temperatures, reduced strength, and increased gas desorption. Another common material is oxygen-free copper for its high electrical and thermal conductivity. Tungsten, tantalum, and molybdenum are suitable for heat-resistant elements such as source fibres due to very high melting points. Impressive material is invar for its properties, which is unfortunately magnetic or titanium, which is very expensive. Metals generally contain a large amount of gases, and for UHV conditions, they must be degassed by heating under the vacuum or special manufacturing operations [61].

The applicability of plastics is highly debatable due to their characteristic high gas desorption and porosity. Therefore, an effort is made to avoid the use of plastics in UHV or at least to minimize their use. Another significant disadvantage is their stability at higher temperatures.

Kapton is widely used for electrical insulation of conductors and components. Viton elastomer [62] can be used as a spring element or for the production of seals of vacuum systems with lower pressures [63]. Teflon is commonly used inside of vacuum systems since it is a self-lubricating and good electrical insulator [64]. It is relatively resistant to both low and higher temperatures and has a low out-gassing. It is not suitable for a barrier between vacuum and atmosphere, as it is somewhat permeable for gases. Polyether ether ketone (PEEK) is another polymer used in UHV. It offers a unique combination of mechanical properties, resistance to chemicals, wear, fatigue, and creep as well as exceptionally high and low-temperature resistance [65]. Despite the high price of the polymer, the added value that material PEEK brings the possibility to manufacturing and also includes lightweight, strength, or toughness and able to survive longer in harsh environments.

Ceramic materials are mainly used as electrical insulators. These materials are unique because they are almost non-gaseous and do not react with large amounts of chemicals. On the contrary, they are brittle and, therefore, difficult to machine and comparatively expensive. A representative of these materials is Macor, which is a material resistant up to 1000°C and is one of the few ceramic materials that are not hard to machine by conventional metal machining processes. It makes it easy to create a variety of more complex shapes while maintaining precise dimensions [66].

## 4.2. Materials in low temperatures

Low (cryogenic) temperature indicates the state where the temperature of the system reaches less than 150 K. For various applications reaching 77 K, nitrogen is usually used for cooling. Below 77 K, liquid helium is the most often cooling medium because of its boiling point 4.2 K, considering to nitrogen, which has a boiling point just 77 K [67].

## 4.2. MATERIALS IN LOW TEMPERATURES

**Table 4.1:** Thermal expansion of some materials from the room to low temperatures. Adapted from [67].

Material	$\Delta L/L$ (300-100) K	$\Delta L/L$ (100-4) K
Stainless Steel	$296 \cdot 10^{-5}$	$35 \cdot 10^{-5}$
Copper	$326 \cdot 10^{-5}$	$44 \cdot 10^{-5}$
Aluminium	$4156 \cdot 10^{-5}$	$47 \cdot 10^{-5}$
Brass	$340 \cdot 10^{-5}$	$57 \cdot 10^{-5}$
Epoxi	$279 \cdot 10^{-5}$	$47 \cdot 10^{-5}$
Titanium	$134 \cdot 10^{-5}$	$17 \cdot 10^{-5}$

The requirements such as thermal and mechanical stability, electric and thermal conductivity should be observed. Thermal stability links materials with different thermal expansion. The thermal expansion represents the change in size as a function of temper-

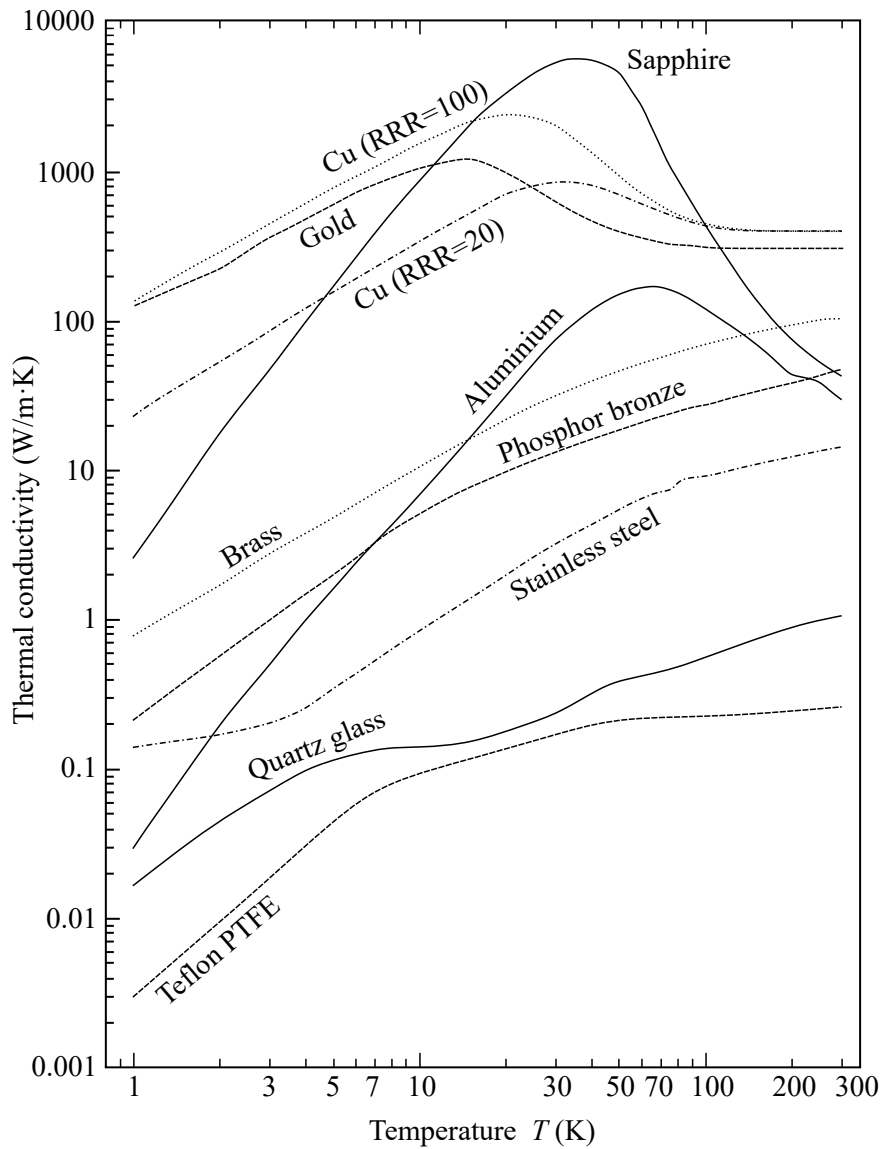


**Figure 4.4:** Thermal conductivity selected materials. Adapted from [68].

ature. The thermal expansion coefficient is assigned as a property of each material. The thermal expansion of selected materials is presented in Table 4.1.

Thermal stability is monitored, especially for materials with very different constants of thermal expansion. Changes in temperature can cause mechanical stress of the connection of the materials and lead to the failure of these materials' connection. Therefore, the difference between these coefficients of the two joined materials is required to be as low as possible.

The thermal conductivity of the material is essential in terms of heat transfer. It must be considered for all parts where the temperature in a specific area of the component changes. This is associated with heat transfer for a certain length of the component since there is no step-change in the temperature of the entire component, but a gradual cooling of the residue. It is also connected with thermal capacity, which is associated with thermal conductivity. It expresses the amount of energy needed for a heating known quantity of a system on the degree [69]. Therefore, for parts that require rapid heating or cooling, it is necessary to choose materials that experience instant heat transfer. The selection of the most used materials is shown in Figure 4.4. An essential property of the material is also embrittlement at low temperatures. In the cryostat inside the magnet, vibrations occur due to the strong magnetic field. Therefore, it is necessary to choose the specific type of material, which does not have a high rate of embrittlement in the low temperatures. It is related to cyclic fatigue of the material during repeated temperature changes. Again, the material may become brittle and subsequently destroyed.

### 4.3. Materials in magnetic field

All materials respond to an applied magnetic field in one way or another. The fundamental quantities in the magnetism are connected by equation

$$\mathbf{B} = \mu_0(\mathbf{M} + \mathbf{H}) \quad (4.2)$$

where  $\mathbf{B}$  is magnetic field,  $\mu_0$  magnetic permeability. Interconnection of the magnetic permeability with the tensor of magnetic susceptibility  $\hat{\chi}$  expresses the equation

$$\mathbf{B} = \mu_0(\hat{\chi} + 1) \cdot \mathbf{H}, \quad (4.3)$$

from which we get that susceptibility is a proportion between magnetization and the magnetic field in the material

$$\mathbf{M} = \hat{\chi}\mathbf{H}. \quad (4.4)$$

Magnetic susceptibility is a property of a material and affects the magnetic behavior of a given material. Each electron in the atom has the orbital dipole magnetic moment and the spin magnetic dipole moment. The resulting vector gives a magnetic nature of the electron and their composition, magnetic nature of the atom. The result obtained for one atom is composed of the results of all other atoms in the sample of the material. If the sum of all these magnetic dipole moments creates a macroscopic magnetic field, the substance is magnetic. There are three main types of magnetism: diamagnetism, paramagnetism, and ferromagnetism.

All materials and substances show diamagnetism. However, it is so weak that it is overlapped when the substance also exhibits paramagnetism or ferromagnetism. If any

#### 4.4. COMPATIBILITY WITH UHV, LOW TEMPERATURE, AND MAGNETIC FIELD

material is placed in the external magnetic field, weak magnetic dipole moments are induced in its atoms, and they are oriented against the external field. However, the resulting action of all induced dipoles is the source of only a weak magnetic field. Dipole moments and thus their weak field disappear if the outer field is removed. Diamagnetic materials have the magnetic susceptibility in range  $-1 < \chi < 0$ .

Paramagnetism show all substances whose atoms have a non-zero angular momentum (e.g., all atoms with an odd number of electrons) and in particular substances containing transition elements, rare earth elements, and actinides. Thus, each atom of such a substance has its magnetic dipole moment, even without external action. However, these moments are randomly oriented in the substance, so that the substance has no resulting magnetic field. The external magnetic field can partially arrange the atomic magnetic moments coincident with the external field, thereby creating a magnetic field in the substance. However, the resulting arrangement ceases when the outer field is removed. The term paramagnetic substance is commonly used for materials that exhibit paramagnetism, but not ferromagnetism. Paramagnetic materials have the magnetic susceptibility in range  $0 < \chi < 1$ .

Ferromagnetism is a property of e.g., iron, nickel, and a few other elements (and their compounds and alloys). Some electrons in these materials align with the resultant magnetic dipole moments and create regions (domains) with strong resultant magnetic dipole moments. The external magnetic field can then align the magnetic moments of these regions to create a strong magnetic field of the substance as a whole. This field is partially retained even when the outer field is removed. Ferromagnetic materials have the magnetic susceptibility  $\chi \gg 1$  [69].

### 4.4. Compatibility with UHV, low temperature, and magnetic field

There are specific conditions for materials used in individual environments. For use in multiple environments simultaneously, the requirements must be met for all environments. In some cases, it is not easy to achieve these conditions from a functional point of view, when the device's function must be taken into account.

The first of the available materials are austenitic stainless steel (304, 316). This kind of steel has a high toughness even at very low temperatures. It also has a low desorption rate of CO, H<sub>2</sub>O, CO<sub>2</sub> and CH<sub>4</sub> under the 1000 K and H<sub>2</sub> under the 600 K, which is sufficient for the applications [70]. The disadvantage is that these steels have a residual ferrite content (3–10 %), which can cause very weak magnetism and work in very high fields with it could be dangerous [71]. A better choice is to use 316Ti stainless steel with titanium additions, which improves the magnetic properties of the steel [72]. However, it is generally not recommended for very high magnetic fields.

Another possible material for the palette is titanium. For this material, it is essential to pay attention to its composition. It is necessary to find titanium that does not contain or contain a tiny percent of additives admixtures such as oxygen due to gassing and the content of iron and other magnetic impurities due to their magnetic behavior [73].

Oxygen-free copper is another very suitable material for use in these environments. Due to the small amount of impurities, especially does not include UHV inappropriate oxygen. It has excellent electrical and thermal conductivity, good weldability, corrosion resistance, and can be used widely as a conductive material. It is widely used for vacuum

seals, capacitors, for microwave tubes and waveguides, as well as in the construction of magnetometers, electromagnets, and other superconductors [74]. Exciting material is also molybdenum. For its high melting point, it is widely used for sample holders or stubs, where a high temperature is required to form the various structures or for the analysis of the samples as well as strength and stability during high temperatures and creeps resistance. It also provides thermal and electrical conductivity and low vapour pressure. It is broadly for electrical and electronic devices, temperature and vacuum furnaces, and semiconductor applications [75].

Phosphor bronze is commonly used material in low temperatures and magnetic fields. It offers an excellent combination of strength, durability, and flexibility under excellent machining conditions. This material is usually used for flexible parts such as retaining components.

Other materials, which are also widely used in HF-EPR systems, are plastics. Plastics are materials easy to machine with a relatively high precision, which is necessary for manufactured components. Nylon is a plastic material suitable to use in multiple environments. It is tough, durable, and abrasion-resistant. The apparent disadvantage is embrittlement after few cycles of temperature changes, which is another requirement for the materials use, especially for insertion into a magnet with significant temperature changes. PEEK is also a plastic material used in multiple environments. It has better cyclic fatigue properties and is tested by our group in the manufacture of other sample holders under these conditions. It has high dimensional stability at different temperatures. Another plastic material is Tufset Polyurethane (Tufnol<sup>TM</sup>). It provides excellent mechanical properties, and it retains its physical properties at low temperatures. Tufset has excellent fatigue resistance and good resistance to stress cracking. To all these plus factors is added good dimensional stability and a hard, abrasion-resistant surface with low friction [76]. Therefore, it is also used mostly for sliding parts such as skids.

All the mentioned requirements and knowledge will be utilized during the design of the mobile vacuum chamber, palette holder, and sample holder developed in this work and described in the following chapter.

# 5. Design of the sample transfer system

This chapter is dedicated to the primary goal of this thesis: the development and design of specific devices for the transport of atmosphere sensitive samples under the UHV conditions. A mechanism for loading samples into HF-EPR and palette holder itself for a certain type of samples it is here developed and designed. The assembled mechanisms will be gradually analyzed, and their components will be described in more detail. Parts described below were done using a student software Autodesk Inventor 2019.

## 5.1. UHV suitcase

The atmosphere sensitive samples can be exposed to the atmosphere, and thus they may oxidize, degrade, or otherwise be damaged. Mobile UHV suitcase must be developed, designed, and manufactured to protect these types of samples and to transfer them safely in the protective atmosphere without any damage. The samples are placed on a palette located inside the suitcase during transport.

The UHV suitcase is primarily built from commercially available UHV components. Conflat-type (CF) flanges were used to connect the individual parts of the suitcase, which guarantee minimum sustainable pressure  $10^{-13}$  mbar [77].

The base of the UHV suitcase, which is shown in Figure 5.1 is a *6-way cross* to which other individual components are gradually attached. The main component is 750 mm long *magnetic linear transport*. At the end of the linear transport, a mechanism for attaching the sample holder called *grabber tool* is connected [78]. In our case, these sample holders are palettes called flag style sample holders. If it is necessary, this mechanism can be removed and used for other sample holder types. Between 6-way cross and magnetic linear transport is placed a *tip-tilt port aligner* [79]. This component is used for tilting the whole magnetic transporter in two perpendicular planes. The tip-tilt port aligner is used to properly attach the palette and compensate for the sag of the magnetic probe caused by an extension.

A *viewport* is connected to another port, which is used to check the correct position of the palette to the linear transporter and also to orient the palette correctly before the insertion into the connected device. On the other side of the viewport, an *ion pump* (small ion pump 5S) for pumping the space inside the chamber is located [80]. *Tee adapter* is connected to the top port of the 6-way cross to which a *vacuum gauge* (Hot cathode/Pirani vacuum gauge, VSH89DL from Thyrocont) is connected [81]. Since the gauge uses a combination of Pirani heat conduction and Bayard-Alpert sensor, it is possible to measure from atmospheric pressure to  $5 \cdot 10^{-10}$  mbar. Furthermore, a *non-evaporable getter* (NEG N100) from Gamma vacuum is connected to the Tee adapter, which pumps

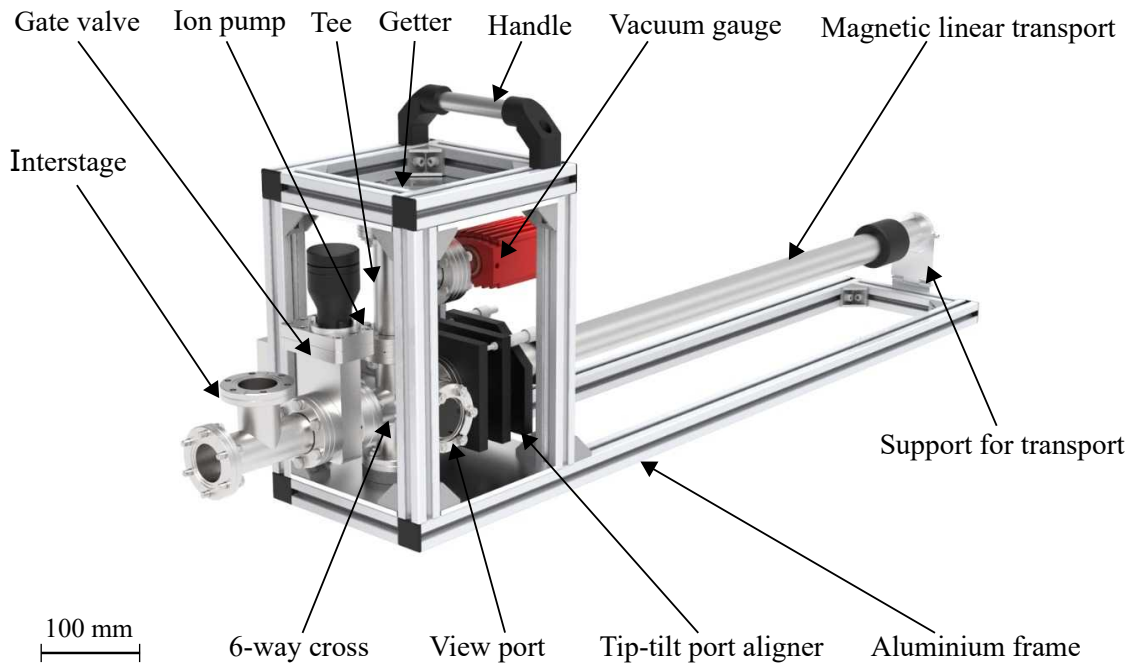


**Figure 5.1:** Proposed design of the mobile UHV suitcase, with indicated main parts. The overall dimensions are (412.4x276.5x1129) mm (without interstage), which allow transport of conventional personal cars trunk. The weight of 20 kg allows one person transport and operation.

especially  $H_2$  and  $CO$  gases [82]. In most commercially available UHV suitcases, the ion pump and getter cartridge are typically connected into one compact device, but it causes lower pumping efficiency. These two devices are separated to increase pumping time and pumping efficiency. There is also a *blank flange* connected to the bottom port of the 6-way cross because it has no use yet. *Manual gate valve* is connected to the last available port [83]. It separates the entire chamber from the surrounding atmosphere. Another tee adapter is mounted to this valve and serves as a connection to any device. Most of the devices also include a valve, so the tee adapter needs to be pumped to avoid contamination of the sample in the UHV suitcase and the connected device during the sample transport. Connected tee adapter is pumped by an external turbomolecular pump connected to the flange, or this port is covered, and space of the tee adapter is pumped through the connected device.

The whole UHV suitcase is placed and fixed to the *aluminium profile frame*, which provides structural support for the chamber and protects against possible impacts. The aluminium frame made of Rexroth square profiles with a T-slot. These profiles are connected by  $90^\circ$  angles using T-nuts and screws. The advantages of this frame are mainly in relative lightness, high strength, and modularity. A handle in the center of mass is attached to the frame by two screws for easier gripping of the entire UHV suitcase. To support linear magnetic transport, a small mechanism called *support for transport* is attached at its end. It is connected to the aluminium frame to prevent damage to the flange due to the weight of the entire magnetic linear transport. Additionally, *safety sleeves* were designed to protect the sample holder and entire magnetic linear transport against going down, when the UHV suitcase is in a vertical position.

Dimensions of the developed UHV suitcase are (412.4x276.5x1129) mm with the weight 20 kg. The suitcase's total price was estimated at 17 243 € (price does not include assembly and testing). In Table 5.1 are described the prices of individual components.

**Table 5.1:** The list of components, which are part of the newly designed assembly of UHV suitcase. The proposal includes parts bought in the Czech Republic, and they are converted to EUR with a uniform exchange rate from the 13. 10. 2019, 1 € = 25.815 Kč.

Parts	Price [€]
UHV and components	8 635
Controllers and devices	8 188
Aluminium frame	210
Fasteners	110
Backup power UPS with 550 W	100

### Comparison with available commercial UHV suitcases

During the design of the UHV suitcase, the possibilities of commercially available and supplied systems were investigated.

In particular, compatibility with the HF-EPR spectrometer and UHV cluster was examined. Further, total dimensions and construction of UHV suitcases were also investigated for the purpose of transport by car.

Most commercial UHV suitcases are offered basically without linear transport, but it is reported that they can be delivered to most of these suitcases. In our case, it is necessary to have this linear transport, because there is no similar component on the spectrometer at CEITEC Nano and it would be difficult, if not impossible, to implement it there.

The broadest portfolio of the mobile UHV suitcases probably offers company Ferrovac, which deals with complete deliveries of UHV systems [84]. This company provides a wide range of mobile chambers with or without linear transport and with flange diameter of 16 mm or 40 mm.

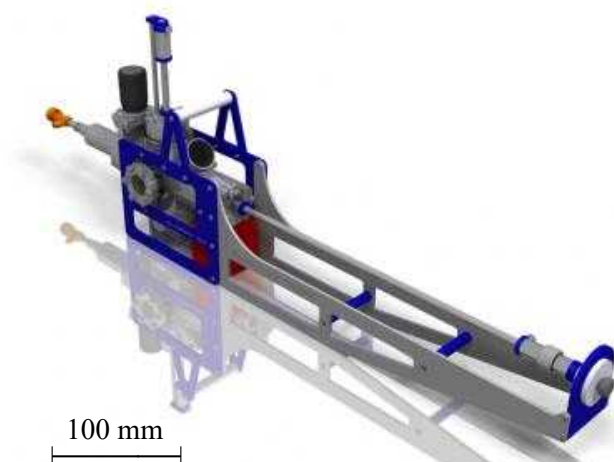


**Figure 5.2:** UHV Suitcase from company Ferrovac equipped with a linear transport sample storage up to three simple sample palettes.

It offers mobile chambers from the simplest chamber without linear transport to the UHV suitcase with a liquid nitrogen dewar for active sample cooling and thermal shields with a temperature measuring kit so that it can transport sensitive samples at cryogenic temperatures under UHV conditions. This company also provides suitcases with sample storage up to 3 samples, which is also seen in Figure 5.2. Dimensions of this UHV suitcase are (274x189x1049) mm with a 650 mm long wobblestick (linear transport with the angle deflection) with the weight about 12 kg and price 31 570 €.



**Figure 5.3:** UHV Suitcase from company CRYOSCAN allowing the movement only in one axis using a linear transport.

The second commercial UHV suitcase is from company CRYOSCAN shown in Figure 5.3. The suitcase has optimized construction concerning volume (without linear transfer). The design of the handle is practical, aesthetical, and performs the functions of the handle and the supporting structure. A possible disadvantage of this product is its instability. It has a short spread making it unstable while the long linear transfer is connected, so it is recommended to use short linear transfer. Therefore, the manufacturer is recommended to use the configuration with the linear transfer connected directly to the device,

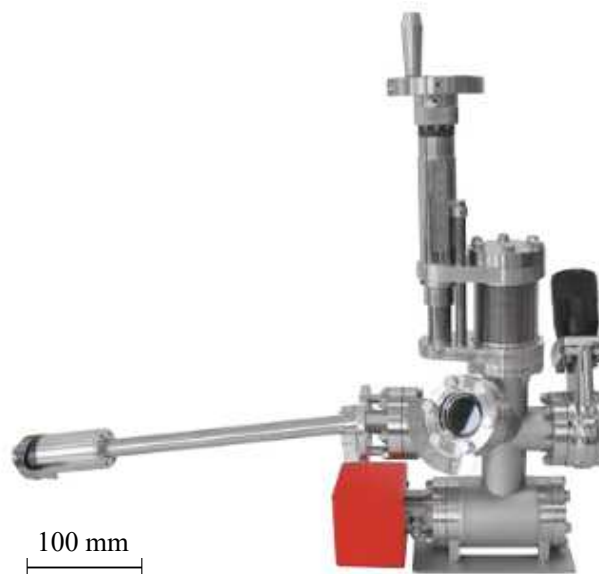


**Figure 5.4:** UHV suitcase from company Henniker-scientific with the linear transport sample holder up to 3 sample palette.

where the suitcase is connected and use the suitcase without the linear transfer. Another disadvantage can be that the linear transfer is fixed without any aligners. The dimensions of the UHV suitcase from CRYOSCAN are (235x116x1233) mm with 450 mm long transfer rod (it is also offered without transfer rod). The weight of this device is 18 kg with the price 29 679 €.

Another UHV suitcase (Figure 5.4) is offered by the company Henniker-scientific [85]. The system is characterized by vacuum components that are tailor-made to the needs. This vacuum suitcase contains the tip-tilt port aligner for precise alignment of the sample position between the main chamber and transfer rod. For this device, longer transfer rods are also offered, but since there is no support for this transfer probe, it will be unlikely to choose the transfer rod longer than 500 mm. The advantage of this suitcase is storage up to 3 flag style sample holders. Dimensions of this suitcase are (481.5x191x608) mm with a weight of 13 kg and price 24 780 €.



**Figure 5.5:** Small and compact UHV suitcase from company Scienta Omicron uses wobblestick as a linear transport.

UHV Suitcase, shown in Figure 5.5, is created by the company Scienta Omicron, well-known for its broad portfolio of products for the vacuum industry. It also has vacuum components tailor-made for needs. It has the considerable advantages of the suitcase, like in small dimensions (340x150x936) mm. Another advantage is storage space for up to six simple flag style sample holder. The exciting thing on this UHV suitcase is his weight, just 9.2 kg makes this device very suitable for transport. The price of this mobile suitcase is 27 150 €. This company also offers a fly case to protect the UHV suitcase on request.



**Figure 5.6:** UHV suitcase from company Enviro™ belonging to the Specs group.

The last featured UHV suitcase is from company Enviro<sup>TM</sup> and is shown in Figure 5.6. This company offers a simple and compact device with dimensions of (276x100x530) mm for transferring samples from one controlled environment to another without the risk of exposure. It is primarily designed to be compatible with their SPECS UHV systems. It is possible to order this mobile suitcase with or without active pumping, which can save the space and weight, but on the other hand, it extends the pumping time, limits the lifetime of the samples inside the UHV suitcase and in author's opinion, slightly complicates for longer transport distances of the sample. The weight of the suitcase is 20 kg with a pumping system, and the price is 26 880 €.

Table 5.2 compares individual commercial devices with the device proposed within this master's thesis. However, the comparison is not 100 % objective, because the parameters of suitcases, such as the length of the linear transfer or the backup power, are not offered for every mobile UHV suitcase.

**Table 5.2:** Comparison of commercially available UHV suitcases with the suitcase developed in this thesis. The achievable pressure is in case of all commercial mobile chambers identical,  $1 \cdot 10^{-10}$  mbar. The length in brackets means the length of the linear transfer for manipulation with samples. \*Price includes only components and materials for manufacture.

Company	Dimensions HxWxL [mm] (length of the linear transfer)	Price [€]
Developed design	412.4x276.5x1129 (750 mm )	17 243*
Ferrovac	372 x189 x1049 (650 mm )	31 570
CRYOSCAN	116 x235 x1233 (450 mm )	29 679
Henniker-scientific	481.5x191 x 608 (400 mm )	24 780
Scienta Omicron	340 x150 x 940 (600 mm )	27 150
Enviro <sup>TM</sup>	276 x100 x 530 (300 mm )	26 880

From the Table 5.2 it can be seen that the developed device is the longest due to the long magnetic linear transport. However, this length is required due to the long distance between the flange and the sample transport device in the UHV cluster on which the samples are transported.

## 5.2. Various sample palettes

In this thesis, two types of samples intended for measurement in the HF-EPR spectrometer were considered. For these samples, it was necessary to devise a sample palettes and guarantee their compatibility with many characterizing devices. These samples and sample palettes are described bellow.

### 5.2.1. Samples

The samples will be characterized and manufactured in cooperation with group Molecular Nanostructures at Surfaces led by doc. Jan Čechal. This section is focused on a description of both types of samples.

The first sample is a crystal of a unique shape fixed into the one type of sample palettes. The crystal is characterized and measured by different techniques, even with deposited molecules on its surface. The second sample is shown in Figure 5.7. The base

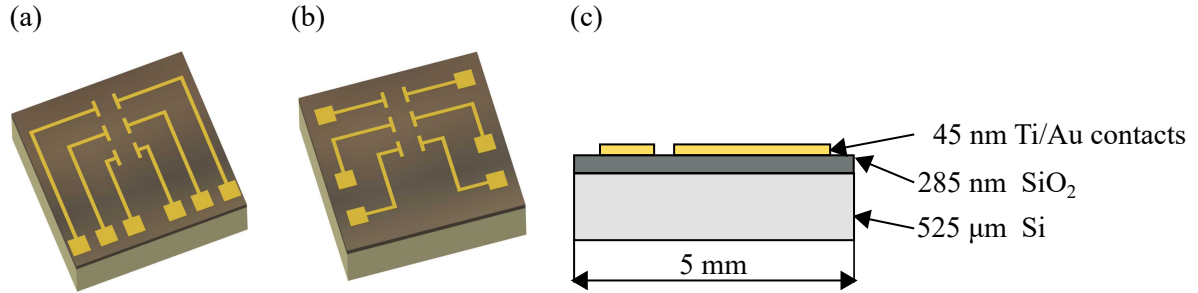


**Figure 5.7:** Si/SiO<sub>2</sub> substrates with the same size 5 mm × 5 mm include Ti/Au contacts. (a) Substrate, which is currently using for measurements graphene and its characterization. (b) Design of substrate with a more suitable placement of Ti/Au contacts for a connection with a chip expander. (c) Side view of the substrate with Ti/Au contacts.

is 525 μm thick silicon used as a substrate with a dimension of 5 mm × 5 mm. On top of silicon substrate is 285 nm native layer of silicon oxide. Furthermore, 3 nm adhesive layer of titan and gold contacts with a thickness of 45 nm are deposited on the oxide surface. The figure shows the distribution of individual contacts on the substrate. The monolayer of graphene will then be transferred to the contacts. Since various holes and defects are created in this monolayer as a result of manufacturing, the sample contains three sets of contacts in order to select the contact where the graphene has not been damaged and is intact in that place.

### 5.2.2. Sample palettes

For the samples mentioned in the section 5.2.1, there are no commercially available sample palettes that are needed for their attachment and subsequent insertion into the device, so it was necessary to manufacture these palettes. The type of crystal palette is already designed and manufactured by a group of doc. Jan Čechal. The second type of sample palette for graphene will be described in the next section.

#### Crystal sample palette

The design of the crystal sample palette shown in Figure 5.8 depends on its use, and it is based on the flag style sample holder. This palette is currently in use for crystals and their characterization in the UHV cluster at CEITEC Nano. The design is derived from multipurpose use in different devices, especially in UHV cluster (4.1). These are, for example, deposition of thin films, scanning tunneling microscopy (STM) for characterization surfaces and molecules on the top of it or LEEM for characterization of crystal pattern. Palette consists of two pieces, top part and bottom part from molybdenum, which are connected by four screws, and the crystal is fixed between these two parts. Each of the two parts also serves to attach the palette to the different devices. The top part is used for STM, while the bottom part serves for mounting into the deposition chamber, LEEM, and other characterization devices. The distance between the top and bottom parts is 5.5 mm from the outer edges.

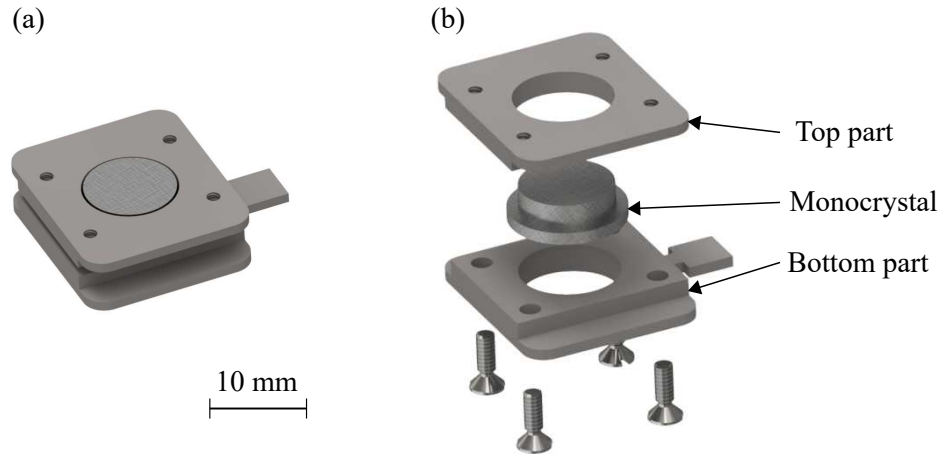


**Figure 5.8:** Crystal sample palette. (a) Model of assembled sample palette. (b) Sample palette disassembled into the individual parts.

### Graphene sample palette

Graphene sample palette shown in Figure 5.9, which is developed in this thesis, is focused on samples with graphene for deposition of the molecules–nanomagnets. As in the previous palette, the design of the components was influenced by the needs for compatibility with the same types of equipment. The sample palette, like the previous type, was based on the flag style sample holder for attaching the entire palette to the linear transporters inside the UHV cluster as well as the grabber tool for transportation using the designed and manufactured UHV suitcase. For mounting in different devices, the palette has the same size as the previous palette, 21.5 mm  $\times$  18 mm. It also consists of *top part* and *bottom part* from the 1 mm thin molybdenum sheet. A *distance washers* had to be used to maintain the same spread 5.5 mm of these two parts from the outer edges as the previous crystal palette. For the beam of electromagnetic radiation passing through the sample, a *reflecting mirror* must be placed under the sample to reflect that radiation back into the detector. A *mirror holder* was designed to hold the mirror right below the sample

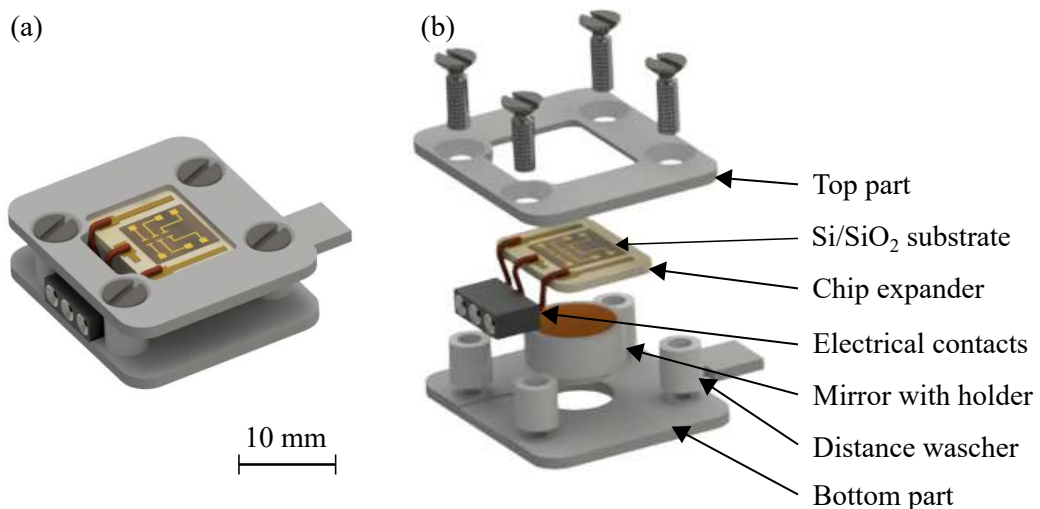


**Figure 5.9:** Graphene sample palette with electrical contacts. (a) Model of assembled palette. (b) Model of palette disassembled into the individual parts.

and also keep the distance between top and bottom sheet. Other part of the graphene palette is *chip expander*. It is a  $7.7 \text{ mm} \times 7.7 \text{ mm}$  plate,  $0.785 \text{ mm}$  thin which is placed into the groove in the top part. On the chip expander, a three gold contacts are deposited. Electrical non-conductivity, possibility of deposition of Au contacts and full transparency or reflectivity are required for the chip expander material. Suitable materials for this purpose are for example polytetrafluoroethylene, alumina based ceramics, corundum or fused quartz [86]. For reflective surfaces, mainly metallic materials are used, which, however, do not meet the condition for the electrical conductivity of the chip expander. A *sample substrate* from Si/SiO<sub>2</sub> with a graphene is placed symmetrically on the top of the chip expander between the contacts. Sample contacts are wire bonded with a contacts on the chip expander. The third, middle contact is connected as a ground with the silicon. The contacts are then routed via copper wires to the pins that are attached to *electrical contacts*. Electrical contacts are fixed in the bottom part. The body of electrical contacts are made from macor and there are 3 holes inside it for the pins. Subsequently the whole graphene sample palette can be inserted to the palette holder and be electrically connected with pins inside the palette holder and subsequently with the waveguide. The waveguide leads the wires to the top of the magnet, where they are further connected to other devices.

### 5.3. Palette holder for EPR measurements

For palettes mentioned above, it was necessary to design and manufacture a holder attached to the end of the waveguide probe. Since there are many types of samples, it was necessary to attach different sample holders, such as the palette holder, carousel sample holder, or chip sample holder to the waveguide probe. For an attachment, a multi-functional mechanism was designed. This mechanism should provide a quick replacement of the holders that ensure minimal time spend between measurements and allow sample preparation during the measurements. The best option was the type of bayonet mechanism shown in Figure 5.10 (a). This type is based on solid stubs in the upper part of the holders, which enter the grooves in the fazette attached to the waveguide probe. This section also contains 24 contacts that are connected to the holder via pins. These con-

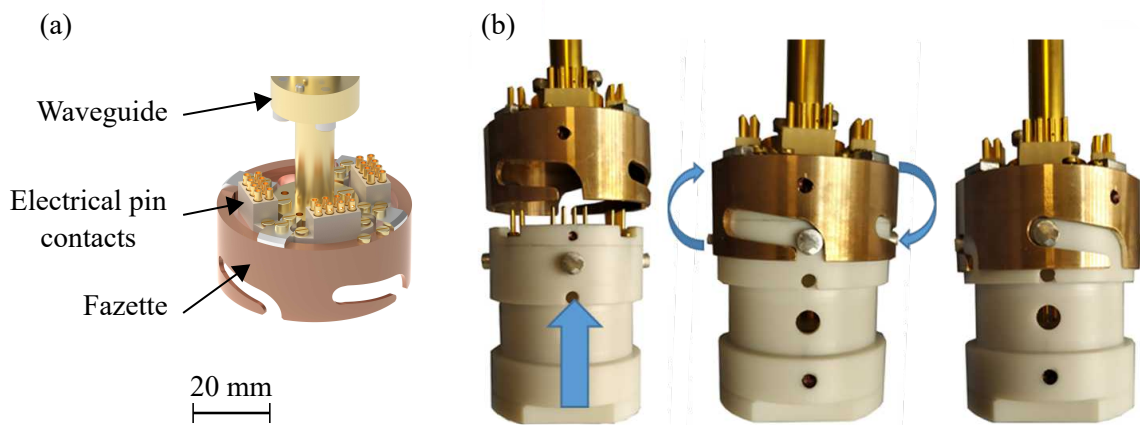


**Figure 5.10:** Bayonet mechanism for easy connection and disconnection of sample holders. (a) 3D model of the end of the waveguide with electrical contacts and fazette. (b) Process of mounting the sample holder to the waveguide.

### 5.3. PALETTE HOLDER FOR EPR MEASUREMENTS

tacts are for the measurement of temperature in the holder, a heater to heat the sample locally, and for controlling the modulation coils, leading the contacts to the sample. This mounting is fast, and no other tools are required. Adam Lagiñ makes the design of the bayonet mechanism in his bachelor thesis [87].

The base of the palette holder (shown in Figure 5.11) is a *body* made of PEEK material, suitable for both low temperature and magnetic field. This part contains holes for *stabs*, which are small cylindrical parts that are pressed into the holes, and they are designed for the bayonet mechanism grooves to attach the entire palette holder to the waveguide probe. The other components are mostly attached to this part. The body also contains various openings for increasing the overall flow of helium as a cooling medium, and thus there is a faster cooling of the sample. Furthermore, the constant flow of the helium then keeps the temperature around the sample more stable. *top coil part* is attached to the body with four screws from the top side. This part contains pins for modulation coil, temperature sensor, and heater that are subsequently connected to the waveguide pins. It also includes one of two Helmholtz coils for modulating the magnetic field inside the holder. There is also a 6 mm hole for a *waveguide tube* that leads electromagnetic radiation to the sample.

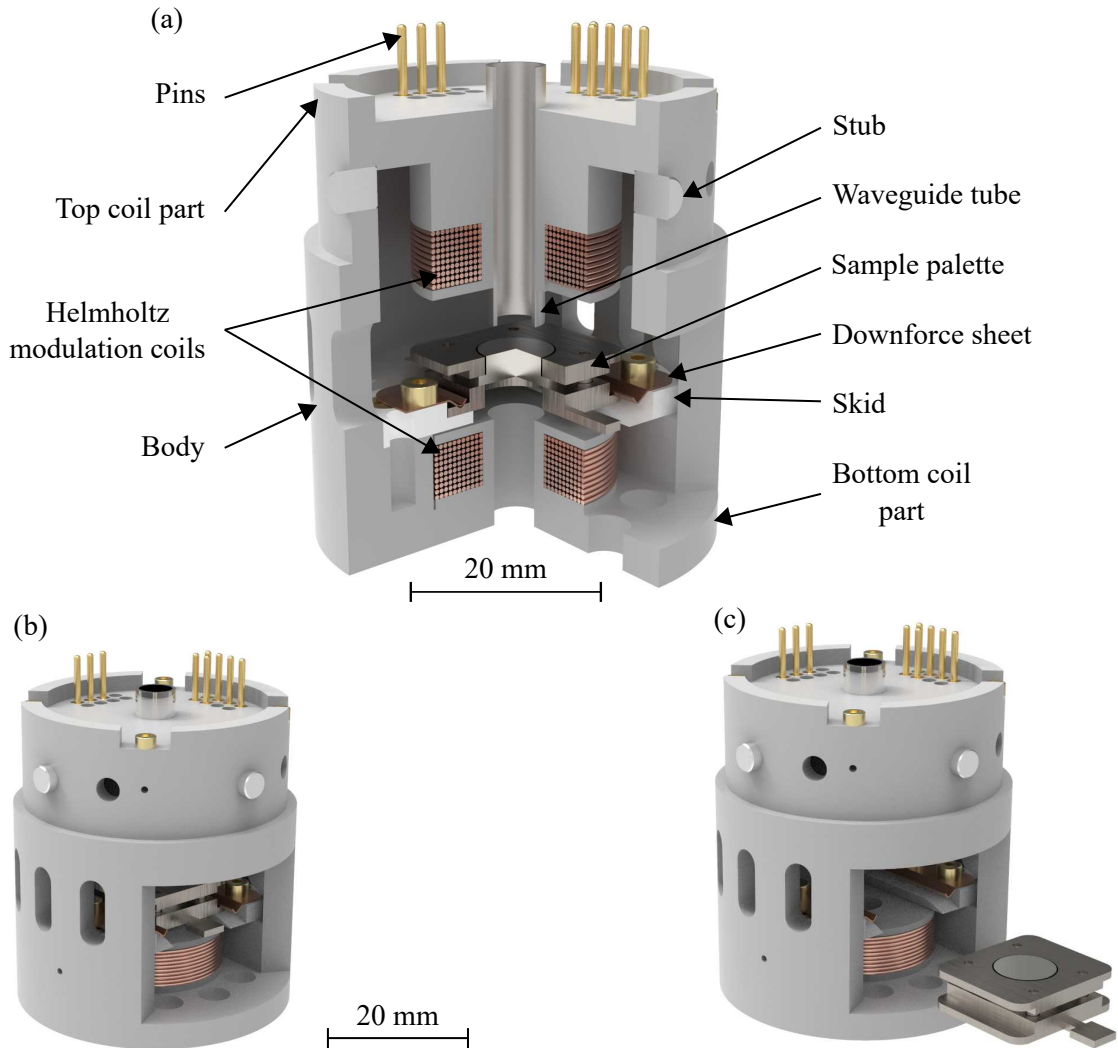


**Figure 5.11:** 3D model of palette holder with the sample palette. (a) Three quarter section view of the assembled palette holder. (b) View of the palette holder with inserted sample palette. (c) View of the palette holder with an ejected sample palette.

*Skids* are another important part of the entire holder. These are two mirror-like parts that support the sample while inserting it into the holder. They are attached to the body of the holder by two countersunk screws on each side. It serves as a support for the palette and the *downforce sheets* used to fix the sample palette in the right position. In the body and skids were also designed holes for the *temperature sensor Corno<sup>x</sup> CX-AA* from Lakeshore cryotronics and *heater* composed of 4 resistors with total resistance 1 k $\Omega$ , which are connected with the pins in the top coil part [88]. Other parts of the holder are *electrical contacts*. They are embedded in the body anchored by two screws and copper plate. Their position corresponds to the position with the sample palette, and so they can be electrically connected. This part is only used for the graphene sample palette. The last part that closes the entire body from the bottom is *bottom coil holder*. This part is connected with a body by three screws, and it contains the second Helmholtz coil. In these parts, there are also several openings for the helium flow.

Already mentioned, Helmholtz coils serve for local influence (modulation) of the EPR signal. The coils are designed that the sample is ideally in the center of these coils and that there is the minimum distance between them. Limiting occurs on the bottom side, where the skids are positioned, so the bottom coil has to be just below them. Frequencies in the range from 1–20 kHz and magnetic field in range from 0.1–1 mT will be used for the modulation. In that case, the coils are designed to fill the largest possible diameter in the body while keeping all the requirements (as the sample in the center of the magnetic field) of the magnet. In appendix A.1 is shown the magnetic field distribution of the Helmholtz coils according to the space occupied by coils and the diameter 0.4 mm of the wire that was used.

## 5.4. Airlock

The airlock is used for loading the waveguide with the attached sample holder to the magnet while preventing helium escaping from the magnet. The waveguide is placed in a hollow non-magnetic tube inserted together with the waveguide into the magnet. This tube is intended for sealing the helium conditions in the magnet from the surrounding atmosphere by a series of o-rings, which are located in the airlock and are separated by teflon rings. In this case, the airlock contained three o-rings. A separate place is created between the o-rings, which serves for differential pumping so that the space between the helium atmosphere in the magnet and the outside atmosphere is vacuum separated, and there is no penetration of the atmosphere. There is no condensation of water vapor in the magnet, which protects the magnet against freezing and functionality loss.

Transfer of the sample under the UHV conditions cannot be avoided without hermetically closing the path between the UHV Suitcase and the spectrometer. The old version of the airlock located on the valve at the top of the magnet did not meet the requirements for the transport of air-sensitive samples due to missing CF flange for mounting the UHV suitcase. Therefore, the newly built version of the airlock, shown in Figure 5.12, contains flanges for both the connection of the mobile UHV suitcase and the viewport for the precise loading of the sample palettes into the palette holder.

For simplicity of production, the airlock is divided into two separate parts. The airlock is also equipped with four o-rings compared to three o-rings in the previous version, which should ensure a better separation of the helium conditions and the outside atmosphere.

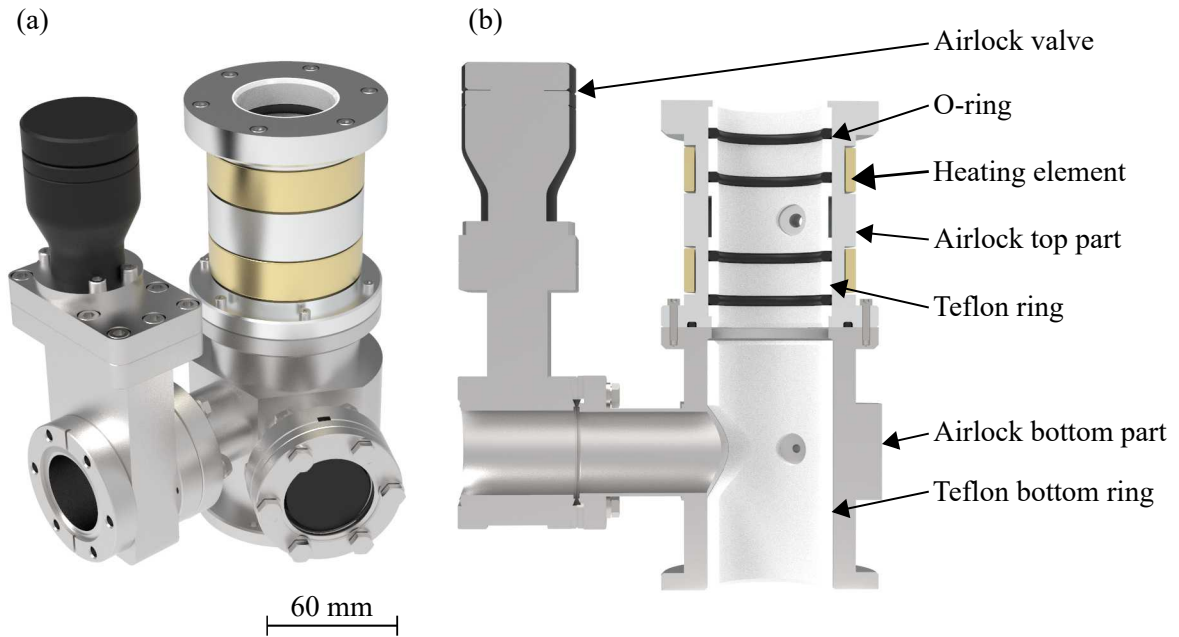


**Figure 5.12:** (a) 3D model of the new version of the airlock. (b) Half section view of the airlock.

## 5.5. Simple suitcase

Part of the work is also the design of equipment for compatibility with the glove box shown in Figure 5.13 (a) located in the laboratories of CEITEC Nano used to transfer the sample to the HF-EPR spectrometer. The glove box is used for sample preparation in various protected atmospheres filled with inert gases, such as argon, but mainly nitrogen. Unfortunately, there are no outputs on this device with which the designed UHV suitcase could be connected. Therefore, the transfer of samples by another device for the glove box and similar types of devices was designed, and it is shown in Figure 5.13 (b).

The main part of the simple suitcase is 300 mm long *wobblestick* [89]. This component allows both linear motion and angular deflection up to a maximum angle of  $20^\circ$ . At the end of the wobblestick rod, there is *grabber tool* for catching the sample palette, just like in the case of the UHV suitcase. A *wobblestick support* is attached to the flange to protect the wobblestick handling rod. A *full nipple* with the length of 110 mm to create space for the grabber tool with the sample is attached to the wobblestick flange. In the end, there is the *gate valve* to close the small chamber and separate the environment inside the simple suitcase from the surrounding environment. For connection of the simple suitcase to the HF-EPR spectrometer, another full nipple is necessary, which serves to connect the valve located on the simple suitcase and the airlock valve. Since the sample will be in a protected atmosphere under normal atmospheric pressure in a simple suitcase, it is not necessary to place the sample under the vacuum, and it will be possible to use a pump connected to the airlock, pump the space in the full nipple and airlock space and fill it with the same inert gas.

The restrictions are, in this case, the dimensions. A load lock chamber of the glove box used for loading samples has a diameter of 400 mm with a length of 600 mm. The proposed simple suitcase must meet this proportion. The simple suitcase is not intended for long transfers, but only for transfers in CEITEC Nano laboratories, therefore the suitcase does not include any active or passive pumping as it is in the case of the UHV

## 5.5. SIMPLE SUITCASE

suitcase. It also does not contain any additional inert gas reservoir. For this reason, the dimensions of a simple suitcase can be very compact, 212x70x530 mm with a weight of 4 kg.

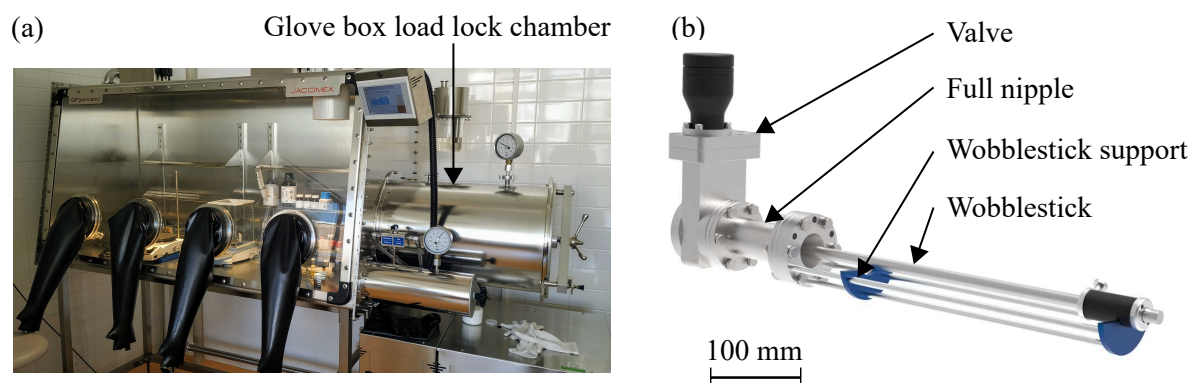


**Figure 5.13:** Transport extension of the atmosphere sensitive samples. (a) Glove box situated in the chemical laboratories at CEITEC. (b) Simple suitcase for transportation atmosphere sensitive samples without the pumping system.

## 6. Performance of the sample transfer system

To verify the functionality of the sample transfer between certain devices using the newly designed UHV suitcase, a set of tests was performed to attest to the functionality of the transport and the compatibility of the UHV suitcase with both the UHV cluster and the spectrometer itself. The testing of components, characterization of test samples, and their transportation will be described as well as a measurement of the representative sample.

Testing and verifying the functionality of the designed components is crucial part of every development process. The first part of this section is dedicated to the testing of the palette holder and its integration with the waveguide (3D printing was used during the design of the UHV suitcase, palette holder and sample palette for prototyping). The functionality of individual parts and their compatibility with each other was checked. With the help of 3D printing, a faster and better design was achieved. Advantages such as fast production, easy adjustment of the produced part were a huge simplification of the design. The following will describe the UHV suitcase testing, subsequent connection to the UHV cluster, and the first loading of the sample into the suitcase. Several tests of the new version of airlock will be described with the subsequent connection of the airlock and spectrometer.

The testing of the rate of contamination process of the sample during transport was described. The connection of the UHV suitcase with the HF-EPR spectrometer was tested, and the first transfer of the test sample was performed. The first measurement of the reference sample was done.

### 6.1. Palette holder testing

Testing the experimental setup of the palette holder (different versions are shown in Figure 6.1) started by assembling all manufactured parts. Some of the parts were partially modified for better assembly handling and also due to manufacturing inaccuracies.

Theoretically calculated 156 turns on one coil, only 144 turns were wound, because during the process of winding, nail polish was used to stick turns together. It caused a reduction in the turns. In this way, the second Helmholtz coil was wound, and subsequently, the bottom coil part could be mounted to the body (In Figure A.2, a method in winding coils and wounded parts are shown). Furthermore, both skids and downforce sheets were also mounted to the right place. Further, the resistors, in case of the heater, were soldered in series with a total resistance of 1 k $\Omega$ . They could be placed as close to the sample as possible, best on a well-conducting material. Due to limited space around the sample palette and handling them, they were glued by thermally conductive glue to the wall of the palette holder's body.

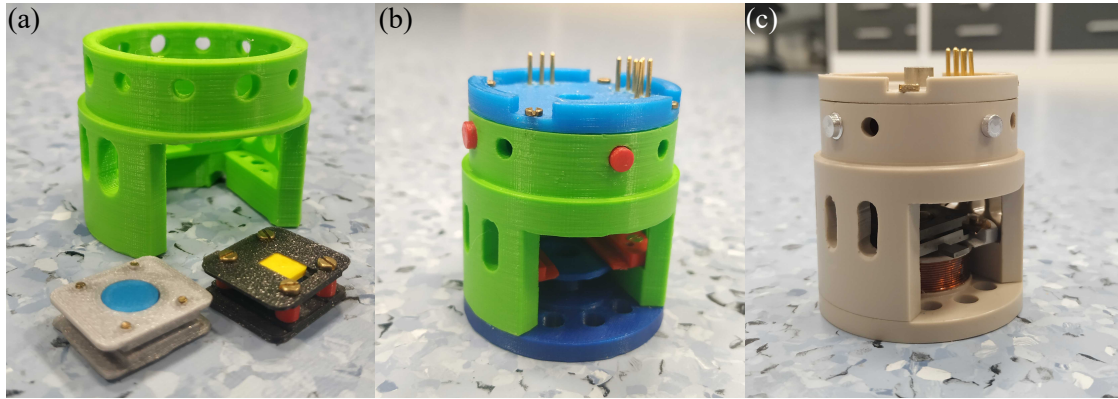


**Figure 6.1:** (a) First version of the palette holder with two types of sample palettes. (b) The last version of the body. 3D printed on a 3D printer Prusa MK3S. (c) Manufactured and assembled palette holder with the inserted reference sample.

Due to the future use of various palettes, the palette holder was designed to be disassemble. A top coil part of the palette holder is screwed into the body and can be removed to reconstruct the internal parts. The ends of the wires of the modulating coils and the heater were fitted by precise headers as well as pins, which were attached to the top coil part of the palette holder for the simple interlocking with each other. In the case of modulating coils, care must be taken to ensure that coils are connected correctly (in series, not in parallel) to avoid disturbance of the magnetic field, which modulates the signal.

The top coil part was equipped with another type of mechanism for connection to the waveguide using two rollers and two screws due to complications in the production of

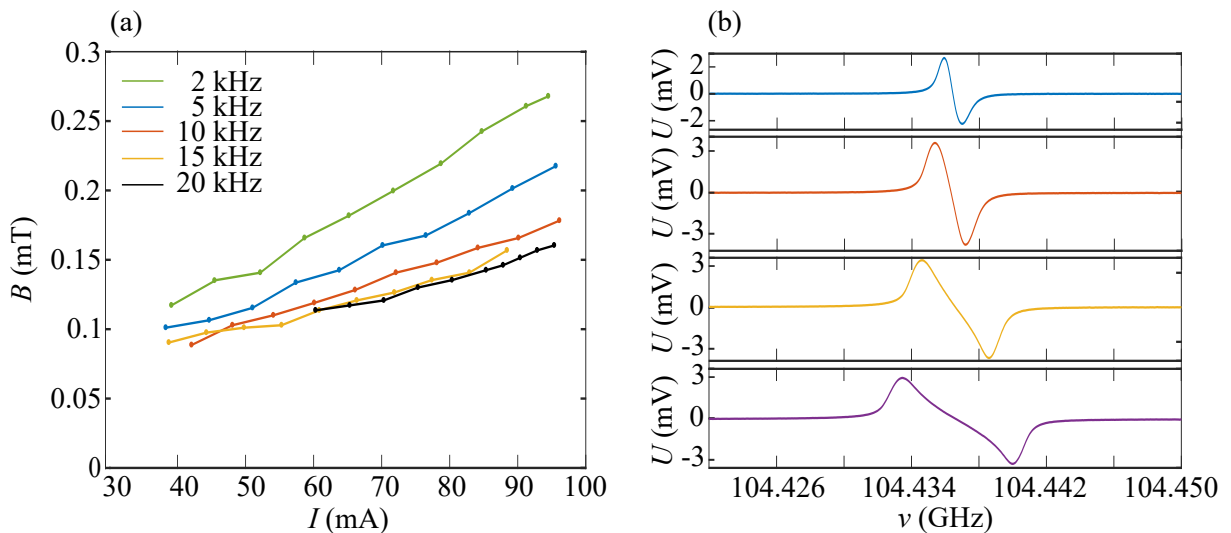


**Figure 6.2:** Calibration of the Helmholtz modulation coils in the palette holder inserted in the magnet. Calibration was done on the reference crystal sample of LiPc. (a) Dependence of the magnetic field in the middle of these two coils on the current flow through the coils. (b) Spectral lines of the LiPc. The input voltage from the modulation source was 9 V. The blue line has a low modulation compared to the red spectral line, which has an optimal modulation. Two spectral lines below reach the maximum amplitude (3.15 mV) of the modulation as the red spectral line, but the two peaks were begun to spread. It means that these two spectral lines are over-modulated, and lower resolution is achieved.

the bayonet mechanism<sup>1</sup>. Then the dummy sample palette<sup>2</sup> was inserted to the palette holder, and the whole process of the inserting sample was troubleshot. The next step was to insert a test LiPc (lithium phthalocyanine) sample with a previously known properties (spin  $s=1/2$ ) and calibrate the modulating Helmholtz coils of the palette holder. This calibration is necessary for proper signal modulation and increases the signal to noise ratio with the use of lock-in technique. The resulting dependence of the magnetic field on the current flows through the coils is shown in Figure 6.2.

## 6.2. UHV suitcase testing

To experimentally verify the functionality of the designed UHV suitcase, it was first necessary to assemble its individual parts. It took place in the EPR laboratory at CEITEC Nano, where all the tools for assembly were available. The first step in assembly was joining the 6-way cross gradually with the blank flange from the bottom, tee adapter from the top, followed by the valve, viewport, and ion pump. Due to the space restriction, it was impossible to use conventional screws with hex head for some flanges. Therefore, threaded rods were used from both ends, fitted with washers and nuts. Threaded rods were also used on the top and bottom of the chamber to attach to an aluminium profile frame. Assembled UHV suitcase is shown in Figure 6.4 (b).

The level of the vacuum was tested with the following procedure. A turbomolecular station with a pre-pumping membrane pump and a pressure gauge was connected from the front side of the UHV suitcase using a reduction<sup>3</sup>. The suitcase was wrapped with heating tapes to bake out the entire system to a temperature of approximately 120 °C, the wrapped suitcase is shown in Figure A.4. Baking causes desorption of the excess gases from the inner surface of the chamber. It was also necessary to heat this pump at the same time as the suitcase, since the ion pump is attached to the 6-way cross and does not contain separate heating. The ion pump contains ferromagnets that could lose their functionality due to heat, so the manufacturer indicates that the ion pump's temperature should not exceed 150 °C. The temperature was controlled with thermocouples, which were connected to the sources of baking. Baking usually takes tens of hours, especially when the system is new, and it was exposed to the atmosphere for a long time before the vacuum apparatus was assembled.

Another important thing was to initiate and activate the non-evaporation getter, which is suitable for passive pumping, especially light molecules. During this process, the controller was connected to the getter, which can be used to control it. First, the getter initiation process, which has already been preset to one hour, was started. In the case of initiation, a large amount of gas was released inside the suitcase, and the associated increase in pressure. During the initiation process, the pressure in the suitcase should not exceed the limit value specified by the manufacturer, which is  $1 \cdot 10^{-4}$  mbar. Probably due to the weak pumping speed of the turbomolecular pump connected to the suitcase, this

---

<sup>1</sup>This additional modification of the holder is not included in the drawings, because it is only a temporary version of the attachment to the waveguide, which will be replaced by the bayonet mechanism in the future.

<sup>2</sup>The dummy sample palette means a part with the same dimensions as a real palette, which is used for testing and it can be possible damaged and thus substitutes the real palette.

<sup>3</sup>It is common to have a CF flange at the outlet of the turbomolecular pump. This turbomolecular station is equipped with a KF flange (Klein Flansche (KF), German, which translates to "Small flange" in English.)

## 6.2. UHV SUITCASE TESTING

limit was reached, and the initiation process was stopped. It was repeated several times until the value of the pressure in the suitcase during the initiation process did not exceed the set limit. Finally, the initiation process was successfully completed. An activation process followed. This process prepared the getter's surface for pumping, and it took the same time as the initial process. It was done by heating the getter under the vacuum up to 450°C.

During the activation of the getter, the pressure increased close to the  $1 \cdot 10^{-5}$  mbar, which should not be exceeded, otherwise, the getter material could be damaged. Therefore, the activation process (just like the initiation process) was switched off and on several times, without completing the entire 60 minutes of the activation process. Ideally, the pressure should be kept below  $1 \cdot 10^{-6}$  mbar during the activation process, recommended by a manufacturer. At the end of the activation process (and also bake out process), the ion pump was turned on for 10-15s to prepare it for work. After switching off the bake out process, the ion pump was gradually turned on, and the valve on entrance of the UHV suitcase was slowly closed down. After two days of pumping, the limit pressure  $1.3 \cdot 10^{-8}$  mbar was reached. The pressure was expected to be lower, so it was decided to test the vacuum chamber with a leak detector.



**Figure 6.3:** UHV suitcase connected to the turbomolecular pump with a pre-pumping leak detector. Some leaks contained in the chamber were detected using this detector.

The leak detector was connected as a pre-pump ahead of the turbomolecular pump, and it was possible to detect a flow rate of helium gas, as is shown in Figure 6.3. The ion pump was turned off, and the valve between the vacuum suitcase and the turbomolecular pump was slowly reopened after achieving approximately the same level of pressure as in the chamber. Then, connected flanges of the suitcase were blown by helium from the outside, and the flow rate of helium was checked on the leak detector. An increase in helium flow during the blowing was found in some flanges, which concluded that these flanges were tightened poorly. Subsequently, the frame was unscrewed from the suitcase, and the flange bolts were tightened, and all connections on the UHV suitcase were checked for safety. Another leak test was performed, and it was found that the helium flow no longer reached such high values as in the previous leak test. Still, it was questionable,

what causes the change of the helium flow in the system. For this reason, another test was performed.

The vacuum suitcase was closed with the valve, and the individual joints were slowly blown with helium. If the suitcase contained another leak, there would be a sharp increase in flow through the detector when the valve was opened. After the blowing started, the detector started to detect some flow again and slowly, but continuously increased, which can be assigned to the background or penetration through other connections than the suitcase contains (suction of helium from the laboratory space). After a sufficient time, the blow was stopped, and the vacuum chamber valve was opened. The helium detector did not detect any differences in the increase of the helium flow in the system. From these findings, it can be concluded that the UHV suitcase does not contain any detectable leaks. Furthermore, it can be seen that the contribution of the helium flow is from the environment.

### 6.2.1. Transport and compatibility with UHV cluster

The transport of the UHV suitcase requires a constant supply of electricity to the ion pump controller for continuous pumping of the chamber to avoid the pressure increase. In this case, the vacuum suitcase was equipped with a portable *backup power supply UPS* (CyberPower green Value) with a power of 550 W [90]. The ion pump controller and the gauge located also on the suitcase were connected to this UPS, which was then connected to an electrical grid. During any power failure and after disconnection from the grid, the UPS serves as a power source for these devices. The endurance test of the backup source with the connected ion pump was performed with a constant consumption power of 11 W at the pressure of about  $10^{-8}$  mbar. Testing took 4.5 h, during which the ion pump was pumping the space of the UHV suitcase.

After successful assembly and testing of the suitcase, together with the controller for the ion pump and UPS, the suitcase was placed on a transport cart equipped with a rubber pad to prevent vibrations during the transport. Cart with the suitcase was transported to the UHV cluster, and it was connected to the load lock chamber of the UHV cluster. It was planned to attach the suitcase to the only possible flange of the load lock chamber located on the top side of the chamber. The valve was connected with the load lock chamber via reduction, where the suitcase should be placed. The valve ensures that after the disconnection of the suitcase from the UHV cluster, the load lock chamber remains hermetically sealed and uncontaminated. After connecting the suitcase with the UHV cluster, the load lock chamber was vented to achieve the same pressure as it was in the tee adapter. After that, the valve could be opened. Subsequently, the load lock chamber and the tee adapter were pumped again.

In order to achieve the best conditions for the transport of the sample from the UHV cluster to the suitcase, it was necessary to bake out the entire load lock chamber with the tee adapter, because tee adapter is exposed to atmospheric pressure and impurities during each transfer of the suitcase into and from the UHV cluster. However, since the UHV parts are made of stainless steel, they have a high thermal conductivity, which would also transfer the heat to the suitcase over the time, in which the pressure would subsequently increase. For this reason, the UHV suitcase was also baked to achieve even better pressure afterward. The baking procedure took place overnight. It was necessary to reactivate the getter before switching off the baking. After the connection of the getter to the controller, it was found that no current flows from the controller to the getter

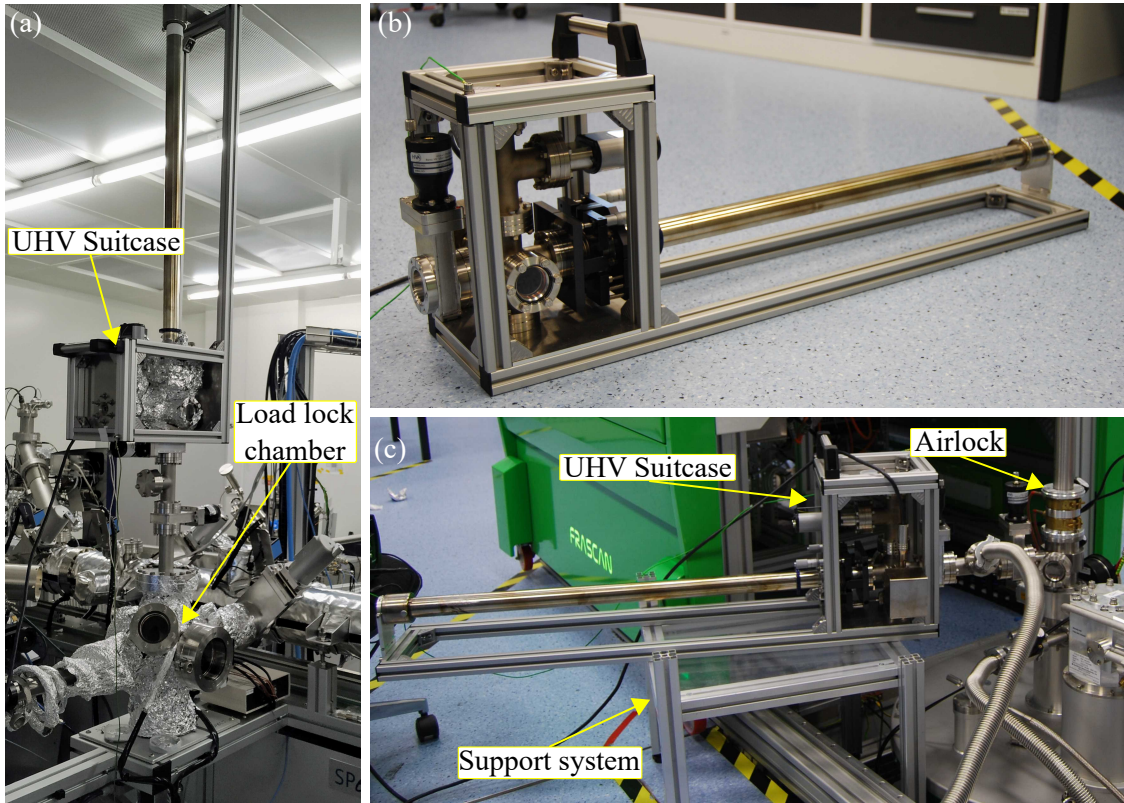


**Figure 6.4:** (a) UHV suitcase connected to the load lock chamber within the UHV cluster. (b) UHV suitcase connected with the airlock and pumped by the turbomolecular pump via tee adapter.

cartridge. After a series of tests, it was found that there would probably be a problem with the getter cartridge itself, where one of the electrical circuits was probably broken. Therefore, further tests were performed without a functional getter. After a series of tests, the getter will be disconnected and sent for a complaint.

The baking procedure was turned off to stabilize the temperature in the chamber, and using a turbomolecular pump, the best possible pressure ( $2 \cdot 10^{-8}$  mbar) was achieved. The ion pump was also turned on so that the space of the UHV suitcase could be closed and pumped during the tests. Meanwhile, the test sample was prepared during the baking procedure. 50 nm thick layer of gold was deposited on the silicon substrate. After that, the test sample was transferred onto the sample palette. The palette was inserted into the load lock chamber and moved to the preparation chamber, where the sample was cleaned. Cleaning comprises two processes: sputtering and annealing. The sample was sputtered for 1 min by argon ions with the energy of 1 keV. Then, the sample was annealed for 1 min at 150 °C.

Following tests were monitored the level of the sample contamination during the transport. There were two types of samples: Au test sample, and Cu test sample with more reactive surface. To measure the sample's level of contamination, the elements of nitrogen, oxygen, and carbon, which are the main polluting elements, were measured.

The XPS method was used for the measurement of the samples<sup>4</sup>. XPS is a surface sensitive method, where counts per second (CPS) as a function of the kinetic energy of

<sup>4</sup>XPS analysis was performed in the photoelectron spectroscopy analysis chamber. The XPS abbreviation will be used when loading the sample into this chamber.

emission electrons from atoms are measured. Offset in  $y$  axis is used in every XPS graphs in this thesis for better spectrum recognition.

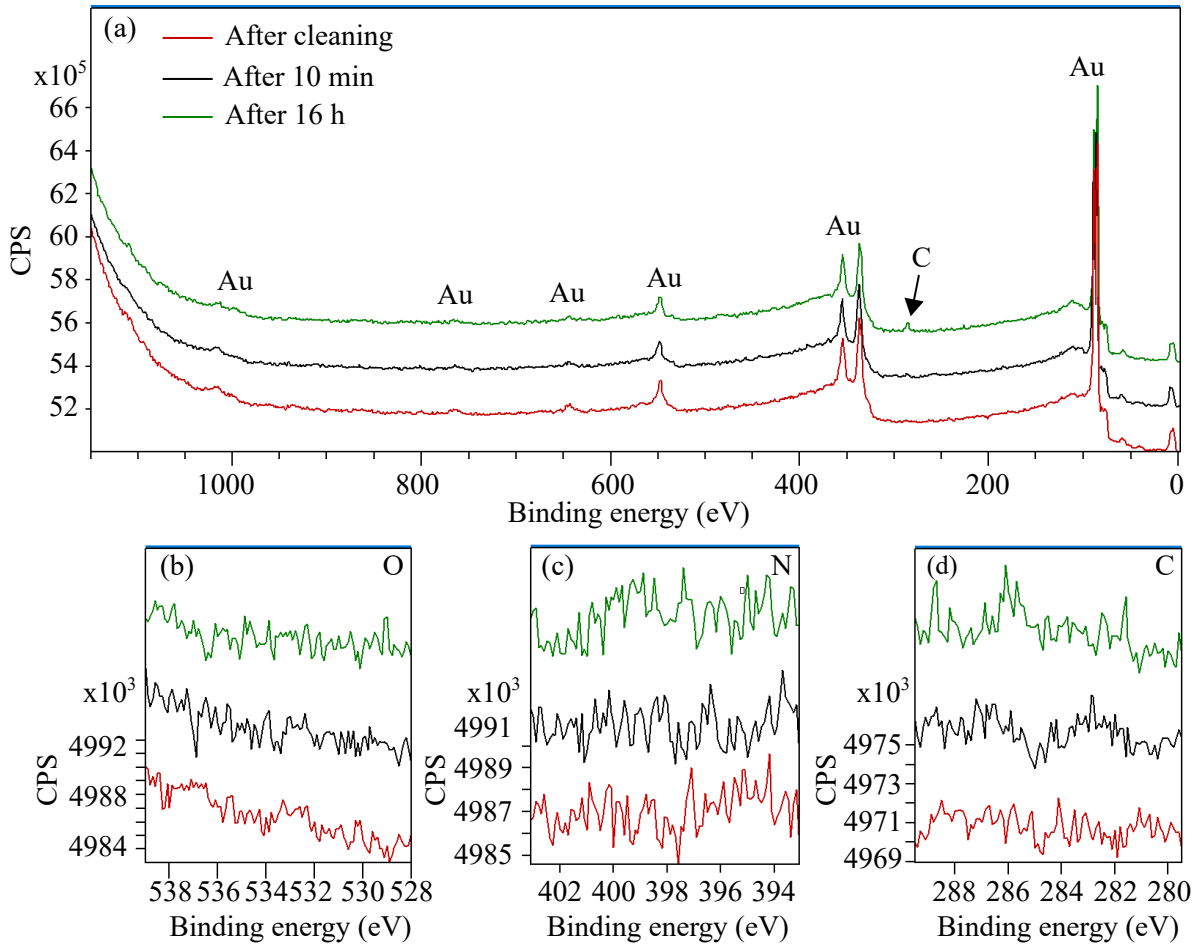


**Figure 6.5:** XPS characterization of the Au test sample. (a) A wide spectrum of the Au test sample. (b) Detail region, where the peak of oxygen should be observed. (c) Detail region, where the peak of nitrogen element should be observed. In (b) and (c), there can be seen just a noise. (d) Detail region, where the small peak of carbon element is observed.

The Au sample was transferred from the preparation chamber to the XPS for reference measurement of the sample spectrum. After the measurement, the sample was transferred to the load lock chamber, from which it was subsequently moved to the suitcase, and the valve was closed. After 10 minutes, the valve was re opened, and the Au sample was transferred back to the XPS, where the spectrum was measured again. A second test measurement followed, where the sample was moved back into the suitcase and left there for 16 hours. During this time, the decrease of pressure exceeded  $1.3 \cdot 10^{-8}$  mbar, and reached a pressure of  $5.7 \cdot 10^{-9}$  mbar. This positive change in pressure was most likely due to repeated baking of the suitcase in the past. The valve was opened, and the sample was again transferred to the XPS to perform the spectrum measurements. The resulting measurement and comparison is shown in Figure 6.5. The red line represents the spectrum of Au immediately after the process of cleaning. The blue line characterizes the spectrum of the sample after 10 min of preservation in the suitcase, and the green line is a spectrum of the sample after 16 hours spent in the UHV suitcase. It is necessary to carefully monitor which peaks (elements) arise during transport. Because, as can be seen, there is a small

peak of carbon after 16 hours of transportation. However, carbon is not as reactive as oxygen, which causes molecular decomposition. It is common that during sample storage in the UHV cluster occurs to adsorption of the carbon on the surface over the time from a residual atmosphere. The resulting small carbon peak may have no effect on the final quality of the sample and its measurement using the HF-EPR spectrometer. It was also important that no increase in oxygen or nitrogen peak was observed even after 16 hours.

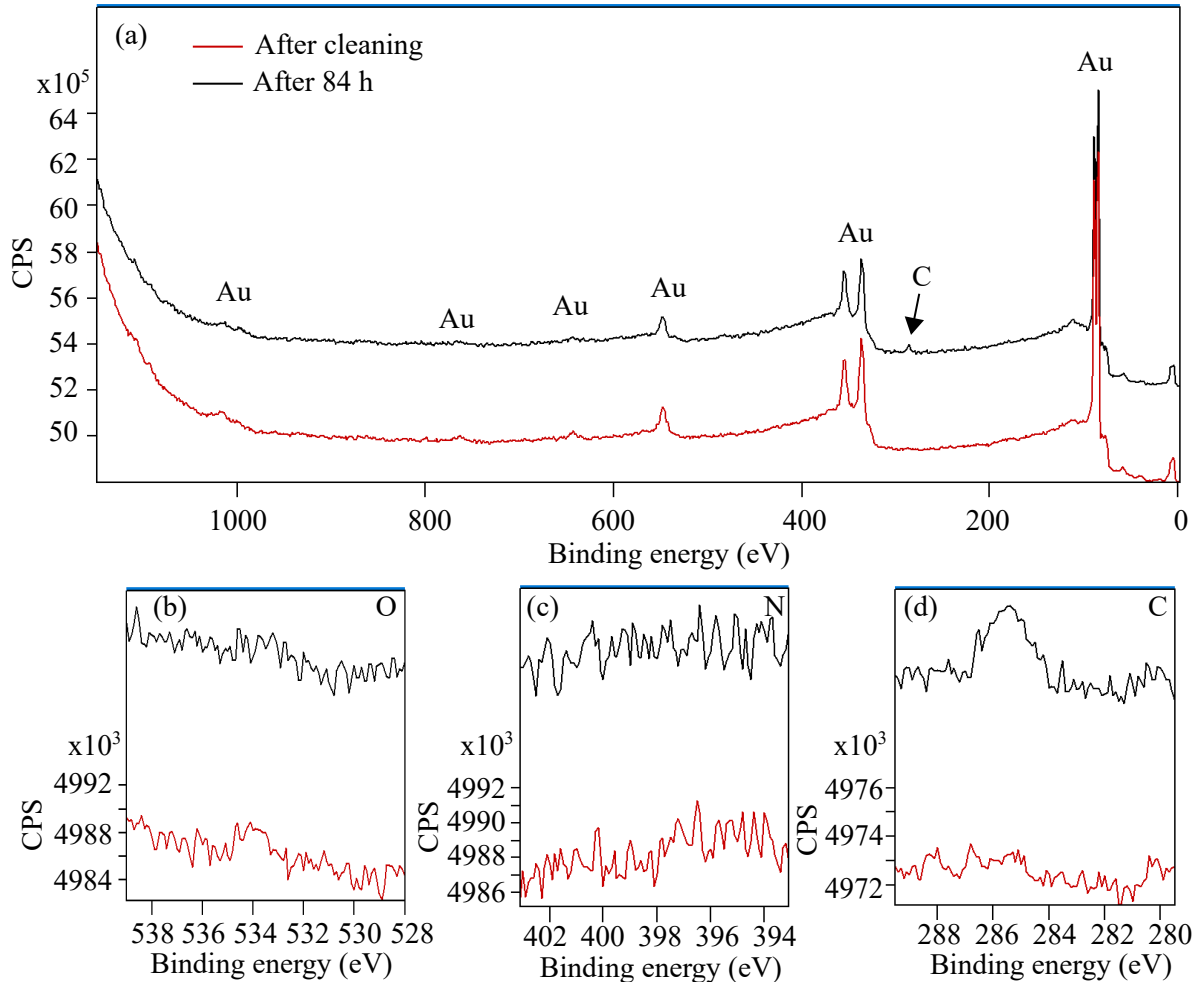


**Figure 6.6:** The second XPS characterization of Au test sample, which tested a longer term in the UHV suitcase. Red was measured before the transport, black after transport. (a) Wide spectrum of the Au test sample. (b) Detailed regional of the oxygen peak. (c) Detailed regional of the oxygen peak. In both cases, there is no occurrence of element peaks in the graph (d) Detailed regional of the carbon peak.

The second test was more extended storage of the test sample in the suitcase. The test sample was placed in the preparation chamber for the repeated cleaning process described above. Then, it was transferred to the XPS for measurement, and after that, it was transferred to the suitcase. After closing the suitcase valve, the load lock was vented so that the tee adapter could be disconnected from the load lock valve. The suitcase was left disconnected for 84 hours and then reconnected. The sample was transferred to XPS, and the sample was measured. A comparison of the reference spectrum and the spectrum after 84 hours is shown in Figure 6.6.

Compared to the previous test, there is a more significant peak of carbon, which means more carbon adsorbed on the surface. However, that corresponds to a longer time spent in the chamber.

For the next tests, as a test sample as it a copper crystal was chosen, which generally has a more reactive surface than gold. The crystal was placed onto the palette and cleaned in the preparation chamber. The test sample was sputtered for 10 minutes with the energy of 1 keV. Then the sample was annealed at 150 °C for one minute, and then re-sputtered. The XPS measurement was also performed in the same way as the gold test sample. The reference spectrum of the cleaned copper sample was measured after 10 minutes and then after 16 hours in the UHV suitcase. The comparison of these spectra is shown in Figure 6.7. The spectrum has the same progression as the previous one.

In comparison with Figure 6.5, after 10 min of staying in the briefcase, even the carbon peak is not recognizable. After 16 h, there is a discernible difference between carbon peaks. It is most likely due to the fact that the surface of copper is more reactive than gold. However, it is a small amount of carbon absorbed on the surface.

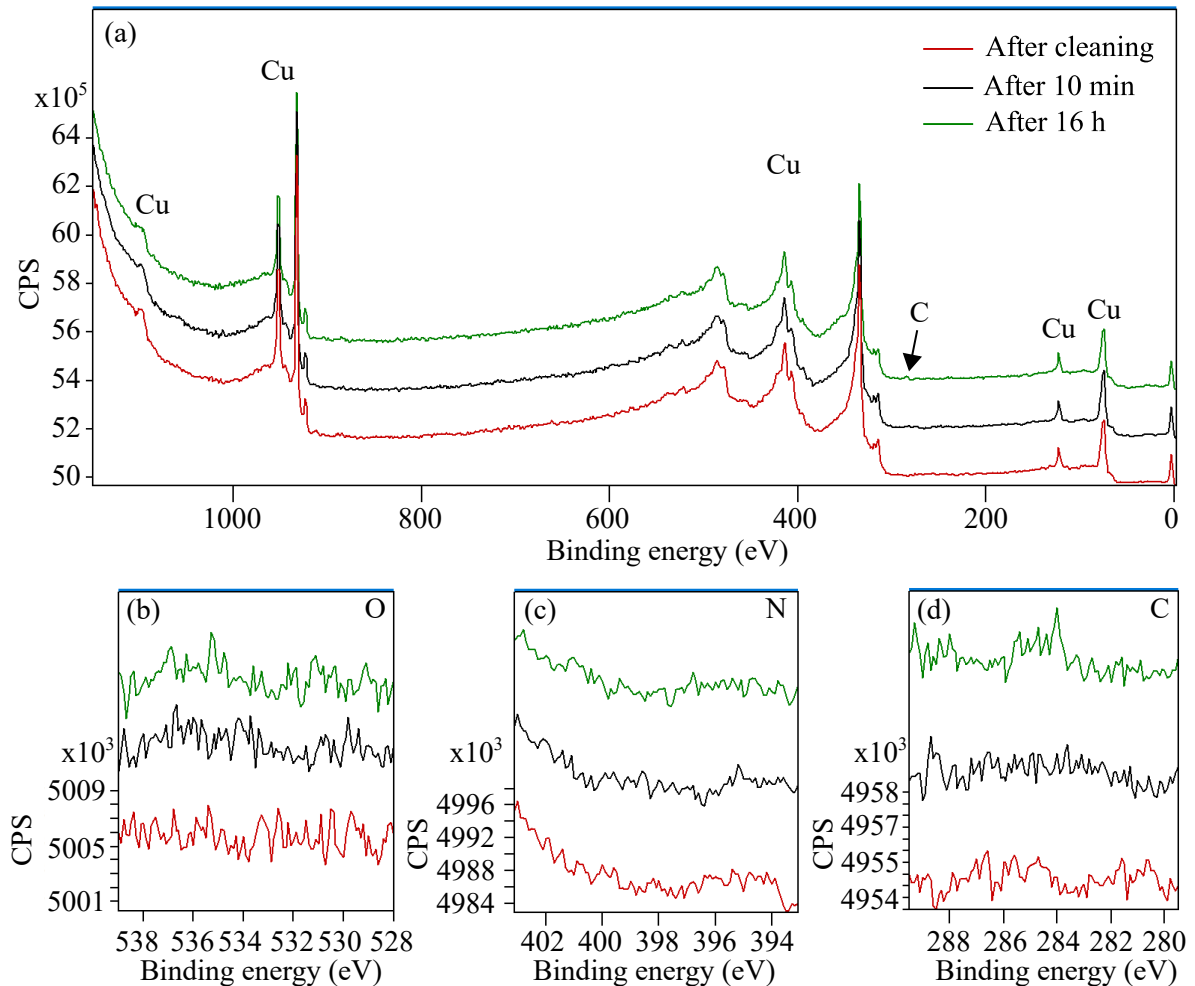


**Figure 6.7:** XPS spectra of Cu test sample after cleaning, 10 min and 16 h. (a) Wide spectrum of the Cu test sample. (b) Detailed measurement section for the characteristic oxygen binding energy. (c) Detailed measurement section for the characteristic nitrogen binding energy. No visible peak oxygen or carbon were displayed. (d) Detailed measurement section for the characteristic carbon binding energy.

XPS measurement showed that transfer itself does not have any measurable effect on sample contamination. All impurities adsorbed from the UHV in order of hours, as is typical for such pressure values. Most important is that short stay in the UHV suitcase leaves the surface intact. Therefore, transfer from the UHV cluster to the HF-EPR spectrometer should not endanger the sensitive sample. 16 hours test was chosen for a long-term transport (e.g., a trip to Stuttgart or synchrotron in Krakow, Poland, or Grenoble in France) and even though there is carbon adsorbed on the surface, it should not have an impact on the EPR measurement.

UHV suitcase was then continuously pumped, and after a few days, it reached a limit pressure of  $4.3 \cdot 10^{-10}$  mbar without the getter pumping. Pumping the UHV suitcase by getter and with the ion pump promises in the future reaches much lower pressure than the current state.

### 6.2.2. Compatibility with HF-EPR spectrometer

The connection of the UHV suitcase to the HF-EPR spectrometer is another goal in the loading of the samples to the HF-EPR spectrometer. In this part, two crucial things were tested, the new version of the airlock and transfer to the spectrometer itself.

#### Airlock testing

It was essential to replace the old airlock with a new one, which was designed and is described in Section 5.4. The replacement includes a supply line for helium to the airlock and also a flange for connecting a pump. Through the connection, the airlock is pumped before the waveguide was inserted to the magnet (it was inserted just in the airlock do seal entire airlock). The pressure did not reach the expectation during the pumping of the new airlock by the turbomolecular pump. Therefore, testing with a helium detector was used again. During this testing, a high flux of helium was recorded even without blowing the whole assembly with helium. After evaluating all of the effects, it was concluded that there is most likely leakage of helium through the valve located on the inlet of the magnet. However, this still did not solve the problem of the ability to pump the entire airlock. Subsequently, the whole assembly was blown by helium. However, due to the relatively high flux of helium passed through the magnet valve, the helium detector's sensitivity decreased, and the additional helium flux was not recorded. Therefore, the airlock assembly was disassembled, and the individual parts were tested separately.

The most critical was the bottom part of the airlock with the mounted viewport and the valve, which was tested first. The parts were sealed with the blank flanges with a rubber seal from above and below. No leaks or other defects have been detected in this part, and it was appropriately pumped. The upper part of the airlock was also tested with teflon seals and o-rings. There were virtual leaks in this part due to the failure to reach the required pressure. In this part, there was a pipe thread for the helium supply and pumping lane. For this thread, a teflon tape is usually used as a sealing. The connection was resealed, but the result was almost identical. Therefore, another problem was considered, consisting of poorly sealing valves in the helium supply and pumping line. Therefore, the valves were replaced for another, for which it was known from the previous testing that their tightness is fine. The problem was not recorded in this change either, so other effects on pressure were considered further. Another test was the removal of teflon rings and o-rings from the assembly and pumped the top part of the airlock again. During

this test, the required pressure was reached. From this it was deduced that the problem was probably in the manufactured teflon rings, which causes virtual leaks between the teflon rings and the wall of the top part of the airlock.

The problem with o-rings was solved by reducing the outer diameters of the teflon rings and holes made in them. The top and bottom parts of the airlock were connected, and the whole airlock assembly was tested again. In the last test, the waveguide was inserted into the airlock, simulating the process of real measurement. This test was successful. All these tests were acceptable, so the airlock was attached to the magnet, and further testing was performed.

Another vacuum test was performed after the connection of the airlock to the magnet. This examination aimed to test the whole airlock assembly connected to the magnet and measure the pressure values in specific periods during the pumping process.

A tee adapter was connected to the airlock valve. Further, the gauge was connected to the same place where the UHV suitcase should be connected during the sample transport. Then, the turbomolecular pump was connected to the last port of the tee. A tube with a waveguide was inserted from the top of the airlock to simulate the real loading of the sample. After switching on the pump, the entire space of the airlock and tee adapter were three times flushed by helium gas to remove possible impurities settled on the inner walls. The pressure was recorded at 0.5 hour, 1 hour and after 16 hours of pumping. The results are summarized in Table 6.1. It can be seen that the decrease in the pressure is not that significant after one hour of pumping. UHV conditions were not achieved, but since it is flushed with helium, it is relatively clean space without major impurities. It should be possible to transfer the sample and insert it into the helium atmosphere quickly without any contamination.

**Table 6.1:** Comparison of measured pressures in the airlock over the time.

Time [h]	pressure $\cdot 10^{-5}$ [mbar]
0.5	3.3
1	2.5
16	1.7

## UHV suitcase connection test

After successfully testing the new version of the airlock, the next step of testing was to connect the UHV suitcase to the airlock. Before the UHV suitcase could be connected to the airlock, it was necessary to design a support system (Figure A.3) on which the UHV suitcase could be placed in the same height as is the airlock's flange for the connection. This support system is composed of aluminium profiles assembled into a square with four support legs. Adjusting screws are attached at the support leg's ends for relatively easy adjustment so that the height of the entire support system can be achieved. On the upper side of the support system, a polycarbonate board was placed to prevent the abrasion of the UHV suitcase frame during the movement on the surface of this board.

Further, the UHV suitcase was transported to the EPR laboratory, placed on the support system, and pushed close to the airlock valve. The exact height of the suitcase flange was set using the adjustable screws. The UHV suitcase was for practice connected to the airlock valve and subsequently disconnected and transferred back to clean rooms to prepare for the transport of the test sample.

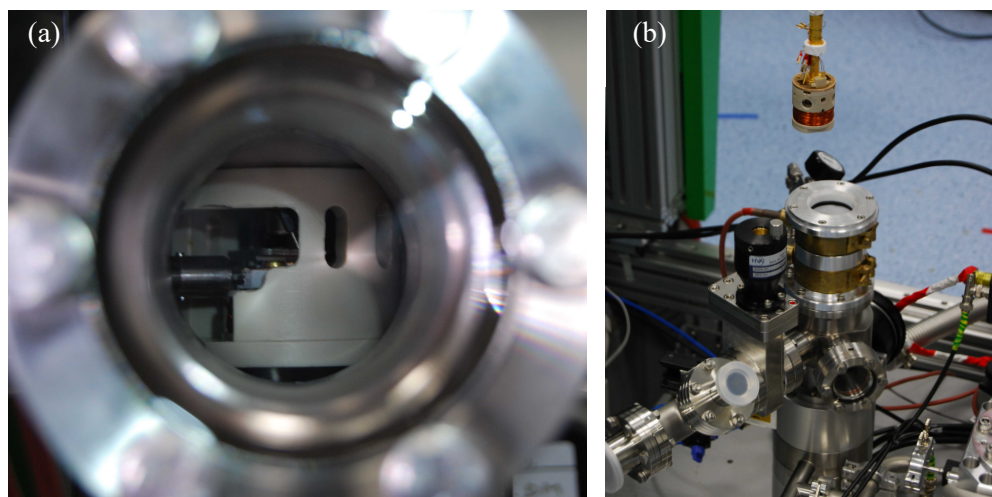


**Figure 6.8:** (a) Airlock inside view through the viewport. Illustration of inserting the sample palette into the palette holder by magnetic linear transfer rod. (b) Waveguide with the holder attached to the bottom inserting to the new version of the airlock.

### UHV suitcase and HF-EPR spectrometer sample transfer

For the test transfer between the UHV cluster and the HF-EPR spectrometer, the same copper test sample was used. The same cleaning procedure for the copper test sample was used as in the previous case, and then the reference spectrum of the clean test sample was measured (Figure 6.9 (red line)). The UHV Suitcase, which was connected to the UHV cluster, was wrapped with baking tapes before the sample was cleaned, and it was also baked with the load lock chamber for 16 hours. Subsequently, for 2 hours, the suitcase and load lock were left to cool down, and after reaching the appropriate pressure, the sample was transferred to the UHV suitcase. Further, the suitcase was disconnected from the UHV cluster and moved to the EPR laboratory. There, the suitcase was placed onto the support system. The suitcase was connected to the airlock valve, the blank flange was removed from the tee adapter, and the external turbomolecular pump was connected in its place. The waveguide with the palette holder was inserted into the airlock (in Figure 6.8 (b) is shown insertion of the waveguide with attached different holder). The valve between the tee adapter and airlock was opened, and the turbomolecular pump was switched on. After switching on the pump, the entire space was three times flushed by helium gas, as in the previous test. The space was pumped for 20 minutes to the pressure about  $5 \cdot 10^{-5}$  mbar, and then the valve between the suitcase and tee adapter was opened. Further, the test sample was moved into the airlock. During the transfer, it was necessary to move with the waveguide, which increased the pressure inside the airlock to  $10^{-4}$  mbar. It caused an increase in the current flowing through the ion pump, and it was turned off for safety reasons. Therefore, in further transfers, the ion pump will be turned off before the valve will be opened. Helium was released to the airlock to simulate the conditions in the magnet during measurement. After that, the sample was transferred back to the suitcase, airlock, and suitcase valves were closed, and the UHV suitcase was disconnected. The UHV suitcase was transferred to the clean rooms, and it was connected to the UHV cluster. The tee adapter was pumped from the side of the load lock chamber, the suitcase valve was opened, and the sample was moved to the XPS, where the characterization was made. A comparison of spectra before and after transportation is shown in Figure 6.9.

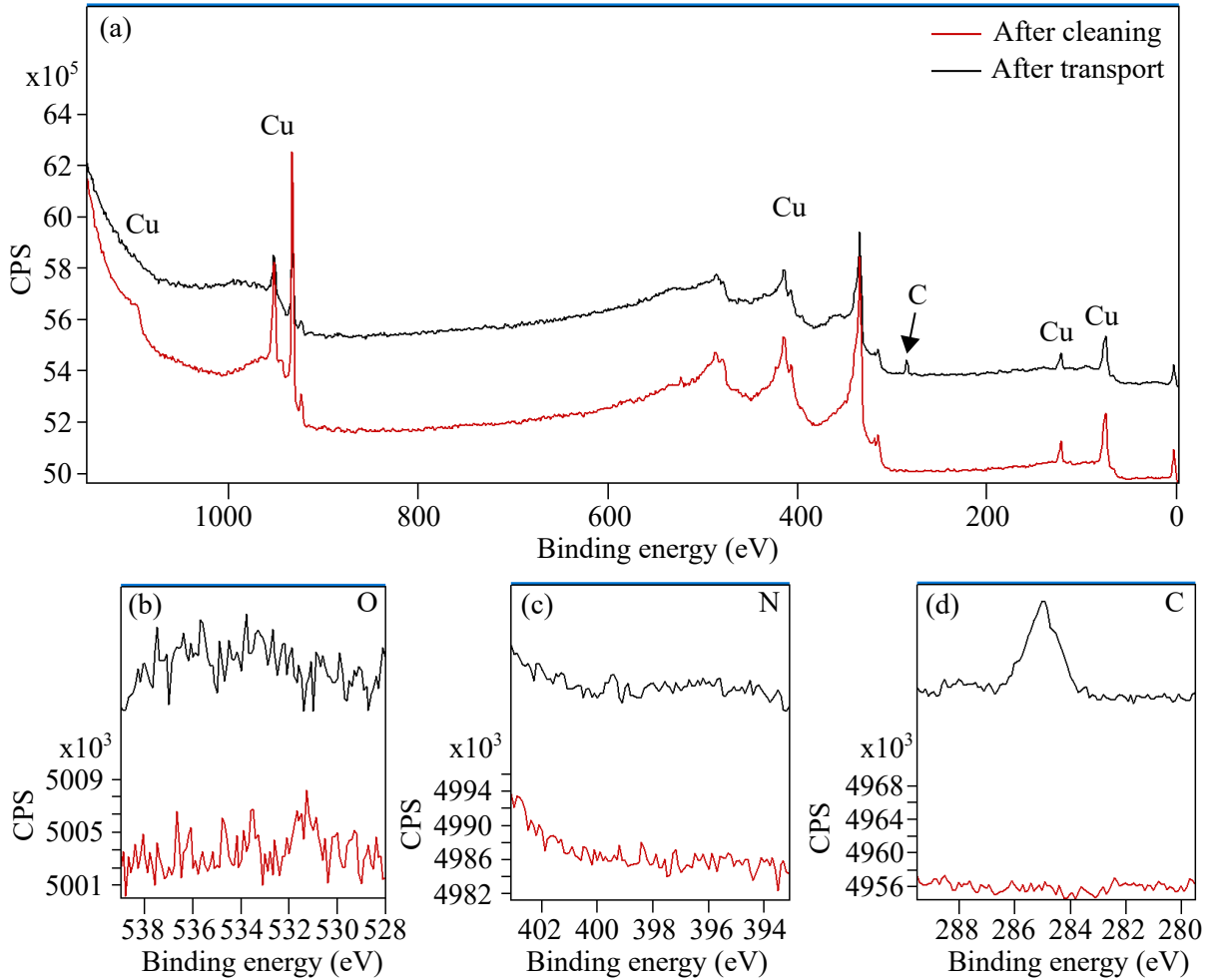


**Figure 6.9:** XPS spectra of the Cu test sample before and after the transport to the HF-EPR spectrometer. (a) Wide field spectrum of the Cu test sample. (b) Detail region, where the potential peak of oxygen should be observed. (c) Detail region, where the peak of nitrogen element should be observed. In (b) and (c), there can be seen just a noise. (d) Detail region, where the peak of carbon element is observed.

From the graph, it can be seen that the carbon peak is in comparison with the previous test of the Cu sample higher. It was probably caused by the low pressure inside the airlock during the transport.

One of the last tests of the UHV suitcase was to verify the possibility of transport for longer distances. In particular, a car will be used for long distance travel. The Škoda Octavia II, the most widespread car in the Czech Republic, was used for the test. For transport from CEITEC Nano laboratories, a transport cart was used, which otherwise served to transport the UHV suitcase between laboratories (Figure 6.10 (a)). The UHV suitcase was loaded into the trunk of a car simultaneously with the ion pump controller and UPS (Figure 6.10 (b)). It verified the possibility to easy transport of the UHV suitcase over a longer distance. It is worth mentioning that the pressure in the UHV suitcase during the transport was changed from  $5 \cdot 10^{-9}$  mbar to  $6 \cdot 10^{-9}$  mbar caused by minor shakes during the transport to the car. During a short transport, the ion pump is powered by UPS, which, as we know from the previous testing, lasts 4.5 hours. For journeys lasting more than 4.5 hours, it would be possible to connect the ion pump, i.e., the UPS, directly to the car.



**Figure 6.10:** (a) UHV suitcase during the transport to the car trunk. (b) UHV Suitcase in the car trunk. The ion pump controller and UPS can also be seen, which has to be connected to the UHV suitcase to avoid pressure decreasing during transport.

### 6.3. Sample test in HF-EPR

Performing the first measurements of atmosphere-sensitive samples in HF-EPR was one of the last goals of this thesis. However, before real measurement of atmosphere sensitive sample is done, reference measurements in HF-EPR have to be performed to verify the functionality of each step of the measurement process.

First of all, a reference sample, which will be comparable, was selected. Iron phthalocyanine ( $C_{32}H_{16}FeN_8$ ) (FePc) was selected as a suitable molecule for the first test measurements. FePc is a very low reactive molecule with the atmosphere, and it will serve for a good comparison. The first substance will be deposited in the UHV cluster onto the surface of the crystal. The second substance of FePc will be in the form of the powder pressed to the pellet. The diameter of the palette for the holder used to measure these types of samples is 5 mm. First, the reference of FePc in the form of a pellet was measured to verify that the measurement works correctly and if it is able to obtain the EPR signal. Required weight of the pellet is from 14 mg to 15 mg. 31.53 mg of FePc in the form of coarse powder was crushed finely. Subsequently, 3.27 mg of Eicosane was added, which is a binder powder without the EPR signal, thanks to which the pellet does not disintegrate. This powder mixture was put to a press, and it was pressed to the pellet. Then it was wrapped by a teflon tape and inserted into the sample holder at the end of the waveguide and moved to the magnet.

The FePc sample was measured in two different frequencies, 181 GHz and 210 GHz in the range from 0 to 12 T. The temperature was, in this case, 5 K. The measured EPR signal is shown in Figure 6.11.

When it was confirmed, that the measurement of the FePc in the pellet is working and it was possible to see a signal, it was approached to the second step, which was a preparation of the single crystal in UHV cluster, deposition of the FePc molecules onto the surface of the crystal and transfer it to the HF-EPR spectrometer via UHV suitcase. Due to the time press, problems with the spectrometer, and several experiments were running in the UHV cluster at that time, and it was not possible to make a deposition of the FePc molecules onto the surface of the crystal and transfer it to the HF-EPR. For this reason, the deposition will be done after the submission of this thesis. If the deposited FePc results are comparable with the pellet sample, it will be the indicator that it works properly. After successful measurements, more atmosphere sensitive molecules (such as

the metal center of Co(II) with ligands according to the description in this article [91]) will be gradually observed.

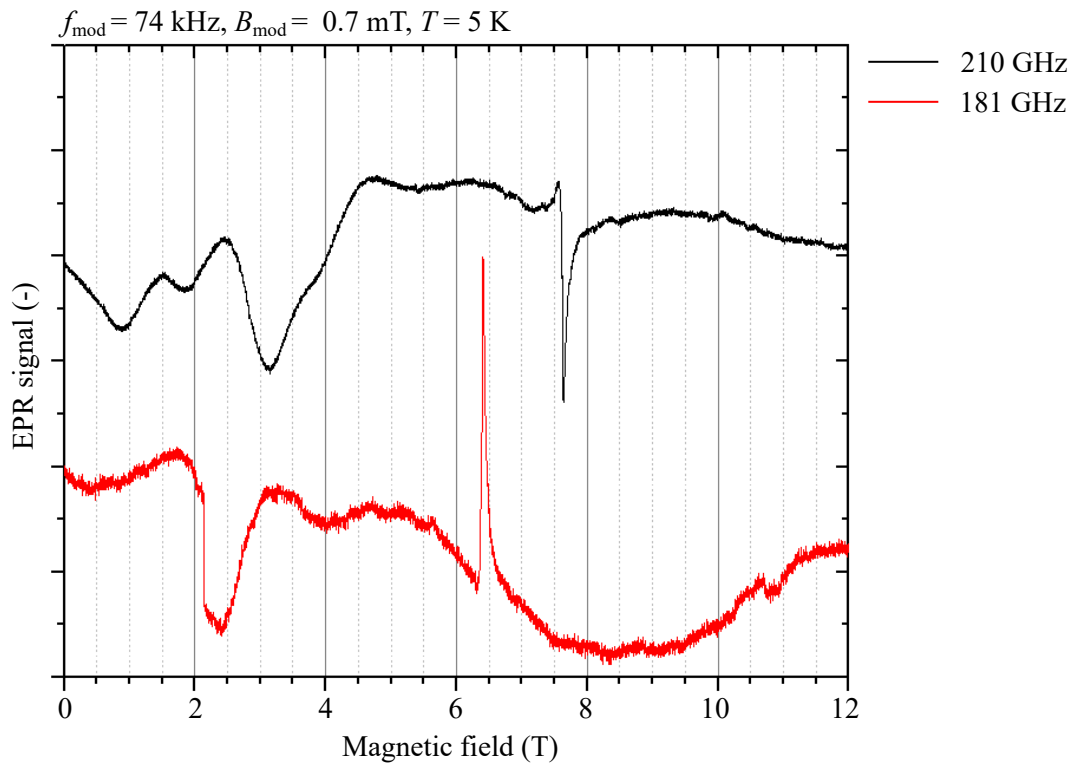


**Figure 6.11:** FePc reference sample in the form of the pellet. The EPR signal with the frequency 181 GHz is swept up from 0 T to 12 T, signal with the frequency 210 GHz is swept down from 12 to 0 T.

## 7. Conclusion

The presented master's thesis deals with the design of the sample transfer system for loading samples into the HF-EPR spectrometer. Elaborated literature review of EPR is presented along with materials and requirements for the proposal of the transfer system, author took advantage during the design of the individual components of the system. The obtained know-how was applied in the design of the individual components of the complex system. This work discusses a unique connection between the UHV cluster and the HF-EPR spectrometer at CEITEC Nano. These systems are powerful tools for sample fabrication and data analysis.

The second chapter introduced EPR spectroscopy, principle of its operation, and applications along with the setup located in the EPR laboratory at CEITEC Nano. Chapter 3 discussed molecular nanomagnets, especially those sensitive to the atmosphere, as their fabrication and characterization stand for the main outcome of the connection between the UHV cluster and HF-EPR spectrometer.

The fourth and fifth chapter focused on the design of the developed sample transfer system and requirement set for the materials used in the UHV system and the HF-EPR spectrometer. Furthermore, mechanical parts, from which the developed systems consist, are described. Part of the thesis was dedicated to design the UHV suitcase and the simple suitcase to transport samples in inert conditions. Furthermore, the palette holder and the sample palette suitable for graphene samples, which can be inserted to the palette holder, were designed as well as the airlock, which is used to connect spectrometer and UHV suitcase. These proposed parts had to meet the required properties for the UHV cluster and HF-EPR spectrometer.

The proposed UHV suitcase was designed to be a compact device to connect the UHV cluster with the HF-EPR spectrometer. 750 mm long transfer rod allows the transfer from multiple UHV chambers of CEITEC Nano, and its aluminium frame protects it from any impacts. Although at the moment, there is the ion pump present in the UHV suitcase, the pressure inside the suitcase reached the limit of  $4.3 \cdot 10^{-10}$  mbar without a functional getter. With a functional getter, much lower pressure will be assured, reaching below  $1 \cdot 10^{-10}$  mbar. The overall dimensions of the UHV suitcase are (412.4x276.5x1129) mm and the weight of 20 kg. Compared to the commercially available suitcases, the UHV suitcase developed in this thesis is the longest one just because it has the longest transfer rod. The rest of the parameters are similar. UHV suitcase is one of the heavier suitcases, but still suitable to operate in most cases in one person. UHV suitcase includes the tip-tilt port aligner, which is a necessary part of the suitcase during the manipulation with the sample palettes. Furthermore, with the price of 17 243 €, it is almost two times cheaper than the second most cheapest suitcase.

The palette holder was designed for the crystal sample palette and the sample palette for graphene. The palette holder should also include three additional electric contacts to

connect the palette holder with the sample palette for graphene, which can be added in the future.

The airlock on the top of the spectrometer magnet was designed to perform the same function as its previous version, but it is extended to enable the connection of the UHV suitcase for transportation atmosphere sensitive samples.

Parts mentioned above were developed, designed, and manufactured. All of these components were thoroughly tested, and their functionality was verified. For the remaining two parts, sample palette for graphene and simple suitcase, only proposals were presented, which will be manufactured in the future.

The calibration of the palette holder coils was carried out to ensure its functionality. Further, a reference measurement of a pellet form FePc was performed. The whole process of the sample transfer, starting with the cleaned test sample, through a connection with the airlock on the top of the magnet, and inserting the test sample into the palette holder was performed. Finally, the test sample was transferred back to the UHV cluster, and the impurity levels were measured.

The possibility of traveling with the UHV suitcase has been verified, which opens up the possibility of connecting unique devices, such as the HF-EPR spectrometer and the UHV cluster, with other devices, which are not located in the CEITEC Nano laboratories.

Furthermore, the molecules on the sample for UHV transfer will be measured. The connection for the preparation, transfer, and testing of samples with the molecular systems that are the basis for nanomagnets is working correctly.

# References

- [1] WEIL, John A and James R BOLTON. *Electron paramagnetic resonance: elementary theory and practical applications*. John Wiley & Sons, 2007.
- [2] GILBERT, Bruce C. *Electron paramagnetic resonance*. Royal Society of Chemistry, 2002.
- [3] GERLACH, Walther and Otto STERN. Das magnetische moment des silberatoms. *Zeitschrift für Physik*. 1922vol. 9, no. 1, 353–355.
- [4] UHLENBECK, George E and Samuel GOUDSMIT. Ersetzung der Hypothese vom unmechanischen Zwang durch eine Forderung bezüglich des inneren Verhaltens jedes einzelnen Elektrons. *Naturwissenschaften*. 1925vol. 13, no. 47, 953–954.
- [5] LEBEDEV, Ya S. High-frequency continuous-wave electron spin resonance. *Modern pulsed and continuous-wave electron spin resonance*. 1990 365–404.
- [6] HAINDL, E. and K. MÖBIUS. A 94 GHz EPR spectrometer with Fabry-Perot resonator. *Zeitschrift für Naturforschung A*. 1985vol. 40, no. 2, 169–172.
- [7] LYNCH, W Bryan, Keith A EARLE and Jack H FREED. 1-mm wave ESR spectrometer. *Review of scientific instruments*. 1988vol. 59, no. 8, 1345–1351.
- [8] KEMPE, Sabine, Hendrik METZ and Karsten MÄDER. Application of electron paramagnetic resonance (EPR) spectroscopy and imaging in drug delivery research—chances and challenges. *European Journal of Pharmaceutics and Biopharmaceutics*. 2010vol. 74, no. 1, 55–66.
- [9] SMITH, GM, JCG LESURF, RH MITCHELL and PC RIEDI. Quasi-optical cw mm-wave electron spin resonance spectrometer. *Review of scientific instruments*. 1998vol. 69, no. 11, 3924–3937.
- [10] BARRA, A.L., L.C. BRUNEL and J.B. ROBERT. EPR spectroscopy at very high field. *Chemical Physics Letters* [online]. 1990vol. 165, no. 1, 107–109. ISSN 00092614. Available from: doi:10.1016/0009-2614(90)87019-N. Available from: <https://linkinghub.elsevier.com/retrieve/pii/000926149087019N>.
- [11] KUTTER, C., H. P. MOLL, J. van TOL, H. ZUCKERMANN, J. C. MAAN and P. WYDER. Electron-Spin Echoes at 604 GHz Using Far Infrared Lasers. *Physical Review Letters* [online]. 1995vol. 74, no. 15, 2925–2928. ISSN 0031-9007. Available from: doi:10.1103/PhysRevLett.74.2925. Available from: <https://link.aps.org/doi/10.1103/PhysRevLett.74.2925>.
- [12] SMITH, G. M., J. C. G. LESURF, R. H. MITCHELL, P. C. RIEDI, J. C. MAAN and P. WYDER. Quasi-optical cw mm-wave electron spin resonance spectrometer. *Review of Scientific Instruments* [online]. 1998vol. 69, no. 11, 3924–3937. ISSN 0034-6748. Available from: doi:10.1063/1.1149200. Available from: <http://aip.scitation.org/doi/10.1063/1.1149200>.

- [13] HALLAK, F. El, J. van SLAGEREN and M. DRESSEL. Torque detected broad band electron spin resonance. *Review of Scientific Instruments*. 2010vol. 81, no. 9. ISSN 0034-6748. Available from: doi:[10.1063/1.3482158](https://doi.org/10.1063/1.3482158).
- [14] ZHANG, Liang, Wenlong HE, Craig R DONALDSON, Adrian W CROSS, Graham M SMITH, Duncan A ROBERTSON and Robert I HUNTER. Smoothly profiled quasi-optical output launcher for a W-band gyro-TWA. In: *2017 10th UK-Europe-China Workshop on Millimetre Waves and Terahertz Technologies (UCMMT)*. 2017 1–2.
- [15] NEUGEBAUER, P, D BLOOS, R MARX, P LUTZ, M KERN, D AGUILÀ, J VAVERKA, O LAGUTA, C DIETRICH, R CLÉRAC, et al. Ultra-broadband EPR spectroscopy in field and frequency domains. *Physical Chemistry Chemical Physics*. 2018vol. 20, no. 22, 15528–15534.
- [16] MIKSCH, Björn, Martin DRESSEL and Marc SCHEFFLER. Cryogenic frequency-domain electron spin resonance spectrometer based on coplanar waveguides and field modulation. *Review of Scientific Instruments*. 2020vol. 91, no. 2, 025106.
- [17] PRISNER, T. and W. KOECKENBERGER. *Dynamic nuclear polarization: new experimental and methodology approaches and applications in physics, chemistry, biology and medicine*. Springer, 2008.
- [18] EATON, Sandra S, Yilin SHI, Lukas WOODCOCK, Laura A BUCHANAN, Joseph MCPEAK, Richard W QUINE, George A RINARD, Boris EPEL, Howard J HALPERN and Gareth R EATON. Rapid-scan EPR imaging. *Journal of Magnetic Resonance*. 2017vol. 280, 140–148.
- [19] LAGUTA, O, M TUČEK, J van SLAGEREN and P NEUGEBAUER. Multi-frequency rapid-scan HF-EPR. *Journal of Magnetic Resonance*. 2018vol. 296, 138–142.
- [20] BELL, John S. *Speakable and unspeakable in quantum mechanics*. Cambridge University. 1987.
- [21] HRUBÝ, Jakub. *Preparation and Characterization of Graphene Based Hybrid Materials*. 2017. Master's thesis. Brno University of Technology.
- [22] RUAMPS, Renaud, Luke J BATCHELOR, Régis GUILLOT, Georges ZAKHIA, Anne-Laure BARRA, Wolfgang WERNSDORFER, Nathalie GUIHÉRY and Talal MALLAH. Ising-type magnetic anisotropy and single molecule magnet behaviour in mononuclear trigonal bipyramidal Co (II) complexes. *Chemical Science*. 2014vol. 5, no. 9, 3418–3424.
- [23] POOLE, Charles P. *Electron spin resonance: a comprehensive treatise on experimental techniques*. Courier Corporation, 1996.
- [24] BRUKER. *What is EPR?* [online]. 2020 [Accessed 2020-06-06]. Available from: <https://www.bruker.com/products/mr/epr/what-is-epr.html>.
- [25] GOSWAMI, Monalisa, Andrei CHIRILA, Christophe REBREYEND and Bas de BRUIN. EPR spectroscopy as a tool in homogeneous catalysis research. *Topics in Catalysis*. 2015vol. 58, no. 12-13, 719–750.
- [26] YASHROY, RC. Magnetic resonance studies of dynamic organisation of lipids in chloroplast membranes. *Journal of Biosciences*. 1990vol. 15, no. 4, 281–288.

- [27] YASHROY, Rakesh C. Protein heat denaturation and study of membrane lipid-protein interactions by spin label ESR. *Journal of biochemical and biophysical methods*. 1991vol. 22, no. 1, 55–59.
- [28] BRUKER. *EPR in Life Science* [online]. 2020 [Accesed 2020-06-06]. Available from: <https://www.bruker.com/products/mr/epr/epr-in-life-science.html>.
- [29] HARRISON, N. Radiation sterilization and food packaging. In: *Irradiation effects on polymers*. 1991.
- [30] BRUKER. *EPR in Material science* [online]. 2020 [Accesed 2020-06-06]. Available from: <https://www.bruker.com/products/mr/epr/epr%2Din%2Dmaterial%2Dscience.html/>.
- [31] BRUKER. *EPR in Physics* [online]. 2020 [Accesed 2020-06-06]. Available from: <https://www.bruker.com/products/mr/epr/epr-in-physics.html>.
- [32] BRUKER. *EPR in Industry* [online]. 2020 [Accesed 2020-06-06]. Available from: <https://www.bruker.com/products/mr/epr/epr%2Din%2Dindustry.html/>.
- [33] GUALTIERI, G, S COLACICCHI, R SGATTONI and M GIANNONI. The Chernobyl accident: EPR dosimetry on dental enamel of children. *Applied Radiation and isotopes*. 2001vol. 55, no. 1, 71–79.
- [34] CHUMAK, V, S SHOLOM and L PASALSKAYA. Application of high precision EPR dosimetry with teeth for reconstruction of doses to Chernobyl populations. *Radiation protection dosimetry*. 1999vol. 84, no. 1-4, 515–520.
- [35] BRUKER. *Electron paramagnetic resonance* [online]. 2020 [Accesed 2020-06-06]. Available from: [https://en.wikipedia.org/wiki/Electron\\_paramagnetic\\_resonance#cite\\_note-17](https://en.wikipedia.org/wiki/Electron_paramagnetic_resonance#cite_note-17).
- [36] MÖBIUS, Klaus and Anton SAVITSKY. *High-field EPR spectroscopy on proteins and their model systems*. Cambridge: Royal Soc. of Chemistry, 2009. ISBN ISBN978-0-85404-368-2.
- [37] GATTESCHI, Dante, Roberta SESSOLI and Jacques VILLAIN. *Molecular nanomagnets*. Oxford: Oxford University Press, 2011. ISBN 978-0-19-960226-1.
- [38] NORTH, Jeremy Micah. *Synthesis and Characterization of Single-Molecule Magnets: Mn12-ac, Fe8Br8, and Analogs*. 2004. Disseration thesis. Florida state university, college of arts, science, department of chemistry, and biochemistry.
- [39] GUO, Fu-Sheng, Benjamin M DAY, Yan-Cong CHEN, Ming-Liang TONG, Ak-seli MANSIKKAMÄKI and Richard A. LAYFIELD. Magnetic hysteresis up to 80 kelvin in a dysprosium metallocene single-molecule magnet. *Science*. 2018vol. 362, no. 6421, 1400–1403.
- [40] SESSOLI, Roberta, Dante GATTESCHI, Andrea CANESCHI and MA NOVAK. Magnetic bistability in a metal-ion cluster. *Nature*. 1993vol. 365, no. 6442, 141–143.
- [41] LIS, T. Preparation, structure, and magnetic properties of a dodecanuclear mixed-valence manganese carboxylate. *Acta Crystallographica Section B: Structural Crystallography and Crystal Chemistry*. 1980vol. 36, no. 9, 2042–2046.
- [42] *Stevens Operators*. [online]. Available from: <http://easyspin.org/documentation/stevensoperators.html>.

- [43] REBECCA, Cebulka. *Light Matter Interaction in Single Molecule Magnets*. 2019. Dissertation thesis. University of Central Florida.
- [44] LIDDLE, Stephen T. and Joris van SLAGEREN. Improving f-element single molecule magnets. *Chemical Society Reviews* [online]. 2015vol. 44, no. 19, 6655–6669. ISSN 0306-0012. Available from: doi:[10.1039/C5CS00222B](https://doi.org/10.1039/C5CS00222B). Available from: <http://xlink.rsc.org/?DOI=C5CS00222B>.
- [45] *A Ten Year (2008-2017) Storage Landscape*. [online]. R. Fontana, G. Decad, 2018. Available from: <https://storageconference.us/2018/Presentations/Fontana.pdf>.
- [46] MIDLÍKOVÁ, Jana. *Design of the far-infrared spectrometer coupling to a super-conductive magnet and magneto-optical measurements in the far-infrared region*. 2018. Master's thesis. Brno University of Technology, Faculty of Mechanical Engineering, Institute of construction.
- [47] *Computing with molecules: A big step in molecular spintronics*. [online]. Kiel University: 2019. Available from: <https://www.sciencedaily.com/releases/2019/12/191223122912.htm>.
- [48] ZADROZNY, Joseph M., Dianne J. XIAO, Mihail ATANASOV, Gary J. LONG, Fernande GRANDJEAN, Frank NEESE and Jeffrey R. LONG. Magnetic blocking in a linear iron(I) complex. *Nature Chemistry* [online]. 2013vol. 5, no. 7, 577–581. ISSN 1755-4330. Available from: doi:[10.1038/nchem.1630](https://doi.org/10.1038/nchem.1630). Available from: <http://www.nature.com/articles/nchem.1630>.
- [49] CORNIA, Andrea, Matteo MANNINI, Philippe SAINCTAVIT and Roberta SESSOLI. Chemical strategies and characterization tools for the organization of single molecule magnets on surfaces. *Chemical Society Reviews*. 2011vol. 40, no. 6, 3076–3091.
- [50] CLEMENTE-LEÓN, Miguel, Hélène SOYER, Eugenio CORONADO, Christophe MINGOTAUD, Carlos J GÓMEZ-GARCÍA and Pierre DELHAËS. Langmuir–Blodgett Films of Single-Molecule Nanomagnets. *Angewandte Chemie International Edition*. 1998vol. 37, no. 20, 2842–2845.
- [51] SAYWELL, Alex, Graziano MAGNANO, Christopher J SATTERLEY, Luís MA PERDIGÃO, Andrew J BRITTON, Nassiba TALEB, María del CARMEN GIMÉNEZ-LÓPEZ, Neil R CHAMPNESS, James N O'SHEA and Peter H BETON. Self-assembled aggregates formed by single-molecule magnets on a gold surface. *Nature communications*. 2010vol. 1, no. 1, 1–8.
- [52] ABDURAKHMANOVA, N., T.-C. TSENG, A. LANGNER, C. S. KLEY, V. SESSI, S. STEPANOW and K. KERN. Superexchange-Mediated Ferromagnetic Coupling in Two-Dimensional Ni-TCNQ Networks on Metal Surfaces. *Physical Review Letters* [online]. 2013vol. 110, no. 2. ISSN 0031-9007. Available from: doi:[10.1103/PhysRevLett.110.027202](https://doi.org/10.1103/PhysRevLett.110.027202). Available from: <https://link.aps.org/doi/10.1103/PhysRevLett.110.027202>.
- [53] KIEFL, Evan, Matteo MANNINI, Kevin BERNOT, Xiaohui YI, Alex AMATO, Tom LEVIANT, Agnese MAGNANI, Thomas PROKSCHA, Andreas SUTER, Roberta SESSOLI, et al. Robust Magnetic Properties of a Sublimable Single-Molecule Magnet. *ACS nano*. 2016vol. 10, no. 6, 5663–5669.

- [54] KOVAŘÍK, Štěpán. *Self-assembled molecular layers on epitaxial graphene*. 2018. Master's thesis. Brno University of Technology.
- [55] MACLEOD, J. M., F. ROSEI, A. LANGNER, C. S. KLEY, V. SESSI, S. STEPANOW and K. KERN. Molecular Self-Assembly on Graphene. *Small* [online]. 2014vol. 10, no. 6, 1038–1049. ISSN 16136810. Available from: doi:[10.1002/sml.201301982](https://doi.org/10.1002/sml.201301982). Available from: <http://doi.wiley.com/10.1002/sml.201301982>.
- [56] CEITEC NANO. *Ultra High Vacuum Preparation and Analytical System* [online]. 2018 [Accessed 2020-06-06]. Available from: <http://nano.ceitec.cz/ultra-high-vacuum-preparation-and-analytical-system-uhv-cluster/>.
- [57] ROTH, Alexander. *Vacuum technology*. Elsevier, 2012.
- [58] HOFFMAN, Dorothy M., Bawa SINGH and John H. THOMAS. *Handbook of vacuum science and technology*. San Diego, CA: Academic Press, 1998. ISBN 01-235-2065-7.
- [59] *Technika vysokého vakua*. Praha: Státní nakladatelství technické literatury, 1981.
- [60] PAVERA, Michal. *Design of low temperature ultra high vacuum scanning probe microscopes*. 2015. Dissertation thesis. Brno University of Technology.
- [61] O'HANLON, John F. *A user's guide to vacuum technology*. 3rd ed. Hoboken, NJ: Wiley-Interscience, 2003. ISBN 04-712-7052-0.
- [62] DUPONT. *DuPont Viton* [online]. 2010 [Accessed 2020-06-06]. Available from: [https://www.ber-pa.it/UserFiles/Download/Viton\\_Brochure%202010.pdf](https://www.ber-pa.it/UserFiles/Download/Viton_Brochure%202010.pdf).
- [63] DUPONT. *DuPont: Kapton polyimide film* [online]. 2020 [Accessed 2020-06-06]. Available from: <https://www.dupont.com/electronic-materials/kapton-polyimide-film.html>.
- [64] LEE, G. *Materials for Ultra-High Vacuum* [online]. Aug. 15, 1989 [Accessed 2020-06-06]. Available from: <https://lss.fnal.gov/archive/tm/TM-1615.pdf>.
- [65] OMNEXUS. *Polyetheretherketone (PEEK)* [online]. 2020 [Accessed 2020-06-06]. Available from: <https://bit.ly/3i8MkQq>.
- [66] CORNING. *Macor brochure* [online]. [Accessed 2020-06-06]. Available from: <https://psec.uchicago.edu/ceramics/MACOR%20Data%20Sheet.pdf>.
- [67] DAVID, E. Materials for cryogenics applications. In: *12th International scientific conference on achievements in mechanical and materials engineering, AMME*. 2003.
- [68] LAKE SHORE CRYOTRONICS. *Temperature Measurement and Control Catalog* [online]. [Accessed 2020-06-06]. Available from: [https://www.lakeshore.com/docs/default-source/product-downloads/lakeshoretc\\_1.pdf?sfvrsn=511d733a\\_3](https://www.lakeshore.com/docs/default-source/product-downloads/lakeshoretc_1.pdf?sfvrsn=511d733a_3).
- [69] HALLIDAY, David, Robert RESNICK and Jearl WALKER. *Fyzika*. Brno: VUTUM, 2000. ISBN 80-214-1868-0.
- [70] BACHER, J.-P., C. BENVENUTI, P. CHIGGIATO, M.-P. REINERT, S. SGOBBA and A.-M. BRASS. Thermal desorption study of selected austenitic stainless steels. [online]. 2003vol. 21, no. 1, 167–174. ISSN 0734-2101. Available from: doi:[10.1116/1.1527953](https://doi.org/10.1116/1.1527953). Available from: <http://avs.scitation.org/doi/10.1116/1.1527953>.
- [71] TERAPOL S.R.O. *Hlavní skupiny nerezových ocelí: Austenitická nerezová ocel* [online]. [Accessed 2020-06-06]. Available from: <http://www.terapol.cz/clanek/no-vap-hlavni-skupiny>.

- [72] ATIMETALS. *ATI 316Ti<sup>TM</sup>* [online]. 2014 [Accessed 2020-06-06]. Available from: [https://www.atimetals.com/Products/Documents/datasheets/stainless-specialty-steel/austenitic/ati\\_316ti\\_tds\\_en\\_v1.pdf](https://www.atimetals.com/Products/Documents/datasheets/stainless-specialty-steel/austenitic/ati_316ti_tds_en_v1.pdf).
- [73] INKOSAS A.S. *Titanové slitiny Grade 1-11 - titanové plechy, tyče, trubky, dráty, příruby* [online]. [Accessed 2020-06-06]. Available from: <https://www.inkosas.cz/templates/titanove-slitiny-tyce-plechy-draty-trubky.php>.
- [74] CUSTOMCABLE.CA. *Oxygen Free Copper and its Applications* [online]. [Accessed 2020-06-06]. Available from: <https://customcable.ca/oxygen-free-copper-and-its-applications/>.
- [75] LUNK, Hans-Joachim and Hans HARTL. Discovery, properties and applications of molybdenum and its compounds. *ChemTexts*. 2017vol. 3, no. 3, 13.
- [76] TUFNOL COMPOSITES LTD. *TUFNOL Tufset* [online]. [Accessed 2020-06-06]. Available from: <https://tufnol.com/materials-full/themoplastics/tufnol-tufset.aspx>.
- [77] COMPANZ, Kurt J. Lesker. *CF Flanges Technical Notes* [online]. [Accessed 2020-06-06]. Available from: [https://www.lesker.com/newweb/flanges/flanges\\_technicalnotes\\_conflat\\_1.cfm](https://www.lesker.com/newweb/flanges/flanges_technicalnotes_conflat_1.cfm).
- [78] LEWVAC. *Magnetically Coupled Single Shaft Linear and Rotary Transporters* [online]. 2020 [Accessed 2020-06-06]. Available from: <https://www.lewvac.co.uk/product/magnetically-coupled-single-shaft-linear-rotary-transporters/>.
- [79] LEWVAC. *Precision Tilt Port Aligners* [online]. 2020 [Accessed 2020-06-06]. Available from: <https://www.lewvac.co.uk/product/precision-tilt-port-aligners/>.
- [80] GAMMA VACUUM. *Small TiTan Ion Pumps* [online]. 2020 [Accessed 2020-06-06]. Available from: <https://www.gammavacuum.com/index.php/product?id=70>.
- [81] THYRACONT VACUUM INSTRUMENTS. *Smartline Digital Vacuum Transducers* [online]. 2020 [Accessed 2020-06-06]. Available from: <https://thyracont-vacuum.com/en/product/vshxd1-smartline-pirani-bayard-alpert/>.
- [82] GAMMA VACUUM. *Non-Evaporable Getters* [online]. 2020 [Accessed 2020-06-06]. Available from: <https://www.gammavacuum.com/index.php/product?id=31>.
- [83] LEWVAC. *Gate Valve – CF Flanges with Viton® Bonnet Seal* [online]. [Accessed 2020-06-06]. Available from: <https://www.lewvac.co.uk/product/gate-valve-cf-flanges-viton-bonnet-seal/>.
- [84] GMBH, Ferrovac. *NexGeneration UHV Suitcases* [online]. 2020 [Accessed 2020-06-06]. Available from: <https://www.ferrovac.com/?tool=ProductList&category=UHV+Suitcase>.
- [85] PREVAC. *Transport box vacuum suitcase* [online]. 2020 [Accessed 2020-06-06]. Available from: <https://bit.ly/3dF0m7k>.
- [86] BEHREND, Ralph, Corina DORN, Volker UHLIG and Hartmut KRAUSE. Investigations on container materials in high temperature microwave applications. *Energy Procedia* [online]. 2017vol. 120, 417–423. ISSN 18766102. Available from: doi:10.1016/j.egypro.2017.07.191. Available from: <https://linkinghub.elsevier.com/retrieve/pii/S1876610217327613>.

- [87] ADAM, Lagiň. *Design of the non-rezonance sampleholder*. 2020. Bachelor thesis. Brno University of Technology, Faculty of Mechanical Engineering, Institute of construction.
- [88] LAKE SHORE CRYOTRONICS. *Cernox® Specifications* [online]. 2020 [Accessed 2020-06-06]. Available from: <https://www.lakeshore.com/products/categories/specification/temperature-products/cryogenic-temperature-sensors/cernox>.
- [89] LEWVAC. *Magnetically Coupled Wobblesticks Single Shaft* [online]. 2020 [Accessed 2020-06-06]. Available from: [https://www.lewvac.co.uk/product/magnetically-coupled-wobblesticks-single-shaft/?fbclid=IwAR2b0RWgCJlo0brBRR5YUkAk1\\_SaQFN-fp497HqN\\_MMJ7ikVa62p5iImzvU](https://www.lewvac.co.uk/product/magnetically-coupled-wobblesticks-single-shaft/?fbclid=IwAR2b0RWgCJlo0brBRR5YUkAk1_SaQFN-fp497HqN_MMJ7ikVa62p5iImzvU).
- [90] CZC.CZ. *Záložní zdroje UPS* [online]. 2020 [Accessed 2020-06-06]. Available from: <https://www.czc.cz/cyberpower-green-value-ups-600va-360w-lcd/174851/produkt>.
- [91] KAUR, Sukhdeep and Subodh KUMAR. Photoactive chemosensors 3: a unique case of fluorescence enhancement with Cu (II). *Chemical communications*. 2002no. 23, 2840–2841.

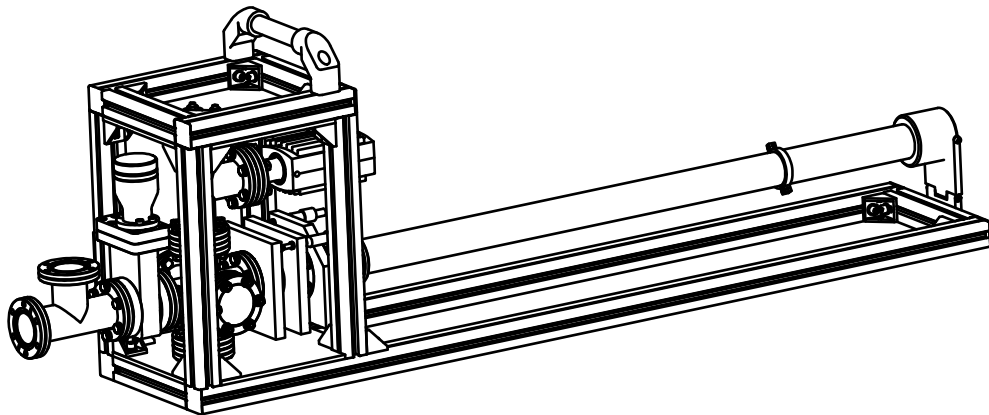
# List of abbreviation and symbols

EPR	Electron paramagnetic resonance
HF-EPR	High-frequency electron paramagnetic resonance
XPS	X-ray photoelectron spectroscopy
CEITEC	Central European Institute of Technology
MOTeS	Magneto-Optical and THz Spectroscopy
UHV	Ultra-high vacuum
ESR	Electron Spin Resonance
VTI	Variable Temperature Insert
SMMs	Single-molecule magnets
SIMs	Single-ion magnets
SCMs	Single-chain magnets
MNMs	Molecular nanomagnets
AFM	Atomic force microscopy
STM	Scanning tunneling microscopy
SEM	Scanning electron microscopy
HDD	Hard disk drive
SSD	Solid-state drive
SAM	Self-assembled monolayer
LV	Low vacuum
HV	High vacuum
LEIS	Low energy ion spectroscopy
LEEM	Low energy electron spectroscopy
PEEK	Polyether ether ketone
CF	Conflat-type
CPS	Counts per second

# List of attachments

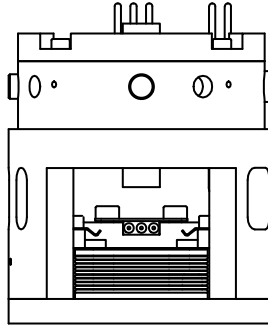
The complete drawing documentation is attached to this work in the boards, electronically in the format PDF.

## UHV Suitcase



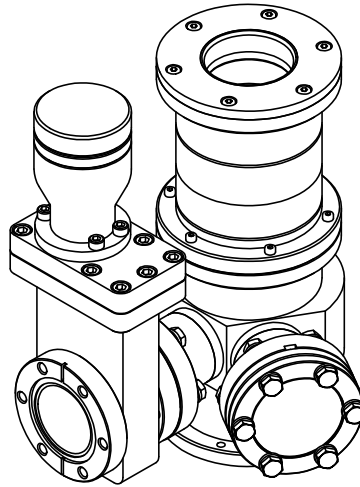
Part Number	Part Title	Paper size
UHVS-420-00	UHV Suitcase	A3
UHVS-420-07	Frame	A3
UHVS-420-07-01	Rexorth 30x30-224	A4
UHVS-420-07-02	Al sheet bottom	A4
UHVS-420-07-03	Al sheet top	A4
UHVS-420-07-04	Rexorth 30x30-155	A4
UHVS-420-07-05	Rexorth 30x30-287.4	A4
UHVS-420-07-06	Rexorth 30x30-1075.3	A4
UHVS-420-14	Safety sleeve 1	A4
UHVS-420-15	Safety sleeve 2	A4
UHVS-420-16	Linear transport holder 1	A4
UHVS-420-17	Linear transport holder 2	A4
UHVS-420-18	Linear transport holder 3	A4
UHVS-420-19	Linear transport holder rod	A4

## Palette holder



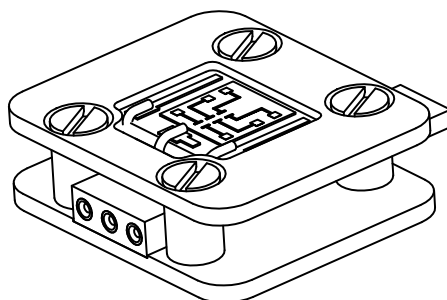
Part Number	Part Title	Paper size
PH-420-00	Palette holder	A3
PH-420-02	Top coil part	A2
PH-420-03	Stud 5mm	A4
PH-420-04	Stud 4mm	A4
PH-420-05	Body	A2
PH-420-06	Guide tube	A4
PH-420-07	Cu sheet for pins	A4
PH-420-09	Bottom coil part	A3
PH-420-10	Downforce sheet-left	A4
PH-420-11	Skid-left	A4
PH-420-12	Downforce sheet-right	A4
PH-420-13	Skid-right	A4

## Airlock assembly



Part Number	Part Title	Paper size
AL-420-00	Airlock assembly	A3
AL-420-01	Airlock-tefflon cover	A4
AL-420-02	Teflon ring-3	A4
AL-420-03	Airlock top center part	A3
AL-420-04	Teflon ring-1	A4
AL-420-05	Teflon ring-4	A4
AL-420-07	Teflon ring-2	A4
AL-420-09	Airlock bottom-weldment	A3
AL-420-09-01	Airlock bottom center part	A3
AL-420-10	Teflon ring-bottom	A3

## Sample holder for graphene



Part Number	Part Title	Paper size
SHG-420-00	Graphene sample palette	A3
SHG-420-01	Top plate	A4
SHG-420-02	Distance washer	A4
SHG-420-03	Bottom plate	A4
SHG-420-05	Mirror holder	A4
SHG-420-06	Chip expander	A4
SHG-420-09	Si/SiO <sub>2</sub> -Au contacts	A4

# A. Appendix

## A.1. Helmholtz magnetic coils

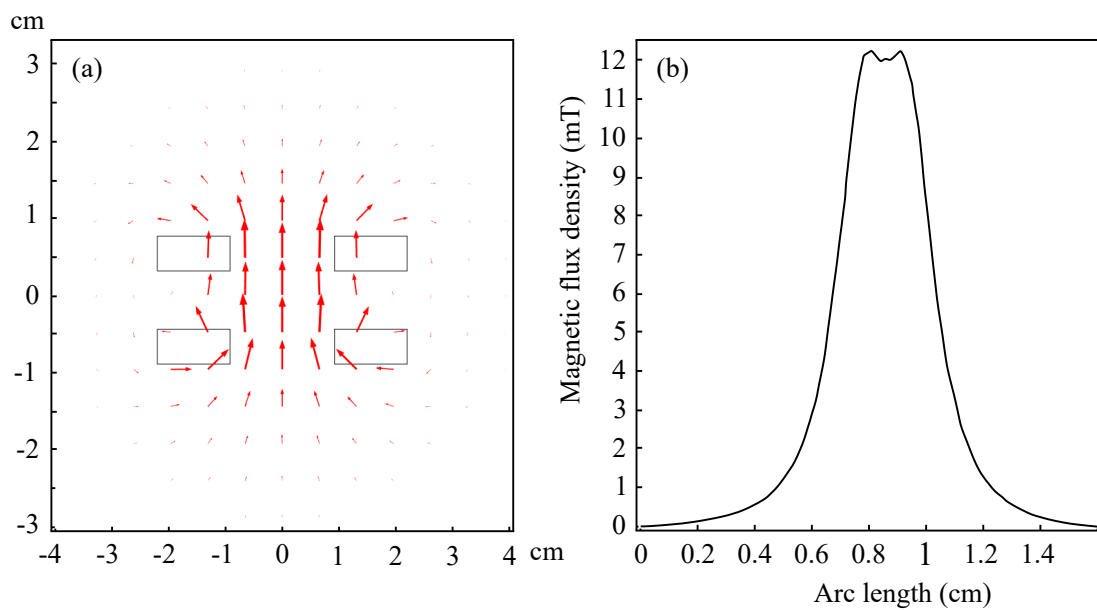


**Figure A.1:** Simulation of the Helmholtz modulation coils designed in thesis with a static magnetic field. Each coil has 156 turns and current  $I = 0.5$  A. (a) Arrow surface – magnetic flux density. (b) Distribution of the magnetic flux density in the plane of the sample.

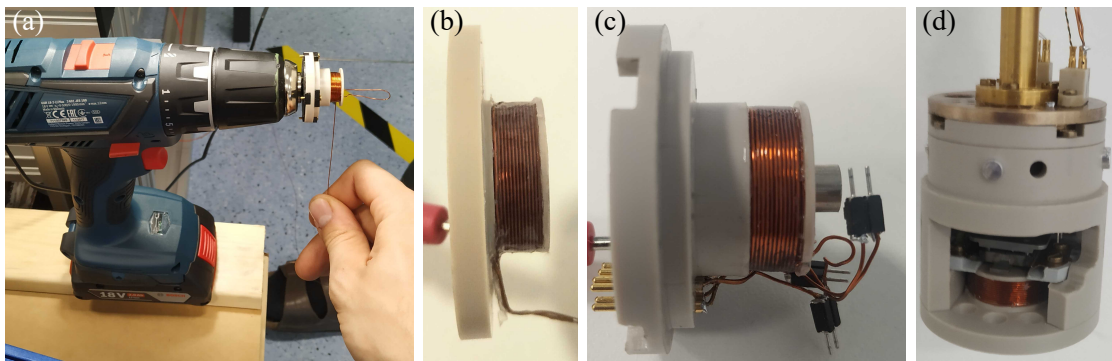


**Figure A.2:** (a) Method of winding coils using a cordless drill. (b) Detailed view on the bottom coil holder with wound coil. (c) Detailed view on the pincoil holder with wound coil. (d) The whole palette holder with the sample palette inside connected to the waveguide.

## A.2. Support system



**Figure A.3:** Support system consists of aluminium profiles. At the end of the each leg, there is an adjustable screw leg for easy adjustment.

## A.3. UHV suitcase



**Figure A.4:** View of the baking procedure of the UHV suitcase. The entire suitcase is wrapped with baking tapes and heated up to 120°C. Temperature was controlled by two controllers showed in (b).